Universidade Federal do Rio Grande do Sul
Instituto de Ciências Básicas da Saúde
Programa de Pós Graduação em Bioquímica

ANÁLISE DENSITOMÉTRICA E ESTEREOLÓGICA DO SISTEMA NERVOSO CENTRAL EM DIFERENTES MODELOS EXPERIMENTAIS

Léder Leal Xavier

Orientadora
Profa. Dra. Matilde Achaval Elena

Co-orientador
Prof. Dr. Carlos Alexandre Netto

Tese apresentada ao Programa de Pós Graduação em CB:Bioquímica, da Universidade Federal do Rio Grande do Sul, como requisito parcial para a obtenção do grau de Doutor.
PORTO ALEGRE
2004

"Os homens criam as ferramentas,
as ferramentas recriam o homem"

Marshall McLuhan

Este trabalho é humildemente dedicado

ao "velho Santiago"

Agradecimentos

A minha eterna orientadora, Prof[a] Dr[a] Matilde Achaval, por três motivos: primeiro, pelo incrível senso crítico e seriedade profissional com que conduziu não apenas este, mas todos os trabalhos realizados no Laboratório de Histofisiologia Comparada; segundo, pela paciência e dedicação que tem para com todos os seus alunos; terceiro, por compreender, como poucos, as capacidades e limitações do ser humano.

Ao meu co-orientador Prof Dr Carlos Alexandre Netto, que com seus atos e ensinamentos, me fez compreender melhor virtudes como a serenidade, o bom senso e a diplomacia.

Ao meu mestre Prof Dr Luis Manuel Cruz-Orive (Laboratório de Estereologia, Departamento de Matematicas, Estadistica y Computacion, Facultad de Ciencias, Universidad de Cantabria), por ter me recebido tão bem em seu Laboratório, por seus ensinamentos, pela paciência em responder meus e-mails, e acima de tudo por suas lições de bom humor.

A Dra Marta Garcia-Fiñana (Magnetic Resonace and Image Analysis Research Centre (MARIARC), University of Liverpool) pela sua amizade, e por todas as tardes que foram perdidas explicando-me as bases matemáticas do cálculo de coeficiente de erro.

A todos os colegas dos Laboratórios de Histofisiologia Comparada, Fisiologia Animal e Isquemia, sem os quais, a execução deste trabalho seria uma tarefa impossível, mas em especial aos jovens estudantes Giordano Viola e Paulo Worm, que foram incansáveis durante toda a realização deste trabalho.

A Pati, por todas as coisas que realizamos e que não realizamos, graças a este trabalho.

Ao CNPq pela bolsa recebida.

Índice

Sumário

O sistema nervoso central (SNC) pode ser analisado com a utilização de distintas abordagens metodológicas, sendo que, o progresso das avaliações bioquímicas/histológicas do SNC está vinculado intimamente ao desenvolvimento da microscopia óptica, das técnicas histológicas, histoquímicas e imunohistoquímicas.

Neste sentido, os avanços no processo de análise das imagens digitalizadas obtidas a partir da utilização destas técnicas, são de fundamental importância para uma interpretação fidedigna dos resultados obtidos.

Neste trabalho, foram padronizados, implementados e descritos os seguintes procedimentos de análise de imagens: 1- O procedimento de análise semi-quantitativa por medida de densidade óptica, no software Image Pro Plus 4.1; 2-O procedimento de análise estereológica, pela aplicação do método de Cavalieri e o protocolo de cálculo do coeficiente de erro do método de Cavalieri associado a técnica de contagem de pontos, no software Microsoft Excel.

A padronização, implementação e descrição destes procedimentos, nos permitiu a análise das imagens geradas a partir da realização de distintos procedimentos histológicos (hematoxilina-eosina); histoquímicos (citocromo oxidase) e imunohistoquímicos (proteína glial fibrilar ácida (GFAP), substância P e tirosina hidroxilase) em diferentes modelos experimentais (SNC de rãs, tartarugas e ratos) em distintas regiões do SNC (medula espinhal, amígdala medial, substância nigra, área ventral tegmental e hipocampo).

Além dos resultados experimentais, foram descritas as vantagens e as limitações destes procedimentos de análise de imagem, assim como as peculiaridades metodológicas inerentes aos diferentes experimentos realizados.

1. Introdução

O sistema nervoso central (SNC) pode ser analisado *in vivo* ou *in vitro*, com a utilização de diversas ferramentas de investigação como por exemplo: o comportamento animal, a lesão estereotáxica, o uso de anticorpos, a autoradiografia, o raio X, a ressonância magnética, a tomografia computadorizada, o uso de infusões intraencefálicas, os slices encefálicos, as culturas celulares, a pesquisa clínica, os modelos computacionais, o eletroencefalograma, os estudos epidemiológicos, o uso de potenciais evocados, os registros eletrofisiológicos intra e extracelulares, a espectroscopia, a cromatografia gasosa, a cromatografia líquida de alta performance, a microdiálise, o *"patch clamp"*, a medida do binding de receptores, entre outras (Martin, 1997; Celis, 1998).

Todas estas técnicas de investigação científica tem as suas vantagens e as suas limitações, mas certamente contribuem de forma inequívoca para um melhor entendimento do SNC. Contudo, o detalhamento da composição bioquímica do tecido nervoso, assim como suas variações frente a diferentes situações patológicas e/ou funcionais, está vinculado, de forma muito íntima ao tema central deste trabalho, que é, o desenvolvimento da microscopia óptica, das técnicas histológicas, histoquímicas e imunohistoquímicas e os avanços nas metodologias de análise de imagem.

1.1 O microscópio óptico

É difícil descrever com exatidão, a localização temporal dos experimentos prévios que levaram a invenção do microscópio óptico, entretanto, existem registros de que os primeiros estudos

sobre as propriedades ópticas das superfícies curvas, foram realizados por Euclides (390 aC), Ptolomeu (127-151 dC) e Alhazan no século XI (Singer, 1931; De Robertis *et al.*, 1963).

Provavelmente, o primeiro uso prático destes estudos, que versavam sobre a amplificação gerada à partir destas superfícies curvas, ocorreu na Itália no ano de 1285 quando Salvino Degli Armanti inventou os óculos. Contudo a aplicabilidade destas investigações não terminara no invento de Armanti, no século XVI, Leonardo da Vinci e Francisco Maurolyco insistiam nas vantagens inerentes à aplicação destas lentes para o estudo de pequenos objetos (Singer, 1931; De Robertis *et al.*, 1963).

Neste mesmo período, em 1590, dois irmãos holandeses que trabalhavam na fabricação de óculos em Middleburg, Zacarías e Francisco Janssen, baseando-se nos estudos de seu pai, um renomado óptico da época, combinaram duas lentes convexas no interior de um tubo, obtendo assim um instrumento óptico capaz de amplificar a imagem de objetos. O impacto da invenção dos Janssen foi tão grande, que no mesmo ano, um dos mais importantes cientista da época, Galileo Galilei, construiu seu próprio instrumento óptico, combinando duas lentes em um tubo, a partir de rumores de que um holandês havia feito o mesmo (Singer, 1931; De Robertis *et al.*, 1963).

O instrumento óptico criado pelos irmãos Janssen se popularizou, e recebeu a denominação de microscópio por Jaime Faber de Bamberg, um médico residente em Roma, que trabalhava para o papa Urbano VII, sendo que a palavra microscópio derivou-se da associação dos vocábulos gregos *mikros* = pequeno e *skopein* = ver, examinar (Singer, 1931; De Robertis *et al.*, 1963).

Em 1665, Robert Hooke modificou o instrumento dos Janssen, intercalando uma terceira lente entre a objetiva e a ocular, no intuito de eliminar a aberração cromática, e apresentou a Real Sociedade de Londres os resultados de sua investigação científica sobre "A textura da cortiça, por meio de lentes de aumento". Neste trabalho, Hooke descreveu pequenos poros nas secções de cortiça e chamou estes de células (do grego *kytos* = espaço vazio), este foi o ponto de partida para a

obtenção de todos os conhecimentos que temos atualmente sobre a organização microscópica da matéria viva (Singer, 1931; De Robertis *et al.*, 1963, Alberts *et al.*, 2002).

1.2 A Histologia

O uso de colorações nas secções teciduais analisadas ao microscópio era extremamente raro até 1860, ainda que Hooke em 1660 já fosse conhecedor de colorações a base de campeche e de cochonilha e que Antony van Leeuwenhoek, um humilde mercador holândes responsável pela descoberta das bactérias e dos protozoários, em 1714 utiliza-se o açafrão para melhorar a visibilidade das fibras musculares ao microscópio (Conn, 1977).

A criação do termo histologia (do grego *histos* = rede) é atribuída a um anatomista alemão chamado Mayer em 1819. A primeira utilização da hematoxilina como corante histológico foi realizado por Böhmer em 1865, embora Waldeyer tenha empregado esta sem sucesso em 1863. O progresso da histologia era tal que, em 1875 Ranvier já enumerava seis corantes sintéticos, a base de anilina, para estudos histológicos (De Robertis *et al.*, 1963; Conn, 1977).

Embora a utilização da histologia como ferramenta de estudo aumentasse de forma vertiginosa no final do século XIX, os resultados obtidos com o emprego das técnicas histológicas para coloração do SNC não eram muito empolgantes, a principal técnica neurohistológica da época baseava-se na coloração com hematoxilina e carmin, um procedimento razoavelmente adequado para o estudo de outros tecidos, mas insatisfatório para a maioria das investigações do SNC, uma vez que as imagens reveladas por esta técnica eram incompletas, mostrando, na melhor da hipóteses, os segmentos iniciais dos dendritos, impedindo o discernimento correto sobre a natureza da célula estudada, o que fez com que muitas vezes células neuronais e gliais fossem classificadas em um mesmo grupo, e chamadas de grânulos (Pannese, 1996).

Em 1873, o italiano Camillo Golgi descobriu uma técnica de vital importância para o estudo do SNC, fundamentada na impregnação do tecido nervoso com dicromato de potássio e nitrato de prata, a reação negra, conhecida atualmente como técnica de Golgi (Pannese, 1996).

Camillo Golgi publicou as observações iniciais de sua técnica em 2 de agosto de 1873 na Gazzetta Medica Italiana de Lombardia, publicando novamente esta, sem sucesso ainda, em outros dois periódicos alemães (Pannese, 1996).

A técnica desenvolvida por Golgi não ficaria adormecida por muito tempo, pois a associação entre o surgimento de uma nova técnica de investigação e a inquietude de um gênio constituem o terreno adequado para o desenvolvimento do conhecimento científico, e neste sentido é impossível não citar a importante contribuição dada no fim do século XIX e início do século XX pelo espanhol Santiago Ramón y Cajal, que utilizando-se das técnicas de impregnação argentica desenvolvidas por Golgi e de adaptações próprias destas, realizou a maior obra histológica conhecida até os dias atuais, no que diz respeito à descrição da circuitaria e da morfologia neuronal do SNC de seres humanos e diferentes animais (Pannese, 1996; De Felipe e Jones, 1992; Ramón y Cajal, 1909).

1.3 As técnicas histoquímicas e imunohistoquímicas

Os numerosos estudos neurohistológicos realizados até o final dos anos 30, constituíram uma base morfológica extremamente sólida para as investigações futuras, ainda que estes trabalhos tenham sido extremamente importantes, com raras exceções, até aquele momento, a grande maioria das técnicas histológicas permitiam apenas investigações descritivas, sendo que com o uso da histologia convencional pouco podia ser avaliado a respeito das alterações bioquímicas e funcionais da célula frente a situações distintas (De Robertis *et al.*, 1963, Conn, 1977).

Esta situação começou a se modificar a partir da década de 30, graças aos progressos paralelos de ciências como a bioquímica e a biofísica, que, à partir da complexa associação de moléculas que constituem a célula, conseguiram isolar substâncias como lipídeos, glicogênio, ácidos nucleícos, vitaminas hormônios e enzimas (Conn, 1977). Por outro lado, houveram grandes avanços nos campos da enzimologia e da bioquímica dinâmica, que estabeleceram as bases para os estudos sobre o metabolismo das substâncias, desde que estas penetram nas células até sua excreção, bem como, de que modo estas são transformadas em energia ou incorporadas a própria célula (De Robertis *et al.*, 1963, Conn, 1977).

Entretanto, os ensaios bioquímicos desenvolvidos em soluções, embora extremamente precisos, não são adequados para o estudo detalhado de estruturas encefálicas complexas, ainda que procedimentos modernos e sofisticados como a dissecação regional e a extração tecidual localizada "*punch biopsy*" tenham melhorado significativamente a discriminação espacial das técnicas bioquímicas, estes ainda constituem ferramentas inadequadas, para a avaliação dos resultados de experimentos que necessitem de uma localização tecidual/celular extremamente precisa, devido a heterogeneidade regional e celular do sistema nervoso (Hammond *et al.*, 1996).

Os histologistas e os bioquímicos não podiam ficar indiferentes a um problema desta magnitude, e deste modo, a histologia e a bioquímica associaram-se criando as técnicas histoquímicas, que passaram então a representar um forte elo entre a sutil abordagem morfológica da histologia e a precisa interpretação química obtida por métodos bioquímicos clássicos. Esta associação permitiu a localização tecidual exata dos mais variados eventos bioquímicos (topoquímica), bem como a avaliação de suas variações frente a diferentes situações experimentais. (De Robertis *et al.*, 1963, Conn, 1977, Hammond *et al.*, 1996).

Embora as primeiras reações histoquímicas sejam normalmente atribuídas a Gomori e Takamatsu, que em 1939 demonstraram a presença de fosfatase alcalina em secções teciduais,

devemos lembrar que o primeiro experimento histoquímico propriamente dito foi a descoberta do glicogênio realizada pelo fisiologista francês Claude Bernard em 1857 (De Robertis *et al.*, 1963, Conn, 1977).

Paralelamente ao desenvolvimento das técnicas histoquímicas podemos observar o surgimento de outra ferramenta originada da histologia clássica, a imunohistoquímica, que é caracterizada pelo uso de anticorpos marcados com reagentes específicos para a localização dos constituintes teciduais (antígenos) *in situ* (Polak e Van Noorden, 1992).

A imunohistoquímica foi criada por Albert Coons e seus colaboradores em 1941, quando estes marcaram um anticorpo com uma substância fluorescente, o isocianato de fluoresceina, que emite um brilho verde quando excitada por um comprimento de luz de 490 nm (Polak e Van Noorden, 1992).

Após os primeiros estudos, o uso da técnica imunohistoquímica foi grandemente expandido, novos anticorpos foram produzidos e marcados com distintas substâncias como o isocianato de rodamina e a peroxidase, que atualmente é o marcador mais utilizado na revelação das reações imunohistoquímicas, atuando sobre um cromógeno como a diaminobenzidina gerando um polímero indamínico, eletron-denso, insolúvel e de cor marrom característico (Sternberger, 1986; Polak e Van Noorden, 1992).

O desenvolvimento das técnicas histoquímicas permitiram progressos consideráveis na investigação da organização bioquímica tecidual, atualmente são identificadas cerca de 80 diferentes enzimas através dos métodos histoquímicos, entre estas diferentes hidrolases, oxigenases, dehidrogenases, diaforases, e enzimas proteolíticas, além de ácidos graxos, fosfolipídeos, glicídeos, lipoproteínas, ácidos nucleicos e metais (Polak e van Noorden, 1992; Alberts *et al.*, 2002; Hardie *et al.*, 2002).

Por outro lado, o avanço das técnicas imunohistoquímicas em secções de tecido nos fornecem informações valiosas sobre a localização de diferentes antígenos no SNC, determinando quais tipos celulares e/ou regiões de uma mesma célula são imunoreativos para proteínas neuronais e gliais, neurotransmissores, hormônios, fatores de crescimento, toxinas, prions etc... (Polak e van Noorden, 1992, Celis *et al.*, 1998; Everbroeck *et al.*, 1999; Alberts *et al.*, 2002).

Ademais, o uso das técnicas imunohistoquímicas não é restrito a investigação dos tecidos normais, sendo amplamente utilizado no estudo das diferentes patologias, uma vez que, com o empregos das técnicas imunohistoquímicas podemos obter importantes informações sobre a natureza dos diferentes tumores (Polak e van Noorden, 1992, Celis *et al.*, 1998; Everbroeck *et al.*, 1999; Alberts *et al.* 2002).

1.4 Avaliação dos resultados obtidos com técnicas histológicas, histoquímicas e imunohistoquímicas

Quanto a interpretação dos resultados obtidos pelas técnicas histológicas, histoquímicas e imunohistoquímicas, podemos dividir esta em três grandes grupos: 1-Avaliações histológicas, histoquímicas e imunohistoquímicas qualitativas que se caracterizam pela identificação e localização dos diferentes compostos químicos dentro, fora das células e nos espaços intercelulares de um determinado tecido (Harley e Bielajew, 1992; Tashima *et al.*, 2000; Lin *et al.*, 2004); 2-Avaliações histológicas, histoquímicas e imunohistoquímicas semi-quantitativas, que utilizando-se das medidas de densidade óptica (DO), avaliam alterações na concentração e/ou atividade dos compostos analisados, entre diferentes tecidos, sem entretanto quantificar com precisão a concentração tecidual exata destes compostos (Gónzalez-Lima e Garrosa, 1991; Knyihar-Csilik *et al.*, 1998; Ruiz-Torner *et al.*, 2001; Alonso-Magdalena *et al.*, 2003; Strazielle *et al.*, 2003) e 3-

Avaliações histológicas, histoquímicas e imunohistoquímicas quantitativas, realizadas através de técnicas fundamentadas em princípios estatísticos e matemáticos sólidos, como as técnicas estereológicas, empregadas para uma estimativa tridimensional precisa de parâmetros como volume estrutural e número total de células em uma determinada estrutura (Pillegard e Ladefoged, 1996; Howard & Reed, 1998; Idrizbegovic *et al.* , 2003; Rodríguez *et al.* , 2004).

1.5 Avaliação semi-quantitativa, por densitometria óptica, dos resultados obtidos com a utilização de técnicas histoquímicas e imunohistoquímica

A análise dos resultados, obtidos à partir da execução de técnicas histoquímicas e imunohistoquímicas no SNC, vem sendo realizada, ao longo dos anos, de modo descritivo e qualitativo, visando apenas o mapeamento topoquímico de diferentes substâncias nas diferentes regiões do SNC em diferentes modelos biológicos (Harley e Bielajew, 1992; Tashima *et al.*, 2001; Chieco *et al.*, 2001; Lin *et al.*, 2004).

Neste tipo de análise qualitativa, usualmente são atribuídos conceitos de acordo com os critérios de análise do investigador, como por exemplo 0 = nenhuma reação; + = reação de intensidade fraca; ++ = reação de intensidade intermediária e +++ = reação de forte intensidade (Harley e Bielajew, 1992; Tashima *et al.*, 2000; Lin *et al.*, 2004).

A análise qualitativa dos resultados obtidos nestes experimentos esta sujeita a todos os problemas encontrados nas análises semi-quantitativas e quantitativas, contudo, a análise qualitativa apresenta o agravante da subjetividade inerente a cada pesquisador, uma vez que, a determinação correta do grau de intensidade de reações histoquímicas e imunohistoquímicas, somente através da observação ao microscópio óptico, está relacionado às expectativas e aos critérios de cada pesquisador, a que tipo de reação histoquímica e imunohistoquímica este observa

normalmente e qual a experiência prévia que este tem na análise de experimentos desta natureza. Portanto, salvo raras exceções, as análises puramente qualitativas que tenham por objetivo comparar diferentes grupos experimentais devem ser realizadas preferencialmente por histologistas extremamente experientes e apenas em situações que inviabilizam totalmente a utilização das metodologias de análise semi-quantitativa e/ou quantitativa (Celis, 1998; Chieco *et al.*, 2001).

A utilização da análise semi-quantitativa por medida de densidade óptica em técnicas histoquímicas e imunohistoquímicas, está associado ao desenvolvimento dos métodos ópticos, para determinação da quantidade de substâncias coloridas encontradas em solução, que atualmente são realizados rotineiramente por espectrofotometria, nos mais variados ensaios biológicos. A investigação por espectrofotometria baseia-se na medida da transmitância (T) através da equação (Fukuda *et al.*, 1978; van Noorden e Butcher, 1991; Celis, 1998; Chieco *et al.*, 2001):

Transmitância (T) = I/I_0

Onde: I = intensidade de luz monocromática que atravessa uma solução colorida; I_0 = intensidade da mesma luz monocromática que atravessa uma solução sem cor (branco), com índice de refração de luz similar ao da solução colorida. Ao multiplicarmos o resultado obtido por 100 obtemos a porcentagem de luz transmitida através da solução colorida (Fukuda *et al.*, 1978; van Noorden e Butcher, 1991; Celis, 1998; Chieco *et al.*, 2001).

A avaliação semi-quantitativa da intensidade de reação obtida através do emprego de técnicas histoquímicas e imunohistoquímicas, pode ser realizada com o uso de *softwares* de análise de imagens, à partir de uma adaptação das técnicas de medida da transmitância por espectrofotometria, conhecida como medida de densidade óptica (DO), também chamada de extinção ou absorbância (Fukuda *et al.*, 1978; van Noorden e Butcher, 1991; Celis, 1998; Chieco *et al.*, 2001).

A medida de DO em técnicas histoquímicas e imunohistoqúimicas é influenciada por fatores como a concentração da substância a ser medida (usualmente a concentração de produto gerado pela reação bioquímica do revelador, lembrando que a revelação da grande maioria das técnicas imunohistoquímicas também é realizada por reações enzimáticas); e a espessura da secção analisada. Estas influências podem ser avaliadas pela Lei de Beer-Lambert, representada na seguinte equação (Fukuda *et al.*, 1978; van Noorden e Butcher, 1991; Celis, 1998; Chieco *et al.*, 2001):

$DO = k. c. d$

Onde: DO = Densidade óptica; k =constante específica ou coeficiente de extinção específico; c = concentração da substância; d = espessura da secção analisada.

Como a intensidade de luz apresenta uma decaimento exponencial, a medida que se aumenta a concentração de matéria dentro da secção analisada, pode-se inferir que a medida de DO é o logaritmo do inverso da transmitância, que é expressa pelas seguintes equações:

$DO = \log I_0/I$; ou $DO = \log 1/$ Transmitância (T)

Atualmente, grande parte das avaliações dos resultados obtido à partir do uso das técnicas histoquímicas e imunohistoquímicas é realizado de forma semi-quantitativa por medida de densidade óptica. Com o uso deste procedimento é possível estimar de forma rápida e precisa as variações de concentração de uma determinada substância existente em uma secção de tecido, medindo a quantidade de luz absorvida por esta secção após o desenvolvimento da reação enzimática. (Fukuda *et al.*, 1978; Gónzalez-Lima e Garrosa, 1991; Chieco *et al.*, 1994; Knyihar-Csilik *et al.*, 1998; Chieco *et al.*, 2001; Ruiz-Torner *et al.*, 2001; Alonso-Magdalena *et al.*, 2003; Strazielle *et al.*, 2003).

Contudo, deve-se ter alguns cuidados básicos na execução das técnicas histoquímicas e imunohistoquímicas, no intuito de que os valores de DO não sejam sub-estimados ou super-estimados.

1-As medidas de DO realizadas em secções obtidas a partir da realização de técnicas histoquímicas e imunohistoquímicas, apresentam uma correlação positiva com o tempo da reação histoquímica e/ou reação do revelador e com a espessura da secção tecidual, e uma correlação negativa com o tempo de fixação e as concentrações dos fixadores e detergentes empregados. A intensidade destas correlações varia de acordo com o tipo de técnica histoquímica ou imunohistoquímica utilizada. Portanto a padronização de variáveis como espessura da secção tecidual utilizada, concentrações dos reagentes empregados e tempos de fixação e incubação podem variar de forma considerável entre as diferentes técnicas histoquímicas e imunohistoquímicas. (Figuras 1, 2 e 3) (Cantu e Nelson, 1994; Gonzales-Lima e Jones, 1994; Hammond *et al.*, 1996; Vaid *et al.*, 1996; Everbroeck *et al.*, 1999; Tangeng *et al.*, 2001).

2-As medidas de DO não podem ser realizadas em secções que apresentem artefatos, rompimentos ou dobraduras, pois estes alteram a espessura da secção e consequentemente alteram as medidas de DO (van Noorden e Butcher, 1991; Chieco *et al.*, 1994; Celis, 1998; Chieco *et al.*, 2001).

3- Algumas vezes, são utilizados diferentes recursos para amplificação e intensificação de reações histoquímicas e imunohistoquímicas fracas, como por exemplo, a intensificação com cloreto de cobalto, sulfato de amônio niquelado e cloreto de magnésio (Adams, 1977, De Olmos e Heimer, 1977). O aumento do número de moléculas produzido pelo uso destes procedimentos pode gerar um obstáculo estérico acentuado, que conduz a perda da estequiometria, fazendo com que ,nestes casos, a medida de DO se torne uma tarefa sem sentido.

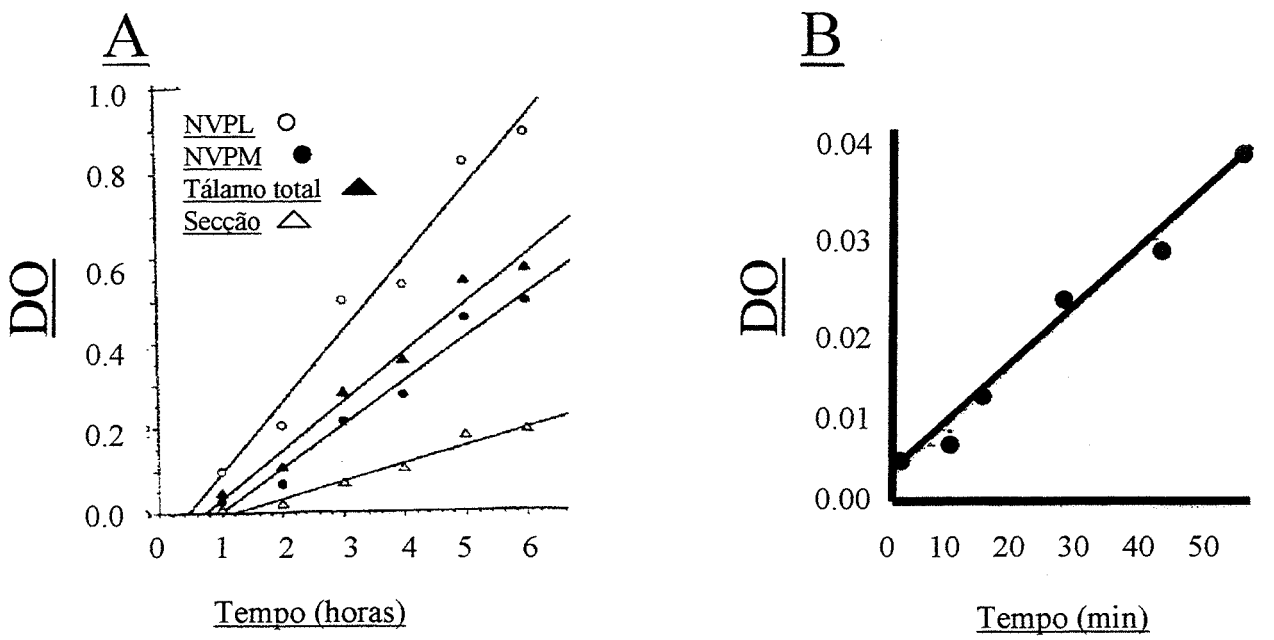

Figura.1. A intensidade da medida de DO é proporcional ao tempo de incubação da reação histoquímica e/ou ao tempo de revelação da técnica imunohistoquímica. A- Observar que as variações de intensidade de coloração, representada pela medida de DO, gerada pela aplicação da técnica histoquímica para revelação da enzima acetilcolinesterase em secções de diferentes estruturas encefálicas de ratos Sprague-Dawley adultos são diretamente proporcionais ao tempo de incubação (NVPL- núcleo ventro póstero lateral talâmico ; NVPM- núcleo ventro póstero medial talâmico). B- Efeito do aumento do tempo de incubação sobre a medida de DO em secções do encéfalo de gerbilos da mongólia (*Meriones unguiculatus*) (40µm) submetidos a técnica histoquímica para detecção da enzima mitocondrial citocromo oxidase (Adaptado de Gonzales-Lima e Jones, 1994 e Hammond, 1996).

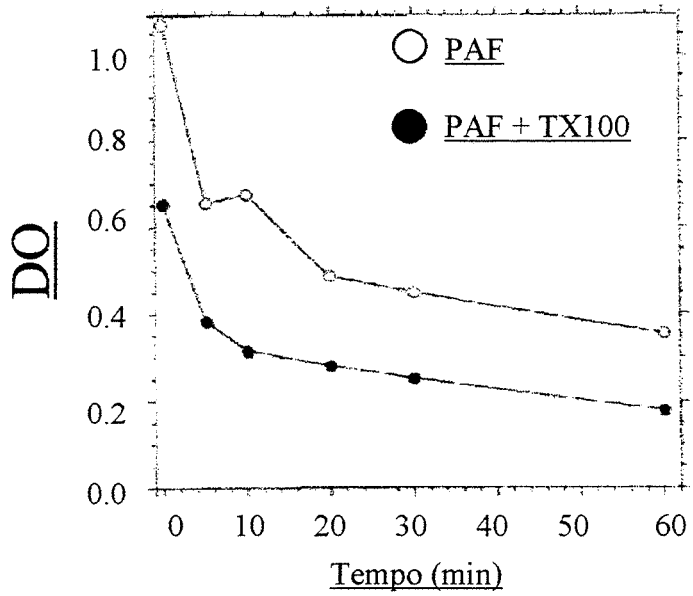

Figura 2. A intensidade da mediada de densidade óptica (DO) é influenciada pelo processo de fixação e tratamentos com detergentes. Neste gráfico podemos observar o efeito dos diferentes tempos de fixação e do uso de detergentes em secções do encéfalo de ratos Spague Dawley (10µm) processadas para detecção histoquímica da enzima acetilcolinesterase. As secções foram montadas em lâminas histológicas e previamente a realização da técnica histoquímica para revelação da enzima acetilcolinesterase foram banhadas com duas soluções distintas, uma de paraformaldeído tamponado (4%) (PAF) , e outra com o mesmo paraformaldeído adicionado do detergente Triton X 100 (0,5%) (PAF + TX100) em diferentes intervalos de tempo (0,10,20,30,40,50 e 60 minutos), Note a queda de reatividade gerada pelo aumento do tempo de fixação e pela utilização do detergente (Adaptado de Hammond, 1996).

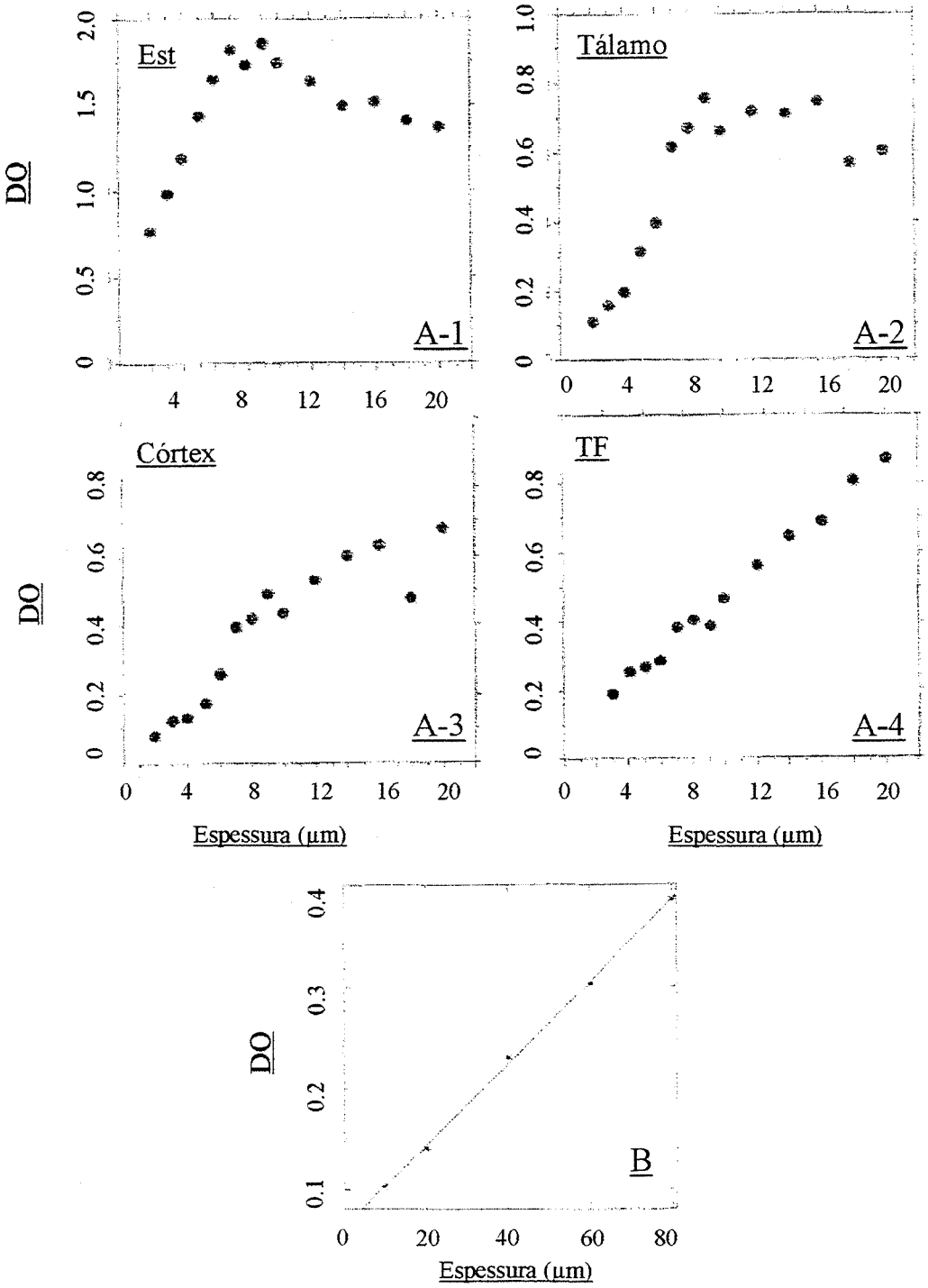

Figura 3. A intensidade da medida de DO é influenciada pela espessura da secção tecidual. Nos gráficos A-1; A-2; A-3 e A-4, podemos observar a intensidade da coloração gerada pela técnica histoquímica para revelação da enzima acetilcolinesterase, representada pela medida de DO, e as alterações encontradas em secções com espessuras distintas em diferentes regiões do encéfalo de ratos Spague-Dawley adultos. Note que neste experimento, utilizando-se um tempo de incubação de 5 horas, obtemos a saturação da medida de DO no tálamo e no estriado (Est) em secções de 8 e 10 µm, enquanto a medida de DO no córtex cerebral não apresenta saturação até a maior espessura testada (20µm), enquento a coloração não específica, tinção de fundo (TF), aumenta indefinidamente, comportando-se como uma função linear da espessura. No gráfico B observamos o efeito das variações de espessura da secção tecidual em secções do encéfalo de gerbilos da mongólia (*Meriones unguiculatus*) submetidos a técnica histoquímica para detecção da enzima mitocondrial citocromo oxidase por uma hora a 37° C, note que a medida de DO apresenta uma correlação positiva ótima com a espessura da secção e que não há saturação da DO até a maior espessura testada (80µm). Portanto a espessura da secção tecidual à ser analisada, deve ser escolhida de acordo com o tipo de técnica histoquímica e imunohistoquímica empregada, a natureza da região encefálica investigada analisada, e os tempo de incubação utilizado. (Adaptado de Gonzales-Lima e Jones, 1994 e Hammond, 1996).

4-Um procedimento utilizado rotineiramente nas técnicas histoquímicas e imunohistoquímicas é a contracoloração com alguma técnica histológica tradicional, objetivando uma localização histológica mais precisa destas reações. Este tipo de procedimento deve ser utilizado apenas se for extremamente necessário, e o corante empregado na contracoloração obrigatoriamente não deve absorver luz no mesmo comprimento de onda absorvido pelo revelador destas técnicas (Fukuda *et al.*, 1978; van Noorden e Butcher, 1991; Celis, 1998; Chieco *et al.*, 2001).

A medida DO, usualmente, se caracteriza pela utilização de imagens digitalizadas das secções teciduais, obtidas ao microscópio óptico que são posteriormente convertidas para tons de cinza, normalmente em uma escala de 8 BPP, ou 8 bits por pixel (*picture element* ou pixel é a menor área dentro da imagem digitalizada, geralmente medindo cerca $0.021cm^2$ da imagem obtida, não da secção analisada, ou menos), ou seja, cada pixel pode apresentar 256 diferentes tons de cinza, variando de 0-255 onde 0 = preto absoluto e 255 = branco absoluto. O emprego de qualquer método de contracoloração altera a intensidade do tom de cinza encontrado no pixel, deste modo, a contracoloração associada à medida de DO não pode ser realizada em imagens que são convertidas para tons de cinza, uma vez que, neste caso, qualquer contracoloração conduz a uma alterações das medidas de DO (Fukuda *et al.*, 1978; van Noorden e Butcher, 1991; Celis, 1998; Chieco *et al.*, 2001).

Portanto, a contracoloração associada a medida de DO pode ser empregada somente nas medidas de DO realizadas em imagens digitalizadas coloridas do tipo RGB (Red, Green, Blue), também referidas como cor verdadeira, sendo que corantes como hematoxilina e eosina não devem ser utilizados, nem mesmo neste caso, pois estes absorvem luz em praticamente todo o espectro de luz visível, gerando alterações significativas da DO (Celis, 1998; Chieco *et al.*, 2001).

5- Um problema relativo à análise densitométrica das técnicas histoquímicas imunohistoquímicas é a comparação freqüentemente realizada entre técnicas realizadas em diferentes ocasiões e portanto com soluções distintas. Embora estas reações mantenham constantes parâmetros como tempos de incubação e concentrações dos reagentes empregados, a simples realização das mesmas em dias distintos, pode modificar de forma significativa os resultados obtidos devido a uma maior ou menor coloração do tecido não reativo (tinção de fundo), o efeito negativo deste procedimento é potenciado nas análises qualitativas, entretanto este pode atingir inclusive as avaliações por densitometria óptica, uma vez que, caso não haja uma subtração prévia da tinção de fundo no processo de medida da DO, esta pode interferir nos resultados obtidos, gerando uma superestimação das medidas de DO (Celis, 1998; Chieco *et al.*, 2001).

Além das precauções relativas a execução das técnicas histoquímica e imunohistoquímicas, devemos ter importantes cuidados no processo de aquisição da imagem digitalizada da secção, para uma correta mensuração da DO, como por exemplo:

1-As lentes do microscópio e da câmera digital devem ser limpas periodicamente, para evitar que pequenas manchas possam aparecer na imagem digitalizada da secção, alterando a medida de DO (Hardie *et al.*, 2002).

2-O procedimento de Köhler deve ser realizados previamente a cada medida de DO para garantir a uniformidade da intensidade de luz que atravessa o material (Celis, 1998; Hardie *et al.*, 2002).

3-O microscópio deve ser sempre colocado sobre uma bancada rígida, no intuito de minimizar as vibrações (Hardie *et al.*, 2002).

4-A fonte de luz do microscópio e da câmera responsável pela obtenção das imagens devem estar conectadas a um aparelho regulador de voltagem, que elimina as flutuações de corrente que podem alterar a qualidade da imagem adquirida (Hardie *et al.*, 2002).

5- Conforme podemos observar na lei de Beer-Lambert a medida de DO é influenciada diretamente por fatores como intensidade de luz e contraste, (que afetam o coeficiente de extinção específico) utilizados no processo de digitalização da imagem. Portanto, a comparação entre grupos experimentais distintos, exige que o processo de obtenção das imagens digitalizadas destas seções seja padronizado, de modo que se mantenham constantes parâmetros como: a intensidade de luz, o brilho, a abertura numérica etc....(Celis, 1998; Chieco *et al.*, 2001; Hardie *et al.*, 2002).

Além destas precauções técnicas, a análise de imagens por DO apresenta alguns problemas peculiares, como por exemplo o fato de que a fórmula utilizada para cálculo da densidade óptica, DO= log 1 / Transmitância (T), embora correta, não contemple variáveis importantes como as variações máximas e mínimas de intensidade de luz captadas pelo sistema de análise de imagens, a correção do *background*, a subtração da tinção de fundo e as relações desta fórmula com as medidas de intensidade de tons de cinza de cada pixel. Ademais a maioria dos artigos científicos que avaliam a atividade histoquímica e/ou imunohistoquímica por densitometria não apresentam e forma clara os algoritmos e macros utilizados para facilitar a medida de densidade óptica nos diferentes *softwares* de análise de imagem (van Noorden e Butcher, 1991; Chieco *et al.* , 1994; Celis, 1998; Chieco *et al.*, 2001; Hardie *et al.*, 2002).

Uma limitação inerente ao uso da análise das técnicas histoquímicas e imunohistoquímicas por densidade óptica, é que os incrementos ou diminuições reais de DO, não produzidos por variações na tinção de fundo, podem ser gerados por fatores distintos, tais como o aumento ou diminuição do número de células; o aumento ou diminuição do número de células reativas; o aumento ou diminuição da área celular reativa; aumento ou diminuição da reatividade intracelular; maior ou menor exposição dos epítopos relacionada às variações nos métodos de fixação; o aumento ou diminuição da expressão gênica ou síntese proteíca. Muitas vezes a natureza destes fatores não pode ser avaliada somente pela medida de densidade óptica, necessitando de outros

experimentos complementares para uma melhor elucidação do problema biológico (van Noorden e Butcher, 1991; Chieco *et al.* , 1994; Celis, 1998; Chieco *et al.*, 2001).

1.6 Avaliação das técnicas histológicas, histoquímicas e imunohistoquímicas por estereologia com aplicação do método de Cavalieri

Um dos grandes desafios inerentes à avaliação de técnicas histológicas em geral, incluindo as histoquímicas e as imunohistoquímicas, é a estimativa precisa de variáveis quantitativas como volume estrutural e o número total dos diferentes tipos celulares presentes nesta estrutura, em diferentes situações experimentais (Cruz-Orive e Weibel, 1990).

Neste sentido, pode-se enumerar uma série de problemas práticos relacionados a estimativa correta destas variáveis, como por exemplo: 1-A determinação do volume estrutural de uma forma geométrica simples, como um cubo por exemplo, pode ser obtida facilmente elevando se o valor da medida de um dos seus lados (L) ao cubo (L^3), contudo, podemos nos perguntar - Qual fórmula matemática, é capaz de estimar com precisão o volume de estruturas encefálicas, que naturalmente não constituem formas geométricas simples, com por exemplo, um hipocampo? 2-Supondo-se que em uma secção tecidual com 40 μm de espessura tivéssemos quatro neurônios nos 20 μm superiores e nenhum nos 20 μm inferiores, e fosse necessário uma estimativa precisa da relação (número de neurônios/volume estrutural), lembrando que a imagem obtida no microscópio óptico é bidimensional, se analisássemos uma imagem obtida dos 20 μm superiores provavelmente obteríamos uma superestimação desta relação, por outro lado, na análise dos 20 μm inferiores provavelmente obteríamos uma subestimação desta mesma relação (Howard e Reed, 1998).

Além dos problemas práticos relativos à análise quantitativa dos resultados obtidos à partir do emprego de técnicas histológicas, histoquímicas e imunohistoquímicas, podemos citar também alguns problemas "filosóficos" sobre o casamento das velhas técnicas histológicas com as modernas ferramentas de análise matemática (Cruz-Orive, 1994):

1- São muito distintos os formatos de um artigo científico publicado na área da matemática e de um artigo publicado na área das ciências biológicas/biomédicas. Artigos científicos publicados na área da matemática, geralmente não apresentam discussão, uma vez que as regras do jogo são bem definidas nos resultados. Portanto, ponderar sobre a consistência dos resultados apresentados, caracteriza-se como um exercício redundante. Por outro lado, os resultados obtidos em experimentos biológicos certamente não são teoremas, e portanto deve haver algum espaço, na discussão, destinado à interpretação dos resultados numéricos obtidos, sendo que, muitas vezes, a discussão também é utilizada para encobrir as diferenças inerentes ao emprego de metodologias imprecisas (Cruz-Orive, 1994).

2- Novos métodos matemáticos quantitativos tendem a ser adotados por pesquisadores das ciências biológicas/biomédicas apenas quando julgados como reproduzíveis em uma grande quantidade de experimentos realizados em diferentes laboratórios (Cruz-Orive, 1994).

3-Os pesquisadores das ciências biológicas/biomédicas normalmente hesitam em modificar seus métodos de análise, devido a uma série de razões, como a impossibilidade de comparar os novos resultados obtidos com os resultados antigos; a problemática inerente à publicação de uma nova metodologia que pode conduzir a resultados distintos aos relatados na literatura corrente (Cruz-Orive, 1994).

Mas o fato é que, a precisão é obtida somente através do argumento estatístico matemático, e este geralmente é pouco compreendido pela grande maioria dos pesquisadores da área biológica (Cruz-Orive, 1994).

No intuito de solucionar estes problemas, no início dos anos 80, alguns neuromorfologistas apropriaram-se de conceitos estatísticos e matemáticos que começaram a ser organizados já nos anos 60, a estereologia (do grego *stereos* = espacial ou tridimensional) para a criação de uma poderosa ferramenta de análise quantitativa no SNC a neuroestereologia (Howard e Reed, 1998).

O termo estereologia foi criado por Elias em 1961, e serve para designar um conjunto de métodos simples, eficientes e precisos, fundamentados nos princípios da geometria e da probabilidade, utilizados para a quantificação das características tridimensionais de um objeto como por exemplo: volume, superfície de área, comprimento, etc...(Haug, 1986; Cruz-Orive e Weibel, 1990; Cruz-Orive, 1997; Howard e Reed, 1998).

As técnicas estereológicas podem ser aplicadas em qualquer imagem digitalizada (microscópio óptico, microscópio confocal, ressonância magnética, tomografia computadorizada etc...), desde que o observador possa identificar nitidamente os limites da estrutura analisada (Howard e Reed, 1998).

Estas características tornaram às técnicas estereológicas ferramentas imprescindíveis para desenvolvimento dos diferentes campos das ciências biológicas, destacando-se entre estes, a morfologia. Neste sentido, o emprego de técnicas estereológicas vem ganhando especial destaque na avaliação quantitativa dos resultados obtidos à partir das técnicas histológicas, histoquímicas e imunohistoquímicas no SNC, constituindo uma das principais ramificações da neuroestereologia (Howard e Reed, 1998).

A estimativa de volume estrutural com a utilização de metodologia estereológica, foi inicialmente desenvolvida por Gundersen e Jensen, em 1987, que utilizaram o teorema descrito em 1635 por Bonaventura Cavalieri, como um arquétipo para a criação de um estimador estereológico, que tem como única necessidade natural uma amostragem sistemática randomica e uniforme (Cavalieri, 1635; Gundersen e Jensen, 1987).

A estimativa volumétrica pelo método de Cavalieri, fundamenta-se na divisão de uma estrutura em secções paralelas de igual distância (T), sendo na neurohistologia algo equivalente a cortes coronais ou sagitais. Após esta divisão, é realizada a medida da área da estrutura inerente a cada secção (A), sendo que o volume desta estrutura (V) pode ser estimado à partir da soma das medidas de área da estrutura inerentes as secções multiplicada pela distância entre as secções, representada pela fórmula: $V=\Sigma A . T$ (Gundersen e Jensen, 1987; Cruz-Orive, 1997) (Figura 4).

Conforme citado anteriormente, um dos princípios do método de Cavalieri é o emprego de uma abordagem sistemática randomica e uniforme. Neste tipo de amostragem o pesquisador deve realizar estimativas piloto, no intuito de definir o tamanho do intervalo entre as amostras, T, de modo que se obtenha um coeficiente de erro reduzido. Após a definição do intervalo entre as amostras, o pesquisador deve definir com o auxílio de uma tabela de números aleatórios a localização da primeira amostra dentro do intervalo T (por exemplo, secciona-se uma determinada estrutura encefálica em 100 partes eqüidistantes, com um intervalo T=10 partes, obtemos em uma tabela de números aleatórios o número 3, deste modo a amostragem será composta das secções 3,13,23,33,43,53,63,73,83,93). Este tipo de amostragem garante o princípio estatístico básico de que cada secção tenha a mesma chance de ser selecionada no processo de amostragem (Gundersen e Jensen, 1987; Thune e Pakkenberg, 2000).

Contudo, a realização da medida de área da estrutura inerente à secção, com o auxílio de *softwares* de análise de imagens, geralmente é uma tarefa demorada e cansativa ao pesquisador, uma vez que depende de um delineamento preciso da área estrutural da imagem obtida a partir da microscopia óptica. No intuito de tornar mais eficiente o processo de estimativa volumétrica, a estimativa da área da estrutura analisada inerente a secção, pode ser realizada pelo método de contagem de pontos (uma metodologia de estimativa de área proposta pelo geólogo russo Glagolev

em 1933) (Haug, 1986; Gundersen e Jensen, 1987; Cruz-Orive, 1997; Howard e Reed, 1998; Gundersen *et al.*, 1999).

A metodologia de contagem de pontos fundamenta-se na sobreposição de uma grade de pontos sobre a imagem digitalizada da secção, obtida ao microscópio óptico, determina-se que cada ponto é representativo de uma área (A/P =área ponto), sendo contados todos os pontos que se sobreponham à área analisada na imagem digitalizada da secção (Haug, 1986; Gundersen e Jensen, 1987; Cruz-Orive, 1997; Howard e Reed, 1998; Gundersen *et al.*, 1999) (Figura 5).

Com objetivo de que não ocorra uma superestimação ou subestimação do volume estrutural realizada pelo método de contagem de pontos, os pontos da grade de pontos devem ser divididos em quatro ângulos, sendo que cada ângulo é representativo de uma área/ponto, portanto, somente um destes ângulos, previamente determinado por uma tabela de número aleatórios, deve ser considerado no processo de contagem de pontos (Cruz-Orive, 1997). A determinação do tamanho da área/ponto e a magnificação das imagens é feita de acordo com a estrutura analisada, considerando-se que, na prática para uma estimativa precisa do volume estrutural, com um coeficiente de erro em torno de 5%, devem se contados entre 100 e 200 pontos, utilizando entre 3 a 15 secções por estrutura, por encéfalo (Gundersen e Jensen, 1987; Cruz-Orive, 1997; Thune e Pakkenberg, 2000). A estimativa final do volume das diferentes regiões, pode ser obtida pela equação:

$$\text{Volume (estimado)} = \text{T. a/p.} \sum_{i=1}^{n} Pi$$

onde: $V_{(est)}$= Estimativa do volume; T= Distância entre as secções analisadas, neste exemplo 120 µm; A/P= Área ponto; ΣP= Soma dos pontos.

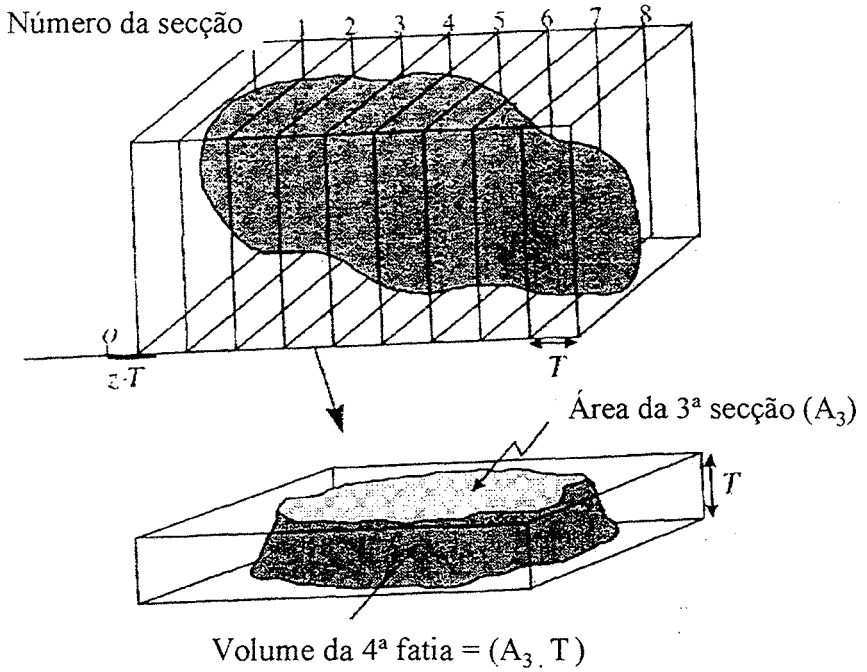

Figura 4. Ilustração do método de Cavalieri, onde um objeto é seccionado em uma série de planos paralelos separados por uma distância (T). A estimativa de volume de cada uma destas fatias seccionadas pode ser obtida multiplicando-se a área da secção (A) pela distância entre elas (T); V_1=A.T, a soma da estimativa de volume de todas as fatias (V_1+V_2+...Vn) constitui uma estimativa precisa do volume total do objeto. Adaptado de Howard e Reed, 1998;

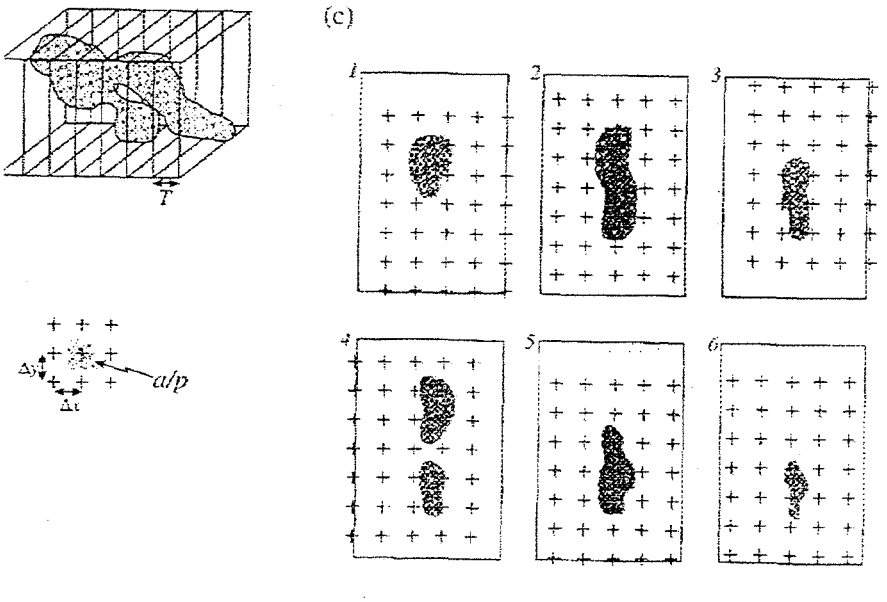

Figura 5. Ilustração do método de contagem de pontos mostrando um objeto seccionado em uma série de seis planos paralelos separados por uma distância (T). Sobre a imagem da área destas secções é sobreposta uma grade pontos equidistantes, sendo que cada ponto é representativo e uma determinada área ponto a/p. A área das secções (A) pode ser estimada pela soma dos pontos que tocam a imagem da secção (P*i*) multiplicada pelo valor da área ponto (a/p): A*n* =*(a/p).Pi* . A estimativa de volume das fatias que compõem o objeto pode ser obtido pala fórmula Vn= (a/p).Pi_n.T; enquanto a estimativa de volume estrutural (V_{est}) é obtida pela soma da estimativa de volume de todas as fatias $V_{(est)}$= (V_1+V_2+...Vn).Adaptado de Howard e Reed, 1998;

A determinação de área estrutural pode ser realizada por ambos: pelo método de contagem de pontos ou por delineamento da área da estrutura com o auxílio de *softwares* de análise de imagens. Embora a técnica de contagem de pontos tenha uma fragilidade metodológica aparente, devemos salientar que existem vários estudos comparativos entre as duas abordagens, e estes não mostram qualquer diferença significativa entre os resultados obtidos. Entretanto, o tempo empregado no delineamento da estrutura é significativamente maior do que o empregado na técnica de contagem de pontos, o que atesta uma maior eficiência, e portanto superioridade, da técnica de contagem de pontos sobre o métodos de delineamento estrutural com o uso de *softwares* de análise de imagens (Mathieu *et al.*, 1981, Regeur e Pakkenberg, 1985, Arteni *et al.*, 2003).

Embora extremamente precisa e confiável, a abordagem estereológica pelo método de Cavalieri também apresenta algumas limitações técnicas como por exemplo:

1-A estimativa de volume estrutural pelo método de Cavalieri necessita de limites precisos entre as estruturas a serem analisadas, condição esta, que não é encontrada em muitas das estruturas do SNC (Howard e Reed, 1998).

2-As medidas volumétricas obtidas à partir de material submetido a tratamento histológico estão sujeitas a importantes alterações, devido aos métodos de desidratação e fixação que podem alterar de forma significativa a espessura das secções (eixo Z), alterando portanto a estimativa do volume tecidual (Gardella *et al*, 2003).

3-O cálculo de coeficiente de erro (CE) empregado para a análise de amostragens estatísticas comuns, não é aplicável ao teorema de Cavalieri, uma vez que a medida de área de uma secção obtida á partir de uma amostragem sistemática randomica e uniforme é influenciada pelas medidas de área das secções adjacentes, o que faz com que o cálculo do CE por técnicas estatísticas convencionais normalmente produza valores errôneos de CE. Ademais, os dois diferentes componentes responsáveis pelo CE gerado pela execução do método de Cavalieri associado à

técnica de contagem de pontos (1-O componente relativo a diferença entre as secções; 2-O componente relativo a técnica de contagem de pontos), não podem ser identificados por métodos estatísticos convencionais. (Cruz-Orive, 1997; Howard e Reed, 1998; Gundersen *et al.*, 1999).

1.7 O cálculo de coeficiente de erro da estimativa de volume pelo método de Cavalieri

A estimativa de volume estrutural pode ser realizada de forma rápida e precisa pelo método de Cavalieri. Entretanto, a predição da precisão desta estimativa de volume não é uma tarefa matemática trivial, uma vez que a área das seções são variáveis dependentes entre si, deste modo a fórmula usual para cálculo de coeficiente de erro, onde se divide o desvio padrão de uma amostra pela raiz quadrada do número total de observações, não pode ser aplicada (Cruz-Orive, 1989).

As primeiras estimativas do CE da aplicação do método de Cavalieri associado ao método de contagem de pontos, foram realizados por Gundersen e Jensen em 1987, a partir de uma adaptação das teorias de Matheron (Matheron 1965; Matheron 1971; Gundersen e Jensen, 1987). Em 1993, Roberts realizou um trabalho de estimativa volumétrica de tumores encefálicos estudados por ressonância magnética, e neste documentou que as fórmulas para cálculo de CE propostas por Gundersen em 1987 produziam predições da variância e de CE adequadas principalmente a objetos que apresentassem um formato regular quase elipsoidal (Roberts *et al.*, 1993). Neste mesmo ano Cruz-Orive desenvolveu uma forma alternativa para cálculo de CE que poderia ser utilizado para avaliação de objetos com formatos distintos (Cruz-Orive, 1993), esta fórmula foi testada, com sucesso, por Roberts e colaboradores em 1994, na estimativa de volume fetal por ressonância magnética (Roberts *et al.*, 1994)

Contudo, a fórmula definitiva para o cálculo de CE gerado a partir da aplicação do método de Cavalieri ainda não foi descoberta, e constitui objeto de estudo de vários centros de pesquisa nas áreas da matemática e da estatística em todo mundo. A crescente utilização do método de Cavalieri como ferramenta de investigação tem renovado ainda mais o interesse no problema da predição correta da variância e do coeficiente de erro dentro de amostras sistemáticas que apresentem variáveis dependentes entre si (Cruz-Orive, 1999). Neste sentido, pode-se destacar os progressos significativos produzidos por pesquisadores como Souchet (1995) e Kiêu (1997) que aprimorando a fórmula desenvolvida por Cruz-Orive (1993) construíram a mais precisa fórmula de cálculo de CE conhecida, utilizada por estereologistas do mundo inteiro (Kiêu *et al.*, 1999).

Deste modo, o cálculo de CE, atualmente utilizado, é fundamentado em uma complexa aproximação da variância de acordo com as propriedades geométricas da estrutura analisada (Kiêu *et al.*, 1999).

Para o cálculo coeficiente de erro, os dados relativos a contagem de pontos por área da estrutura inerente a secção P*i* devem ser agrupados em uma planilha, onde se deve calcular os valores de P_i^2; $P_i . P_{i+1}$; $P_i.P_{i+2}$ e $P_i.P_{i+4}$.

Secção	P_i	P_i^2	$P_i . P_{i+1}$	$P_i.P_{i+2}$	$P_i.P_{i+4}$
1					
2					
3					
...n					
Total					
		$\hat{C}_0$	$\hat{C}_1$	$\hat{C}_2$	$\hat{C}_4$

O cálculo de coeficiente de erro começa com a predição da variância da estimativa da área das secções gerada pelo método de contagem de pontos pela seguinte fórmula (Matheron, 1971; Gundersen e Jensen, 1987; Cruz-Orive, 1989)

$$\sum_{i=1}^{n} \hat{\sigma}_i^2 = 0.0724 . \frac{\overline{B}}{\sqrt{\overline{A}}} . \left(n . \sum_{i=1}^{n} Pi \right)^{1/2}$$

No cálculo da variância da estimativa de área das secções gerada pelo método de contagem de pontos, deve-se sempre levar em conta, o cálculo do coeficiente de forma, ou *shape Z*, que é a média do comprimento dos limites das áreas analisadas dividido pela raiz quadrada da média das áreas da secção (por exemplo, um cubo com L=2, seccionado paralelamente a um dos seus eixos principais apresenta: média do comprimento dos limites das áreas analisadas = 8; média das áreas da secção = 4, portanto apresenta um coeficiente de forma no valor de 4) (Matheron, 1971; Gundersen e Jensen, 1987; Cruz-Orive, 1989).

$$\text{Shape Z} = \frac{\overline{B}}{\sqrt{\overline{A}}}$$

Onde:

$\overline{B}$=média do comprimento dos limites das áreas analisadas

$\sqrt{\overline{A}}$=raiz quadrada da média da área da secção

Embora o cálculo do coeficiente de forma, constitua um modo pouco natural, para a estimativa desta variância, uma vez que adapta o cálculo do CE a geometria das diferentes estruturas analisadas, este é o único modo confiável de realizar o cálculo de CE nas distintas regiões encefálicas avaliadas pelo método de Cavalieri (García-Fiñana *et al.*, 2003).

Após o cálculo da variância da estimativa da área das secções gerada pelo método de contagem de pontos pode-se estimar, pela fórmula de Kiêu-Souchet, uma constante que exprime a suavidade da variação entre as medidas de área realizadas no intervalo T (Kiêu *et al.*, 1999) .

$$\hat{q} = (\log 4)^{-1} \cdot \log \left[\frac{3.(\hat{C}_0 - \sum_{i=1}^{n} \hat{\sigma}_i^2) + \hat{C}_4 - 4\hat{C}_2}{3.(\hat{C}_0 - \sum_{i=1}^{n} \hat{\sigma}_i^2) + \hat{C}_2 - 4\hat{C}_1} \right] - \frac{1}{2}$$

Após a obtenção desta constante, calcula-se o coeficiente alfa para estimativa da variância e do coeficiente de erro (García-Fiñana *et al.*, 2003).

$$\alpha(\hat{q}) = \frac{\Gamma(2\hat{q}+2).\zeta(2\hat{q}+2).\cos(\hat{q}\pi)}{(2\pi)^{2\hat{q}+2}.(1-2^{2\hat{q}-1})}$$

Nesta fórmula encontra-se as funções Γ e ζ, gamma e zeta respectivamente, estas funções podem ser obtidas facilmente com o auxílio de tabelas matemáticas ou em *softwares* de processamento matemático. Entretanto se não for possível a obtenção destas, os seguintes polinômios podem prover uma ótima aproximação do valor real do coeficiente alfa e dos resultados encontrado à partir do cálculo deste coeficiente (Cruz-Orive, 1993; Gundersen *et al.*, 1999; García-Fiñana *et al.*, 2003).

Se, o valor da variância da estimativa da área das secções gerada pelo método de contagem de pontos ficar entre 0 e 0.25 utiliza-se o seguinte polinômio (Cruz-Orive, 1993; Gundersen *et al.*, 1999; García-Fiñana *et al.*, 2003).

$$\alpha(\hat{q}) \approx 0.0833 - 0.2153\hat{q} + 0.2820\hat{q}^2 - 0.2890\hat{q}^3$$

Se, for entre 0.25 e 0.75 utiliza-se o seguinte polinômio (Cruz-Orive, 1993; Gundersen *et al.*, 1999; García-Fiñana *et al.*, 2003).

$$\alpha(\hat{q}) \approx 0.0220 + 0.0627(0.5-\hat{q}) + 0.0764(0.5-\hat{q})^2 + 0.0590(0.5-\hat{q})^3$$

Se, for maior que 0.75 utiliza-se o seguinte polinômio (Cruz-Orive, 1993; Gundersen *et al.*, 1999; García-Fiñana *et al.*, 2003).

$$\alpha(\hat{q}) \approx 0.004167 + 0.01693(1-\hat{q}) + 0.02468(1-\hat{q})^2 + 0.01895(1-\hat{q})^3$$

A partir do cálculo do coeficiente alfa podemos estimar a variância da estimativa de volume estrutural pelo método de Cavalieri pela seguinte fórmula (Cruz-Orive, 1993; Gundersen *et al.*, 1999; Garcia-Fiñana *et al.*, 2003):

$$Var(\hat{V}) = \alpha(\hat{q})\, T^2 \left\{ 3\left[\hat{C}_0 - \sum_{i=1}^{n} \hat{\sigma}_i^2\right] + \hat{C}_2 - 4\hat{C}_1 \right\} + T^2 \sum_{i=1}^{n} \sigma_i^2$$

Note que o cálculo da variância total é obtido a partir da soma de dois componentes, um gerado pela variância entre as secções e outro gerado pelo método de contagem de pontos (Cruz-Orive, 1993; Gundersen *et al.*, 1999; García-Fiñana *et al.* , 2003):

$$Var(\hat{V})_{(\text{secções})} = \alpha(\hat{q})\, T^2 \left\{ 3\left[\hat{C}_0 - \sum_{i=1}^{n} \hat{\sigma}_i^2\right] + \hat{C}_2 - 4\hat{C}_1 \right\} \qquad Var(\hat{V})_{(\text{contagem de pontos})} = T^2 \sum_{i=1}^{n} \sigma_i^2$$

A variância gerada pelas secções, usualmente é muito maior do que a variância gerada pelo método de contagem de pontos (Gundersen, 1988). Portanto, para uma estimativa mais precisa do volume estrutural, com um valor de CE reduzido, é recomendável o aumento do número de amostragens por estrutura, no intuito de reduzir o intervalo (T), ao invés de uma diminuição da área ponto, com um conseqüente aumento do número de pontos contados por secção, ou uso de delineamento de área por analisador de imagens, manobras estas que reduziriam apenas o CE relativo a contagem de pontos (Gundersen, 1998).

Para obtenção dos coeficientes de erro (CE) relativos a secção e relativos à técnica de contagem de pontos devemos dividir ambos os lados da equação de cálculo da variância pela seguinte fórmula (Cruz-Orive, 1993; Gundersen *et al.*, 1999; García-Fiñana *et al.*, 2003):

$$T^2 \cdot \left(\sum_{i=1}^{n} Pi \right)^2$$

Deste modo obtemos os dois componentes do CE, um relativo a secção e outro relativo a técnica de contagem de pontos (Cruz-Orive, 1993; Gundersen *et al.*, 1999; García-Fiñana *et al.*, 2003).

$$CE(\text{secção}) = \frac{\alpha(\hat{q})\, T^2 \cdot \left\{ 3 \left[\hat{C}_0 - \sum_{i=1}^{n} \hat{\sigma}_i^2 \right] + \hat{C}_2 - 4\hat{C}_1 \right\}}{T^2 \cdot \left(\sum_{i=1}^{n} Pi \right)^2}$$

$$CE(\text{contagem de pontos.}) = \frac{T^2 \sum_{i=1}^{n} \sigma_i^2}{T^2 \cdot \left(\sum_{i=1}^{n} Pi \right)^2}$$

O coeficiente de erro total, expresso sob forma percentual é obtido a partir da seguinte fórmula (Cruz-Orive, 1993; Gundersen *et al.*, 1999; García-Fiñana *et al.*, 2003).

CE(total)=[CE(secção) + CE(contagem de pontos)] . 100

2-Objetivos

A análise semi-quantitativa por medida de densitometria óptica e a análise estereológica são ferramentas que se complementam para uma interpretação adequada de distintos resultados histofisiológicos. Assim, a análise semi-quantitativa por medida de densitometria óptica caratteriza-se perfeitamente para uma avaliação rápida, objetiva e precisa da intensidade de coloração gerada com a utilização de técnicas histoquímicas ou imunohistoquímicas. Enquanto que a avaliação estereológica constitui uma ferramenta quase que indispensável para a avaliação de diferentes parâmetros quantitativos como o volume estrutural. Portanto, a análise correta dos resultados obtidos com o emprego das técnicas histológicas, histoquímicas e imunohistoquímicas deve tentar contemplar, sempre que possível, a associação entre as técnicas semi-quantitivas densitométricas as técnicas quantitativas estereológicas, objetivando a obtenção de resultados cada vez mais fidedignos neste tipo de investigação científica (Conn, 1977; Howard e Reed, 1998; Chieco *et al.*, *2001*).

O objetivo principal principal deste trabalho foi contribuir para o estabelecimento, aprimoramento e desenvolvimento destas técnicas de análise de imagens no Laboratório de Histofisiologia Comparada da UFRGS, visando a criação de um Laboratório de Análise de Imagens no DCM-ICBS-UFRGS, onde possam ser realizados procedimentos precisos e de fácil execução para análise de diferentes técnicas histológicas, histoquímicas e imunohistoquímicas, atendendo as necessidades locais e regionais, neste sentido, este trabalho apresentou os seguintes objetivos específicos:

1-Padronizar e implementar os procedimentos de avaliação da atividade histoquímica e da reação imunohistoquímica por meio de densitometria óptica, executando este de forma semi-automática em um dos *software* de análise de imagens mais utilizados um todo mundo, o Image Pro

Plus 4.1 (IPP 4.1) (Media Cybernetics, MA, USA). Para tanto, serão criadas macros com a linguagem Auto Pro, um subconjunto da linguagem BASIC, de acordo com a sintaxe Visual Basic.

2-Padronizar e implementar de forma rotineira a técnica de estimativa de volume estrutural baseada no teorema de Cavalieri, executando esta de forma semi-automática no *software* de análise de imagens IPP 4.1

3-Padronizar e implementar de forma rotineira os procedimentos para o cálculo de coeficiente de erro inerente a aplicação do teorema de Cavalieri, executando estes de forma semi-automática em planilhas do *software* Microsoft Excel.

4-Após a padronização e implementação destes procedimentos, utilizar estes para a análise dos resultados obtidos com o uso de técnicas histológicas, histoquímicas e imunohistoquímicas distintas, testando a aplicabilidade destes em diferentes modelos experimentais, diferentes técnicas histológicas, histoquímicas e imunohistoquímicas em diferentes regiões encefálicas, analisando as peculiaridades e as dificuldades inerentes a cada uma desta investigações.

Os resultados obtidos na implementação e padronização das técnicas de análise de imagens, assim como, os diferentes experimentos realizados com a utilização destas, serão apresentados na seção de resultados sob forma de artigos cientificos publicados ou submetidos e anexos, listados a seguir:

4.1-Análise semi-quantitativa da atividade imunoreatividade da proteína glial fibrilar ácida (GFAP) na amígdala medial de ratos machos e fêmeas em diestro -Artigo publicado- "Glial fibrillary acidic protein immunodetection and immunoreactivity in the anterior and posterior medial amygdala of male and female rats"; Brain Research Bulletin, 58: 67-75 (2002).

4.2-Análise semi-quantitativa da imunoreatividade para substância P na medula lombosacral de rãs (*Rana catesbeiana*) após a secção de nervo ciático- Artigo publicado- "Sciatic nerve

transection decrease substance P immunoreactivity in the lumbosacral spinal cord of frog *Rana Catesbeiana*"; Comparative Biochemistry and Physiology; 131:807-814 (2002).

4.3-Análise semi-quantitativa da imunoreatividade para substância P na medula lombar de tartarugas *Trachemys dorbigni* após a secção de nervo ciático- Artigo publicado- "Substance P immunoreactivity in the lumbar spinal cord of the turtle *Trachemys dorbigni* following peripheral nerve injury"; Brazilian Journal of Medical and Biological Research, 36: 515-520 (2003).

4.4-Análise semi-quantitativa da imunoreatividade para tirosina hidroxilase na porção compacta da substância nigra e na área ventral tegmental, do encéfalo de ratas tratadas com o agente neurotóxico 6-hidroxidopamina (6OHDA), verificando os possíveis efeitos neuroprotetores da reposição hormonal com estradiol -Artigo publicado- "Failure of estrogen to protect the substantia nigra pars compacta of female rats from lesion induced by 6-hydroxydopamine"; Brain Research, 986: 200-205 (2003).

4.5- Estimativa estereológica, pelo método de Cavalieri, do volume da camada piramidal de CA1 e do giro denteado; correlacionando esta, com as variações da atividade da enzima mitocondrial citocromo oxidase, analisada por medida de densitometria óptica, no hipocampo de ratos controle e submetidos a isquemia letal, a isquemia subletal e ao precondicionamento isquêmico.- Artigo Submetido- "Preconditioning changes cytochrome oxidase activity and hippocampal volume after global cerebral ischemia". Neuroscience Research.

4.6-Protocolo para execução de medida de densidade óptica em imagens digitalizadas obtidas a partir de técnicas histoquímicas e imunohistoquímicas no *software* IPP 4.1, apresentando todos os algoritmos e macros empregadas -Artigo submetido- "A simple and fast densitometric method to analyze tyrosine hydroxilase immunoreactivity in the substantia nigra pars compacta and in the ventral tegmental area"; Brain Research Protocols.

4.7- Protocolo para execução do cálculo de coeficiente de erro gerado á partir da aplicação do teorema de Cavalieri, em planilhas do *software* Micrososft Excel –Anexo.

Brain Research Bulletin, Vol. 58, No. 1, pp. 67–75, 2002

0361-9230/02/$–see front matter

PII: S0361-9230(02)00758-X

Glial fibrillary acidic protein immunodetection and immunoreactivity in the anterior and posterior medial amygdala of male and female rats

Alberto A. Rasia-Filho,* Léder L. Xavier, Paula dos Santos, Günther Gehlen and Matilde Achaval

Laboratório de Histofisiologia Comparada, Departamento de Ciências Morfológicas, Universidade Federal do Rio Grande do Sul, Porto Alegre, RS, Brazil

[Received 21 August 2001; Revised 2 January 2002; Accepted 7 January 2002]

ABSTRACT: The medial amygdala (MeA) has receptors for gonadal hormones and modulates reproductive behaviors in rats. Adult male and female rats were used for the immunodetection, a less accurate technique, and the immunohistochemistry for the astrocytic marker glial fibrillary acidic protein (GFAP) in the anterior and posterior MeA. Both procedures were done using polyclonal anti-GFAP and were quantified by densitometry. The first technique provided no evidence for a difference between sexes in the immunocontent of GFAP in any region of the MeA ($p > 0.1$). Nevertheless, the measure of the intensity of GFAP immunoreactivity (GFAP-IR) showed that females had a higher GFAP-IR in the posterodorsal ($p < 0.01$) and in the posteroventral subregions of the MeA ($p < 0.01$) than males. No sex difference was found in its anterodorsal part ($p > 0.1$). The present results point out the differences between these two above-mentioned techniques but add a new finding to the previously described sexual dimorphism in the MeA, i.e., the GFAP-IR. Data also suggest that probably astrocytes can be affected by sex steroids in this brain area. It is likely that this regionally specific difference in the GFAP-IR may contribute to the distinct functional roles that the MeA subregions have in male and female rats.

KEY WORDS: Amygdaloid complex, GFAP, Sexual differentiation, Glia, Gonadal hormones.

INTRODUCTION

Gonadal hormones modify the morphology and the electrophysiological properties of neurons in the central nervous system (CNS) of several species [38,44,50,51,53,65]. Through plastic changes that occur throughout the animal life, these sex steroids lead to modifications in neuronal morphology and neurochemistry, modulate neuroendocrine function and affect the occurrence of reproductive and non-reproductive behaviors ([23,34,39,44,67,68,82], and see [14]). Moreover, gonadal hormones contribute to the development of sexual dimorphisms that became evident in the structure and function of specific CNS areas [26,30,47,54,62,79]. For example, the synaptic organization of the hypothalamic arcuate nucleus of rats, which is involved with the preovulatory surge of gonadotrophin releasing hormone (GnRH), is markedly influenced by the neonatal and adult sex steroid environments and shows a clear functional differentiation between males and females [10,19].

Amygdala is the name given to an anatomically and functionally heterogeneous group of nuclei that are located near the ventral surface of the temporal lobe of rats ([2,63], but see [1,64,78]). Among them is the medial nucleus of the amygdala (MeA), a superficial nucleus part of the conceptual "extended amygdala" ([2,52], but see [7]), which has many intranuclear, intra-amygdaloid, interamygdaloid and extra-amygdaloid connections [63]. It basically receives inputs from the prefrontal cortex, bed nucleus of stria terminalis, and hypothalamus [63]. On the other hand, the MeA sends efferents to the olfactory bulb and vomeronasal organ, hippocampus, ventral striatum and pallidum, bed nucleus of the stria terminalis, several hypothalamic nuclei (such as the medial preoptic area, the ventromedial nucleus, and the ventral premammillary nucleus, for example) thalamus, periaqueductal gray, ventral tegmental area and midbrain raphe [7,8,63]. Besides, it is noteworthy that receptors for testosterone and estrogen receptors α and β are remarkably found in the MeA [56,72,74], the area of this nucleus appears to be larger in males than in female rats [30,47], and it modulates the sexual behavior in both sexes [25,43,45,52,66,82]. Therefore, based on the presence of neural cells that are influenced by gonadal hormones in the MeA and the connections made by this nucleus, it is likely that the MeA participate in a sex steroid-responsive and sexually dimorphic circuit that integrates chemosensory information and hormonal signals for the occurrence of behaviors in males and females [4,6,18,26,42,52,82]. In addition, it appears that the MeA becomes integrated with information about the animal's internal and external milieu by virtue of its reciprocal connections with the hypothalamus and via parallel intra-amygdaloid pathways [52,63].

It has been described that glial cells are relevant for CNS functions such as migration and maturation of neurons, myelin ensheathing, regulation of ionic concentrations, metabolism of chemical transmitters, synaptic integration, energy supply to neurons, and response to brain injury [5,31,35,41]. Notwithstanding, glial cells could also be considered as participant in the process of sexual differentiation of the CNS [10,17,19]. Neuronal-glial interactions can affect the synaptic patterning in the developing

* Address for correspondence: Alberto A. Rasia-Filho, Ph.D., Fundação Faculdade Federal de Ciências Médicas, Depto. Ciências Fisiológicas, R. Sarmento Leite, 245, Porto Alegre, RS 90050-170, Brazil. Fax: +55-51-33163092; E-mail: aarf@ufrgs.br

brain as well in the adult CNS [19,20,48]. Recent *in vivo* and *in vitro* experimental findings have shown that immunoreactivity, enzymatic activity, and gene expression of astrocytes are modified by sex steroids [10,40,46,77]. Astrocytes may respond to gonadal hormones via their interaction with neurons that possess receptors for these steroids [13]. Glial cells have receptors for progesterone, androgen and estrogen [13,33] and participate in the metabolism of sex steroids [9].

The morphology of astrocytes and the amount or the distribution of the astrocytic marker glial fibrillary acidic protein (GFAP), which is the major intermediate filament protein of differentiated astrocytes, are sexually dimorphic and can be altered by the level of the gonadal hormones [22,40]. However, the effects of the gonadal hormones on GFAP seem to be dependent on the brain area in which these steroids act [29]. For example, cyclic hormonal variation of estrogen and progesterone in females are able to down- and up-regulate the GFAP synthesis in the hypothalamus, in the hippocampus, and in the interpeduncular nucleus [19,20,29,40]. In the arcuate nucleus, estradiol induces an increase in GFAP levels during the proestrous [19,21]. On the other hand, castration of adult male rats enhanced GFAP mRNA in the hippocampus [13].

The aim of the present study was to investigate a possible sexual dimorphism in the GFAP immunoreactivity (GFAP-IR) in the anterior and posterior subregions of the MeA of male and female rats. The MeA was divided in subregions [2,7] because there are a greater number of androgen receptors present in the posterior part of the MeA of males [72], and estradiol receptors α and β have a heterogeneous expression pattern throughout the MeA of females [56]. In addition, there are sex differences in the dendritic spine density and synaptic connections in the neurons that compose the anterior and posterior aspects of this nucleus [54,65] and they appear to form functionally different circuits of cells [52]. Supposedly, these differences might all alter GFAP-IR in the different subregions of the MeA. Our initial approach used a rather less accurate technique, that is, the dot immunodection for GFAP. Because this procedure may result in an overestimation of the protein content in a specific brain area [80], our next step was to determine the intensity of the reactivity for the GFAP present in the subregions of the MeA using an immunohistochemical technique and a semi-quantitative analysis by densitometry. This latter procedure is a more refined method and was assumed as the main indicator of the GFAP-IR in the MeA of rats. To our knowledge, this is the first report of a sexual dimorphism in the GFAP-IR at a subdivisional level of the rat MeA.

MATERIALS AND METHODS

Animals

Adult male and female Wistar rats 3–6 months old were used ($n = 11$ for males and females in the dot immunodetection study and $n = 5$ for males and females in the GFAP immunohistochemistry study). Animals were bred locally and housed in groups with free access to food and water, temperature around 22°C, and a 12 h light–dark cycle.

Vaginal smears were taken from nulliparous females to determine the different stages of the estrous cycle. Subjects were invariably studied on the morning of the diestrus. This arbitrary criterion was primarily chosen to avoid unpredictable variations in the results due to different levels of sex steroids in circulation. In addition, it was our intention to employ a naturally occurring event and not techniques of endocrine ablation and hormone replacement.

Immunodetection and Immunohistochemical Procedures

For the dot immunodetection, rats were sacrificed by decapitation and the brain dissected. Coronal brain slices (0.4 mm) were cut with a McIlwain chopper and microslices 0.7 mm in diameter were prepared with a punch. The location of the subregions of the MeA was based on previous descriptions [2,7,58]. According to the atlas of Paxinos and Watson [58], samples were taken from the anterodorsal MeA (MeAD) and anteroventral MeA (MeAV), corresponding to the anterior MeA for this initial study (plates 26–29, from 1.80 to 2.30 mm posterior to the bregma, Fig. 1), and from the posteroventral MeA (MePV) and posterodorsal MeA (MePD), corresponding to the posterior MeA in the first part of this study (plates 32–33, from 3.14 to 3.30 posterior to the bregma; Figs. 1 and 2). In order to have enough material for the immunodetection procedure, pools of the anterior part of the MeA (MeAD + MeAV) and pools of the posterior part of the MeA (MePD + MePV) were prepared for each rat from each sex and both sides of the brain were used. The location of the microslices was further confirmed by staining the sampled brain slice with cresyl violet (data not shown).

Three microslices from the anterior and posterior MeA were added to 100 μl of 0.5% sodium dodecyl sulfate (SDS). Solubility of the tissue was completed by homogenization with a microsyringe and further 100 μl of SDS was added. A dose-response curve was obtained (data not shown) and a dilution of 1:7 was chosen. Samples of 40 μl were applied as dots onto a nitrocellulose membrane. The dots were developed by the luminol method using a polyclonal antibody to GFAP (Sigma Chemical Co., USA) [24,69]. The intensity of the dots was quantified by densitometry of the X-ray films, as described previously [69]. To be certain that males and females could be compared directly, a sample from a male was always paired with a sample from a female on the same membrane.

For the GFAP immunohistochemistry, males and females were deeply anesthetized using sodium thiopental (50 mg/kg, i.p.) and were perfused through the left cardiac ventricle with 200 ml of saline solution followed by 200 ml of 4% paraformaldehyde in 0.1 M phosphate buffer pH 7.4. The brains were removed and left for post-fixation in the same fixative solution at 4°C for 2 h. After this, the material was cryoprotected by diving the brain in 30% sucrose in phosphate buffer at 4°C. The brains were embedded in Optimal Cutting Temperature (Sakura Finetek, USA) compound and sectioned (50 μm) on a cryostat (Leitz). The sections were collected in phosphate buffer saline solution (PBS) and processed for GFAP immunohistochemistry following the unlabeled antibody peroxidase–antiperoxidase (PAP) procedure [75]. Free-floating sections were treated in 10% methanol and 3% H_2O_2 for 30 min and washed carefully. Then, the sections were preincubated in 3% normal goat serum (NGS) in PBS containing 0.3% Triton X-100 (PBS-Tx, Sigma Chemical Co.) for 30 min and incubated with polyclonal GFAP antiserum raised in rabbit (Sigma Chemical Co.) diluted 1:150 in 3% NGS in PBS-Tx for 48 h at 4°C. After washing several times with PBS-Tx, tissue sections were incubated in a rabbit anti-rabbit IgG diluted 1:50 in PBS-Tx at room temperature for 2 h. Sections were washed again in PBS and incubated in a rabbit PAP (Sigma Chemical Co.) diluted 1:500 in PBS for 2 h at room temperature. The immunohistochemical reaction was revealed by incubating the sections in a histochemical medium that contained 0.06% 3,3′-diaminobenzidine (DAB, Sigma Chemical Co.) dissolved in PBS for 10 min and then, in the same solution containing 1 μM of 3% H_2O_2 per ml of DAB medium for approximately 10 min. Afterwards, the sections were rinsed in PBS, dehydrated in ethanol, cleared with xylene and covered with Entellan and coverslips. Control sections were prepared omitting the primary antibody by replacing it with PBS [70]. The brains of males and females were fixated and post-fixated for the same time in identical solutions and rigorously processed in pairs, incubated in an identical medium, and during the same time. This caution was taken to reduce the possibility of an overreaction, differences in the chromogen reaction or changes in the background levels.

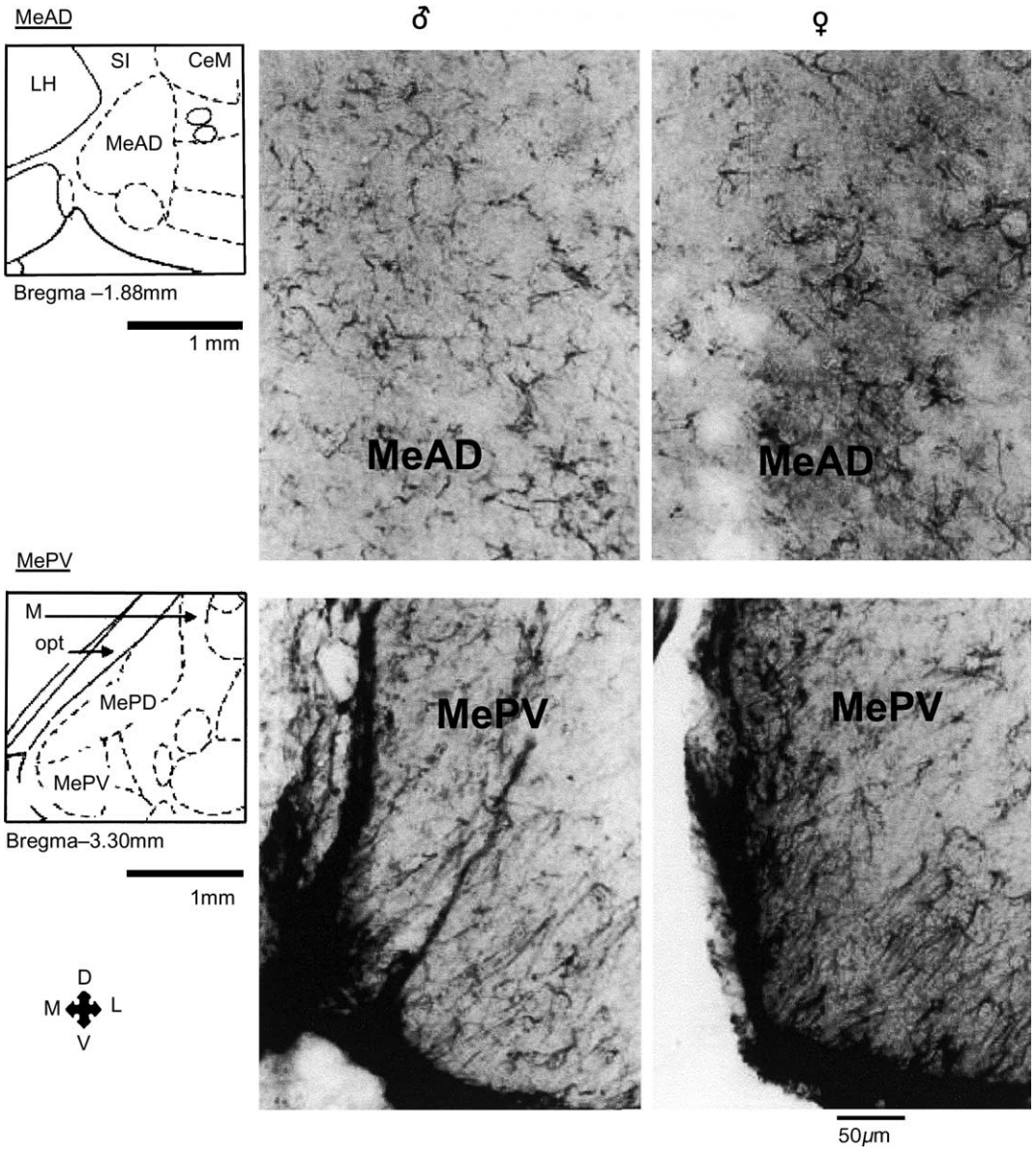

FIG. 1. Anatomical regions analyzed for GFAP-IR in the medial amygdala of rats. Schematic drawings of coronal slices of the rat brain showing the location of the anterodorsal medial amygdala (MeAD, upper part of the figure) and posteroventral medial amygdala (MePV) are shown relative to their distance in mm posterior to the bregma. Photomicrographs are representative for each subregion of the MeA of males and females from which material for the optical density determination of the GFAP-IR was obtained. Scale bars correspond to 1 mm for schematic drawings and to 50 μm for the photomicrographs.

Data Acquisition

For this immunohistochemical study, we selected the MeAD, the MePD, and MePV subregions of the MeA because they are the largest ones in the MeA. The images of GFAP-IR from these three MeA subregions were also compared to the brain slices from the atlas of Paxinos and Watson [58], as described above.

The protocol used for measuring the optical density of GFAP imunohistochemistry was modified from Petito et al. [59]. The intensity of reaction product of GFAP-IR was measured by a semi-quantitative analysis using a Nikon Eclipse E-600 (400×) microscope coupled to a Pro-Series High Performance CCD camera and Image Pro Plus Software 4.1 (Media Cybernetics, USA). Data were obtained and the selected areas were converted in an 8-bit gray scale (0–255 gray levels). A square with 84,000 μm^2 (our area of interest, AOI) was overlaid and the regional optical density was measured. The obvious blood vessels and other artifacts were avoided. Both left and right sides of each brain were used and 20 readings per subregion of the MeA were obtained from each sex (i.e., four sections per subregion obtained from five males and five females). Background staining from a non-reactive place in the slide was determined and used to correct the measures of the optical density. All lighting conditions and magnifications were held constant. Moreover, the investigator was unaware of the experimental groups from which the slices were obtained during the analysis.

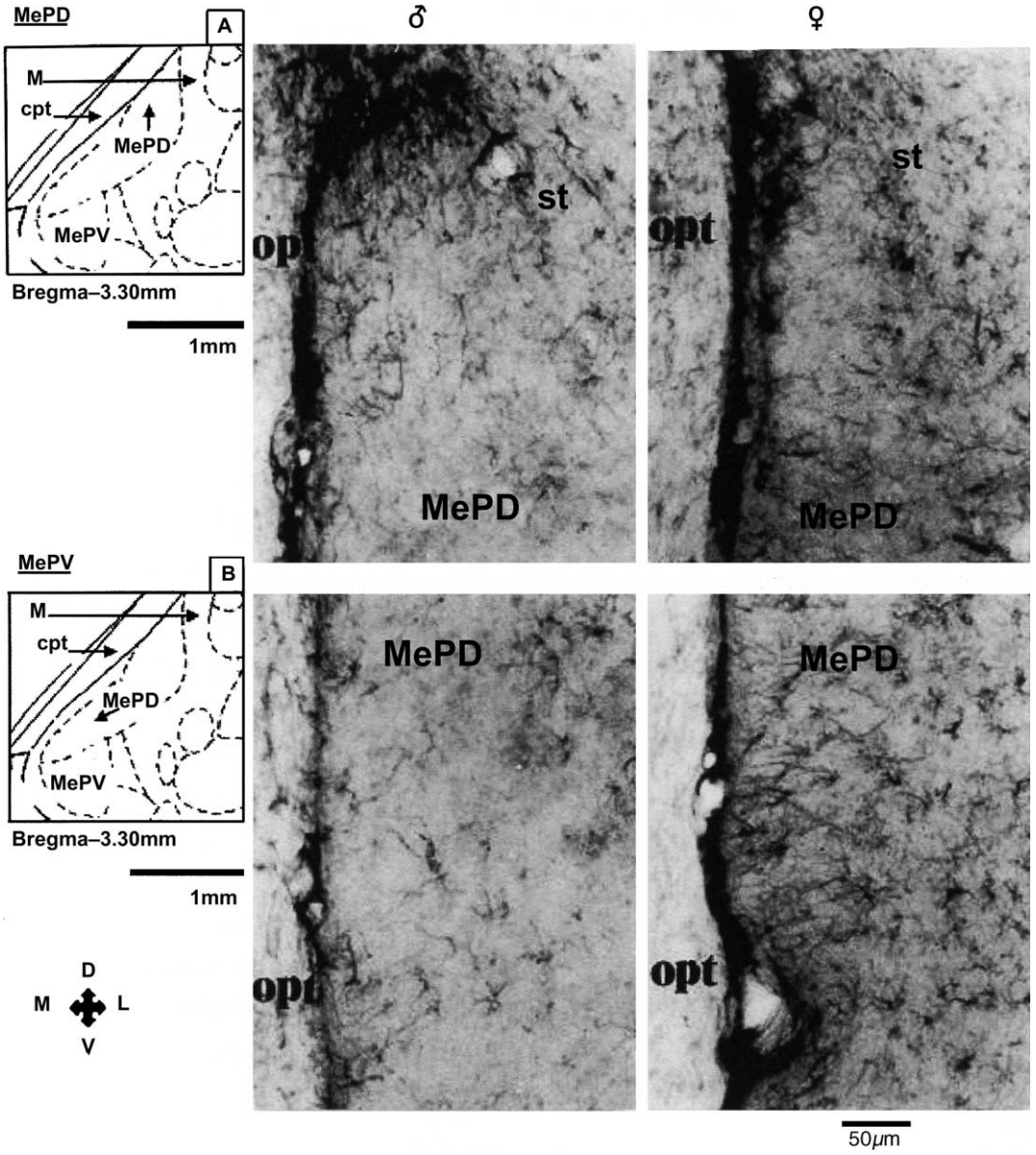

FIG. 2. Anatomical regions analyzed for GFAP-IR in the medial amygdala of rats. Schematic drawings of coronal slices of the rat brain showing the location of the posterodorsal medial amygdala (MePD) relative to its distance in mm posterior to the bregma, in its more dorsal aspect (A) close to the optic tract (opt) and the stria terminalis (st), and in its intermediate aspect (B), lateral to the optic tract, where material for the optical density determination of the GFAP-IR was obtained. Photomicrographs are representative for each aspect of the MePD of males and females. Scale bars correspond to 1 mm for schematic drawings and to 50 μm for the photomicrographs.

The formula for measurement of optical density (OD) used was the following:

$$OD_{(x,y)} = 100 - \left\{ \frac{(BACKGROUND_{(x,y)} - BLACK) - (INTENSITY_{(x,y)} - BLACK)/(INCIDENT - BLACK)}{255} \right\} \times 100$$

where $BACKGROUND_{(x,y)}$ is the intensity of background at $pixel_{(x,y)}$, $INTENSITY_{(x,y)}$ is the intensity at $pixel_{(x,y)}$, BLACK is the intensity generated when no light goes through the material, and INCIDENT is the intensity of the incident light. The results obtained represent the mean of all pixels in the selected area in a 100% scale. In the present study, the thickness of the brain sections used did not lead to immunohistochemical overreactions or saturation of optical density.

The size of the AOI was determined to avoid obtaining data from outside the MeA (from the optic tract or other adjacent amygdaloid

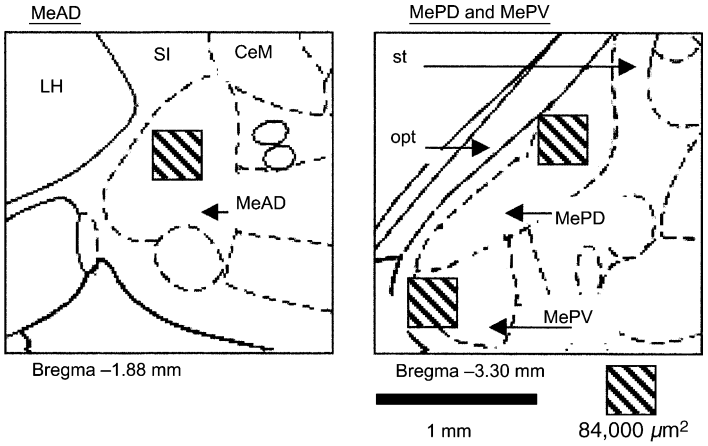

FIG. 3. Schematic drawings of coronal slices showing the localization and relative size of the square (84,000 μm^2) used to determine the optical density of GFAP immunoreactivity in each MeA subregion of males and females. The location of each subregion (MeAD, MePD, and MePV) was the same as described in Figs. 1 and 2.

nuclei, for example) but also to gather a significant number of pixels from the different subregions of the MeA. And, at this point, it is important to describe that the GFAP-IR data used for further comparisons among MeA subregions and between males and females were not selective for one specific layer of GFAP-IR cells, as will be described below. That is, the square with 84,000 μm^2 used to determine the optical density of GFAP-IR in each MeA subregion allowed us to have quantitative results restricted to one MeA subregion but not exclusively from one specific layer of GFAP-IR cells within it (Fig. 3). For example, data obtained in the MePD correspond to all layers of GFAP-IR cells that could be found in its intermediate region, as depicted in Fig. 3.

Statistical Analysis

For the dot immunodetection data, males and females were submitted to the Wilcoxon paired-sample test to compare the results of the densitometry for the GFAP dots in the anterior MeA (MeAV + MeAD) and in the posterior MeA (MePD + MePV) between sexes.

For the GFAP immunohistochemistry, data regarding GFAP-IR from the MeAD, the MePD, and MePV of males and females were compared using a two-way analysis of variance (ANOVA) for repeated measures. A Student–Newman–Keuls *post-hoc* test was employed to detect specific differences of the GFAP-IR for each subregion of the MeA within each sex and between sexes. In both cases, the level of significance was set as $p < 0.05$.

RESULTS

The results of the dot immunodetection will be presented first. The densitometric values for females were normalized to 100% and the values for males are expressed as a percentage compared to this reference value [69,81]. When males were compared to females, no statistical difference was found in the immunocontent of GFAP in the anterior MeA ($p > 0.5$) or in the posterior MeA ($p > 0.2$; Fig. 4).

Immunohistochemical reaction for GFAP was detectable in the three studied subregions of the MeA, that is, the MeAD, the MePD, and MePV (Figs. 1, 2 and 6). In both sexes, few GFAP-IR glial cells were found in the MeAD (Fig. 1). That is, few cell bodies were reliably identified in the MeAD and those that were observed had rod or, more often, stellate shapes. On the other hand, some GFAP-IR processes were present within this nucleus (Fig. 1). As a general view, the MeAD appeared to have less GFAP-IR expression than the adjacent amygdaloid areas (data not shown). And, in females, the posterior subregions of the MeA (MePD and MePV) appeared to have more GFAP-IR than the MeAD (Figs. 1, 2 and 6).

In the posterior MeA of males and females, some general aspects were noteworthy. First, the GFAP-IR in the MePD and in the MePV appeared to be higher in females than in males. Second, the organization pattern of the GFAP-IR cells observed in the most dorsal part of the MePD subregion, close to the stria terminalis, was rather different than the general aspect of the GFAP-IR cells located in the intermediate part of the MePD, in the way to its ventral position. In the most dorsal part of the MePD, many astrocytes with an intense immunoreaction were detected. These cells had variable soma sizes with stellate or rod shapes and some processes (Figs. 2 and 5). In the MePD region intermediate between the MePV and the dorsal portion near the stria terminalis, GFAP-IR astrocytes appeared to form three cellular layers. One medial layer with intense GFAP-IR extended close to the lateral border of the optic tract; a second layer appeared to have less GFAP-IR than the medial one; and, the third and more lateral layer had well-identified astrocytes with large stellate cell bodies (Figs. 2 and 5). And, third, in the MePV another pattern of GFAP-IR cells appeared to occur. From the medial border that accompany the optic tract and going to the ventral surface of this subnucleus there appeared to be a first layer of abundant radially oriented GFAP-IR processes where astrocytes cell bodies were not easily distinguished. In the close vicinity, there appeared to be a second intermediate layer with not so many astrocytes cell bodies but, again, with abundant GFAP-IR processes that follow the ventral shape of the MePV, and a third inner part that looked like as a "core" of this subregion in which there were more cell bodies with stellate or rod shapes (Figs. 1 and 5).

Statistical analysis of the data regarding the immunohistochemical study of the different subregions of the MeA in males and females showed that there was an interaction between sex and subregion of the MeA for the measures of the optical density of GFAP-IR cells [$F(2, 29) = 7.46$, $p < 0.01$]. The *post-hoc*

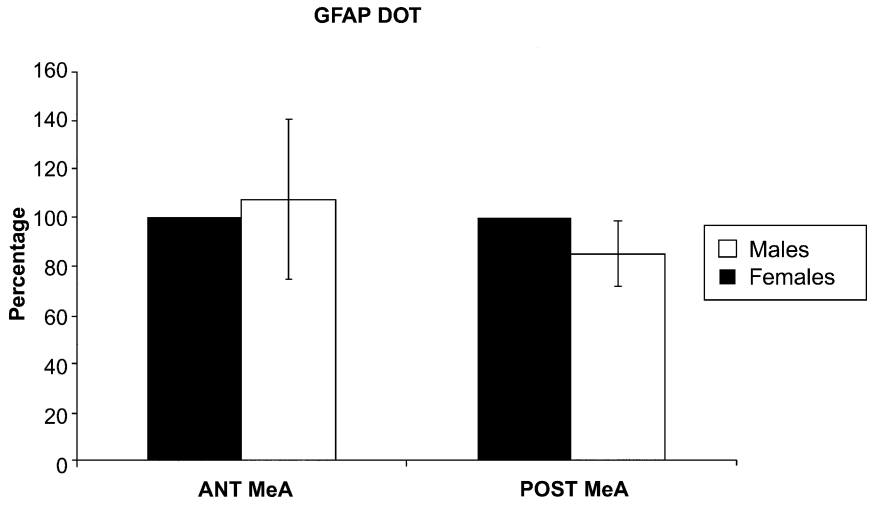

FIG. 4. Immunodetection of GFAP obtained from the anterior medial amygdala (ANT MeA) and posterior MeA (POST MeA) of male (M) and female (F) rats ($n = 11$ in each group). Values are group medians and interquartile intervals of peak heights of duplicate dots determined by densitometry and expressed as a percentage, comparing the results of the females with the males, after the data from females being normalized to 100%. No statistical significance was found.

comparison of the GFAP-IR data obtained from the different subregions of the MeA per sex showed that, in males, there was no difference in the results obtained in the MeAD, in the MePD or in the MePV ($p > 0.05$). The same was not true for females. That is, the values of the optical densities for the GFAP-IR in the MePD and in the MePV were higher than the one obtained for the MeAD ($p < 0.01$ in both cases). Moreover, the GFAP-IR in the MePD is even greater than in the MePV of females ($p = 0.03$). These data are presented in Fig. 6.

Finally, when the data of males and females were compared for each subregion of the MeA, there was no statistical difference in the optical density of GFAP-IR in the MeAD of males and females ($p = 0.22$), but females had a higher GFAP-IR in the MePD ($p < 0.01$) and in the MePV ($p < 0.01$) than males (Fig. 6).

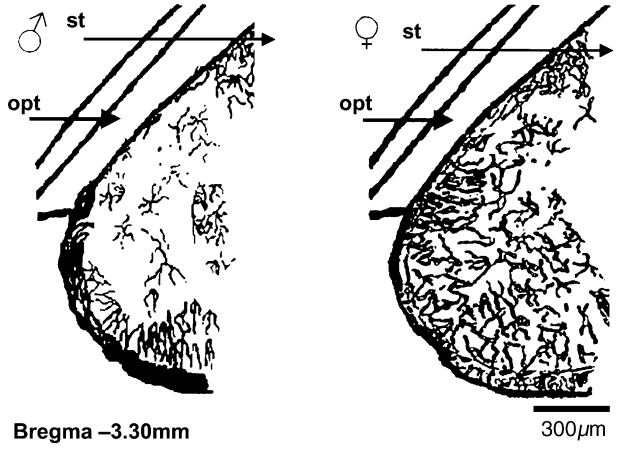

FIG. 5. Camera lucida drawings of GFAP-immunoreactive cells in the MePD and MePV of male and female rats. The locations of each subregion of the MeA are identical to those described in Figs. 1 and 2. The optic tract (opt) and the stria terminalis (st) are indicated. Scale bar corresponds to 300 μm.

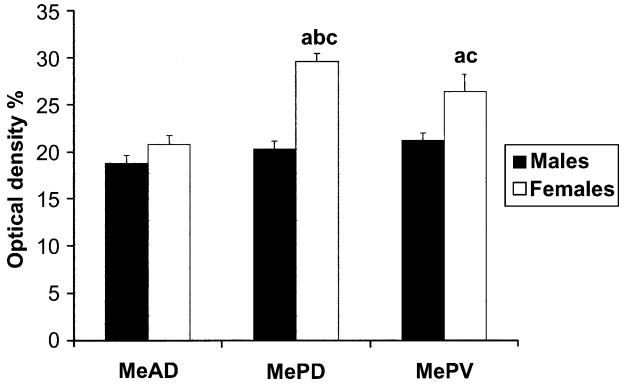

FIG. 6. Percentage of the maximum possible GFAP-IR optical density (mean ± SEM) obtained by immunohistochemical procedure from the anterodorsal (MeAD), the posteroventral (MePV), and the posterodorsal (MePD) subregions of the medial amygdala of male and female rats ($n = 5$ in each group). In males, no statistical difference was found when the GFAP-IR data from the three subregions were compared together. In females, the GFAP-IR in the MePD and in the MePV are greater than in the MeAD ('a' corresponds to $p < 0.01$ in both cases) and the GFAP-IR in the MePD is even greater than in the MePV ('b' corresponds to $p < 0.05$). When the data of males and females were compared together, females had a higher GFAP-IR in the MePD and in the MePV than males ('c' corresponds to $p < 0.01$).

DISCUSSION

The present data point out the differences in the results obtained using two different techniques, the immunodetection using dot–blot and the immunohistochemistry for GFAP-IR. The latter was assumed to be more accurate than the former and, more than this, it is the same immunohistochemical procedure that was used by other authors to demonstrate sexual dimorphisms and the effects of gonadal hormone manipulations on the GFAP-IR in several regions of the rat brain [10,19,29,40]. Based on this, our results add

a new finding to the previously described sexual dimorphism in the MeA (i.e., the GFAP-IR found in the subregions that compose this nucleus) and suggest that probably astrocytes may also be affected by sex steroids in this brain area. Moreover, analysis of GFAP-IR in the MeA showed that sexual dimorphism is regionally specific and occurs mainly in the MePD and MePV.

Different methods may present distinct results when evaluating the GFAP content and immunoreactivity in the MeA. In fact, the immunodot appears to be more susceptible to misleading results because the solution used for tissue fixation, the storage conditions, the number of freeze–thaw cycles, the degree of protein phosphorylation or number of epitopes, and the presence of high calcium content may alter antibody recognition on dot blots [27,28,80]. Based on these possible pitfalls, we decided to consider the results of the GFAP immunohistochemisty as a more realistic indicator of the modulation of the GFAP immunoreaction by gonadal hormones in the different regions of the MeA of male and female rats. In the near future, experiments using *in situ* hybridization and stereological methodologies could be considered for further comparisons with the present findings. Sex differences in GFAP-IR may be due to an increased content of this protein per cell or a higher branching pattern of the glial cell [22]. In this sense, it was demonstrated that estradiol enhanced the number of process-bearing intense GFAP-IR cells in hypothalamic cultures [22] whereas glia cell size or number in the rat hippocampus were not affected by gonadal hormones [13].

In fact, a clear statement about the number of astrocytes within each subregion of the MeA would be very helpful to determine what are the main effects of sex steroids in these brain areas. However, this could not be reliably done here because, when the GFAP immunohistochemistry is used, astrocytes do not have an identifiable nucleolus and it is very hard to identify with precision the borders of the cell nucleus of all astrocytes present in a specific brain area. In addition, a precise estimation of the total number of cells per volume of tissue requires a reliable determination of the borders of the brain area in study. This could be done for the hippocampus [36,61] but, in contrast, the ultimate borders of the different subnuclei of the MeA are still somewhat unsettled (compare the MeAD area in [57,58]). These pitfalls hindered the use of the optical disector and/or precise measurements of the length of each astrocytic process per individual cell. Another method that could be used for quantification of immunohistochemical studies is the evaluation of the surface density of GFAP-IR profiles. Unfortunately, it also could not be done because for this purpose we have to employ vertical sections and it was proved to be very difficult to establish the real borders of each MeA subregion when sections with different angles are used (data not shown). Therefore, we decided not calculate the surface density of astrocytes per MeA subregion and the total number of astrocytes in each MeA region in the present study in order to avoid misleading results [3,12,32].

Although the functional significance of our data deserves further research, they can be viewed in the context of the already described activities of the MeA and the modulatory actions of the gonadal hormones upon it. An interesting relationship between the development of neurons and glial cells exists in the CNS [16,17,76]. The morphology of astrocytes described above may well accompany neuronal morphology, synaptic patterning, and cellular packaging within the MeAD, MePD, and MePV [2,5,30,38,42,47,54,65]. In this sense, although they are interconnected, these three subregions of the MeA appear to have different afferent and efferent connections [7]. Thus, it is likely that the regionally specific differences in the GFAP-IR, within each sex and between both sexes, are related with the distinct aspects of cellular organization and functional roles that the MeA subregions have in male and female rats [2,15,30,54,55,64].

It has been already reported that males have a greater area of the MeA [30,47], and that estrogen modifies dendritic morphology [38] and androgen secretion influences the postnatal development, sexual dimorphism and structural maintenance of the MeA [11,23,42,47,53]. It is possible that the MeA neuropil, where astrocytes can be found, is the main target for the morphological effects of gonadal hormones [65]. Moreover, as astroglia play a role in the synaptic connections of neurons [20] and more dendritic spines are found in the anterior MeA of males [65], it is noteworthy that no sex difference in the GFAP-IR in the MeAD was observed. And this point raises the question of why, supposedly having fewer number of synapses in the MeAD, females have the same quantity of GFAP-IR in this area. Unfortunately, detailed ultrastructural data are still not available to answer all of these questions. And the number of unanswered questions raised in the present study, as occurred for other brain areas [49], emphasizes the need for further knowledge about steroid effects on glial cells in the MeA.

Nevertheless, it is possible that the sex difference in the GFAP-IR described here may be related with the pattern of synaptic contacts, and the functional consequences of them, made on the different subregions of the MeA. Some possible physiological roles for the MeA subregions were recently described in detail elsewhere [1,6–8,26,52,66,71,82]. In males, the MeAD may be involved with the display of a general behavioral arousal and the MePD, more influenced by gonadal hormones, may respond to pheromones and modulate behavioral responses, such as male sexual activity [52]. In females, it is well established that the hypothalamic ventromedial and the arcuate nuclei are influenced by the physiological variations in the circulating levels of ovarian hormones and are relevant sites for the modulation of reproductive behavior of female rats [19,20,51]. The MeAD and the MePV (at least in males) massively innervate different parts of the hypothalamic ventromedial nucleus but only sparse to moderate inputs from the MeA subregions reach the arcuate nucleus [7]. Although the MePD projects only sparsely to the ventromedial nucleus, it appears to be involved with neuroendocrine functions activated by vaginocervical stimulation [60] and projects to the anteroventral periventricular nucleus of the preoptic region to influence gonadotropin secretion [73].

Lesions of the anterior part of the corticomedial amygdala decrease sexual receptivity of female rats, whereas the stimulation of this region has opposite effect [43]. Recently, it was demonstrated that maternal and defensive behaviors involve the MePD in female rats [37,71]. For example, the presence of pups in the same cage promotes avoidance responses in nulliparous females. On the other hand, pups were able to induce maternal behaviors in multiparous ones. In both cases the MePD showed Fos immunoreactivity that, due to its difference, suggest that this subregion is involved with the inhibition of maternal behavior and stimulation of defensive behavior [71]. Pup-induced Fos immunoreactivity in the anterior MeA and in the MePV was equivalent in maternal and nonmaternal subjects [71]. Probably, gonadal hormones can change the activity of the MePD, which in association with interconnected olfactory and hypothalamic areas and in the context of the previous maternal experience, modulates the occurrence of appropriate female behaviors according to environmental circunstances [26,63,71]. Based on these anatomical and functional connections, it remains to be established if GFAP-IR in the MePD can also be affected by the fluctuations of gonadal hormones during the estrous cycle or following parturition. In addition, our present data, which showed that the MePD has the higher GFAP-IR in females, open the possibility to suppose that glial cells in this subregion participate in the modulation of female typical behaviors.

In conclusion, the present findings showed that a sex difference in the GFAP-IR can be found in the posterior, but not the anterior,

subregions of the MeA. Compared to males, females have a higher GFAP-IR in the MePD and MePV. These data seem to be relevant for further understanding of the emotional processing of information and the modulation of defensive and reproductive behaviors with which the subregions of the MeA are involved [8,26,52,71]. However, it is likely that glial cells may be another element involved with the sexual dimorphism in the rat MeA. Further studies may reveal the sex steroid-dependence of GFAP-containing cells and, in order to compare with other CNS areas [19,21,29,40,49], elucidate the functional consequences of this regionally specific sex difference in the MeA.

ACKNOWLEDGEMENTS

Authors thank Dr. R. Rodnight (UFRGS, Porto Alegre, RS, Brazil) for his critical opinion during the preparation of this study and, also, to Dr. E. Rocha (UFRGS) for her suggestions. We are also indebted to Dr. S. Jacques (UFRGS) and Dr. D. Rassier (UNISINOS, São Leopoldo, RS, Brazil) for their help in the statistical analysis. This work was supported by the Brazilian funding agencies FAPERGS, CNPq, PRONEX and FINEP.

REFERENCES

1. Aggleton, J. P.; Saunders, R. C.; The amygdala—What's happened in the last decade? In: Aggleton, J. P., ed. The amygdala: A functional analysis. Oxford: Oxford University Press; 2000:1–30.
2. Alheid, G. F.; de Olmos, J. S.; Beltramino, C. A. Amygdala and extended amygdala. In: Paxinos, G., ed. The rat nervous system. San Diego: Academic Press; 1995:495–578.
3. Baddeley, A. J.; Gundersen, H. J. C.; Cruz-Orive, L. M. Estimation of surface area from vertical sections. J. Microsc. 142:259–276; 1986.
4. Bakker, J.; Baum, M. J.; Slob, A. K. Neonatal inhibition of brain estrogen synthesis alters adult neural Fos responses to mating and pheromonal stimulation in the male rat. Neuroscience 74:251–260; 1996.
5. Bezzi, P.; Volterra, A. A neuron-glia signalling network in the active brain. Curr. Opin. Neurobiol. 11:387–394; 2001.
6. Bressler, S. C.; Baum, M. J. Sex comparison of neuronal Fos immunoreactivity in the rat vomeronasal projection circuit after chemosensory stimulation. Neuroscience 71:1063–1072; 1996.
7. Canteras, N. S.; Simerly, R. B.; Swanson, L. W. Organization of projections from the medial nucleus of the amygdala: A PHAL study in the rat. J. Comp. Neurol. 360:213–245; 1995.
8. Canteras, N. S.; Chiavengatto, S.; Ribeiro do Valle, L. E.; Swanson, L. W. Severe reduction of rat defensive behavior to a predator by discrete hypothalamic chemical lesions. Brain Res. Bull. 44:297–305; 1997.
9. Celotti, F.; Melcangi, R. C.; Negri-Cesi, P.; Paletti, A. Testosterone metabolism in brain cells and membranes. J. Steroid Biochem. Mol. Biol. 40:673–678; 1991.
10. Chowen, J. A.; Busiguina, S.; Garcia-Segura, L. M. Sexual dimorphism and sex steroid modulation of glial fibrillary acidic protein messenger RNA and immunoreactivity levels in the rat hypothalamus. Neuroscience 69:519–532; 1995.
11. Cooke, B. M.; Tabibnia, G.; Breedlove, S. M. A brain sexual dimorphism controlled by adult circulating androgens. Proc. Natl. Acad. Sci. U.S.A. 96:7358–7540; 1999.
12. Cruz-Orive, L. M. Stereology of single objects. J. Microsc. 186:93–107; 1997.
13. Day, J. R.; Laping, N. J.; Lampert-Etchells, M.; Brown, S. A.; O'Callaghan, J. P.; McNeill, T. H.; Finch, C. E. Gonadal steroids regulate the expression of glial fibrillary acidic protein in the adult male rat hippocampus. Neuroscience 55:435–443; 1993.
14. Devauld, L. L.; Morrow, A. L.; Nguyen, U. T. Q. Ovariectomy has minimal effects on neuroadaptations associated with ethanol dependence in female rats. Neurochem. Int. 37:433–442; 2000.
15. Drekic, D.; Malobabic, S.; Gledic, D.; Cvetovic, D. Different neuronal and glial cell groups in corticomedial amygdala react differently to neonatally administered estrogen. Neuroscience 66:475–481; 1995.
16. Fernandez-Galaz, M. C.; Morschl, E.; Chowen, J. A.; Torres-Aleman, I.; Naftolin, F.; Garcia-Segura, L. M. Role of astroglia and insulin-like growth factor-I in gonadal hormone-dependent synaptic plasticity. Brain Res. Bull. 44:525–531; 1997.
17. Fernandez-Galaz, M. C.; Parducz, A.; Naftolin, F.; Torres-Aleman, I.; Garcia-Segura, L. M. Interaction of gonadal steroids and growth factors in brain sex differentiation. Biomed. Rev. 7:67–74; 1997.
18. Fiber, J. M.; Swann, J. M. Testosterone differentially influences sex-specific pheromone-stimulated Fos expression in limbic regions of Syrian hamsters. Horm. Behav. 30:455–473; 1996.
19. Garcia-Segura, L. M.; Cardona-Gomez, G. P.; Trejo, J. L.; Fernandez-Galaz, M. C.; Chowen, J. A. Glial cells are involved in organization and activational effects of sex hormones in the brain. In: Matsumoto, A., ed. Sexual differentiation of the brain. New York: CRC Press; 1999:83–93.
20. Garcia-Segura, L. M.; Chowen, J. A.; Dueñas, M.; Parducz, A.; Naftolin, F. Gonadal steroids and astroglial plasticity. Cell. Mol. Neurobiol. 16:225–237; 1996.
21. Garcia-Segura, L. M.; Luquin, S.; Parducz, A.; Naftolin, F. Gonadal hormone regulation of glial fibrillary acidic protein immunoreactivity and glial ultrastructure in the rat neuroendocrine hypothalamus. Glia 10:59–69; 1994.
22. Garcia-Segura, L. M.; Torres-Aleman, I.; Naftolin, F. Astrocytic shape and glial fibrillary acidic protein immunoreactivity are modified by estradiol in primary rat hypothalamic cultures. Dev. Brain Res. 47:298–302; 1989.
23. Gomez, D. M.; Newman, S. W. Medial nucleus of the amygdala in the adult Syrian hamster: A quantitative Golgi analysis of gonadal hormonal regulation of neuronal morphology. Anat. Rec. 231:498–509; 1991.
24. Gonçalves, C.A.; Gottfried, C.; Kommers, T.; Rodnight, R. Calcium-modulated proteins change their immunoreactivity in the presence of Ca^{2+}: A sudy of antibody recognition in a dot immunoassay for calmodulin, calcineurin (β-subunit), and S100B. Anal. Biochem. 253:127–130; 1997.
25. Gréco, B.; Edwards, D. A.; Michael, R. P.; Clancy, A. N. Androgen receptor immunoreactivity and mating-induced Fos expression in forebrain and midbrain structures in the male rat. Neuroscience 75:161–171; 1996.
26. Guillamón, A.; Segovia, S. Sex differences in the vomeronasal system. Brain Res. Bull. 44:377–382; 1997.
27. Guttenberger, M. Protein determination. In: Celis, J. E., ed. Cell biology. San Diego: Academic Press; 1998:295–303.
28. Guttenberger, M.; Neuhoff, V.; Hampp, R. A dot–blot assay for quantification of nanogram amounts of protein in the presence of carrier ampholytes and other possibly interfering substances. Anal. Biochem. 196:99–103; 1991.
29. Hajós, F.; Halasy, K.; Gerics, B.; Szalay, F.; Michaloudi, E.; Papadopoulos, G. C. Ovarian cycle-related changes of glial fibrillary acidic protein (GFAP) immunoreactivity in the rat interpeduncular nucleus. Brain Res. 862:43–48; 2000.
30. Hines, M.; Allen, L. S.; Gorski, R. A. Sex differences in subregions of the medial nucleus of the amygdala and the bed nucleus of the stria terminalis of the rat. Brain Res. 579:321–326; 1992.
31. Hof, P. R.; Trapp, B. D.; de Vellis, J.; Claudio, L.; Colman, D. R. The cellular components of nervous tissue. In: Zigmond, M. J.; Bloom, F. E.; Landis, S. C.; Roberts, J. L.; Squire, L. R., eds. Fundamental neuroscience. San Diego: Academic Press; 1999:41–70.
32. Howard, C. V.; Reed, M. G. Unbiased stereology. New York: Springer; 1998.
33. Jung-Testas, I.; Renoir, M.; Bugnard, H.; Greene, G. L.; Baulieu, E.-E. Demonstration of steroid hormone receptors and steroid action in primary cultures of rat glial cells. J. Steroid Biochem. Mol. Biol. 41:621–631; 1992.
34. Kanit, L.; Taskiran, D.; Yilmaz, Ö.A.; Balkan, B.; Demirgören, S.; Furedy, J. J.; Pögün, S. Sexually dimorphic cognitive style in rats emerges after puberty. Brain Res. Bull. 52:243–248; 2000.
35. Kettenmann, H.; Ransom, B. R. Neuroglia. New York: Oxford University Press; 1995.
36. Long, J. M.; Kalehua, A. N.; Muth, N. J.; Hengemihle, J. M.; Jucker, M.; Calhoum, M. E.; Ingram, D. K.; Mouton, P. R. Stereological estimation of total microglia number in mouse hippocampus. J. Neurosci. Methods 84:101–108; 1998.

37. Lonstein, J. S.; Greco, B.; De Vries, G. J.; Stern, J. M.; Blaustein, J. D. Maternal behavior stimulates c-fos activity withn estrogen receptor alpha-containing neurons in lactating rats. Neuroendocrinology 72:91–101; 2000.
38. Lorenzo, A.; Diaz, H.; Carrer, H.; Caceres, A. Amygdala neurons *in vitro*: Neurite growth and effects of estradiol. J. Neurosci. Res. 33:418–435; 1992.
39. Lucion, A. B.; Charchat, H.; Pereira, G. A. M.; Rasia-Filho, A. A. Influence of early postnatal gonadal hormones on anxiety in adult male rats. Physiol. Behav. 60:1419–1423; 1996.
40. Luquin, S.; Naftolin, F.; Garcia-Segura, L. M. Natural fluctuation and gonadal hormone regulation of astrocytic immunoreactivity in dentate gyrus. J. Neurobiol. 24:913–924; 1993.
41. Magistretti, P. J. Brain energy metabolism. In: Zigmond, M. J.; Bloom, F. E.; Landis, S. C.; Roberts, J. L.; Squire, L. R., eds. Fundamental neuroscience. San Diego: Academic Press; 1999:389–413.
42. Malsbury, C. W.; McKay, K. Neurotrophic effects of testosterone on the medial nucleus of the amygdala in adult male rats. J. Neuroendocrinol. 6:57–69; 1994.
43. Mascó, D.H.; Carrer, H. F. Sexual receptivity in female rats after lesions or stimulation in different amygdaloid nuclei. Physiol. Behav. 24:1073–1080; 1990.
44. McEwen, B. S.; Coirini, H.; Westlind-Danielsson, A.; Frankfurt, M.; Gould, E.; Schumacher, M.; Woolley, C. Steroid hormones as mediators of neural plasticity. J. Steroid Biochem. Mol. Biol. 39:223–232; 1991.
45. Meisel, R. L.; Sachs, B. D. The physiology of male sexual behavior. In: Knobil, E.; Neil, J. D., eds. The physiology of reproduction. New York: Raven Press; 1994:3–105.
46. Melcangi, R. C.; Riva, M. A.; Fumagalli, F.; Magnaghi, V.; Racagni, G.; Martini, L. Effect of progesterone, testosterone and their 5α-reduced metabolites on *GFAP* gene expression in type 1 astrocytes. Brain Res. 711:10–15; 1996.
47. Mizukami, S.; Nishizuka, M.; Arai, Y. Sexual difference in nuclear volume and its ontogeny in the rat amygdala. Exp. Neurol. 79:569–575; 1983.
48. Mong, J. A.; Glaser, E.; McCarthy, M. M. Gonadal steroids promote glial differentiation and alter neuronal morphology in the developing hypothalamus in a regionally specific manner. J. Neurosci. 19:1464–1472; 1999.
49. Mong, J. A.; Kurzweil, R. L.; Davis, A. M.; Rocca, M. S.; McCarthy, M. M. Evidence for sexual differentiation of glia in rat brain. Horm. Behav. 30:553–562; 1996.
50. Nabekura, J.; Oomura, Y.; Minami, T.; Mizuno, Y.; Fukuda, A. Mechanism of the rapid effect of 17β-estradiol on medial amygdala neurons. Science 233:226–228; 1986.
51. Nelson, R. J. Female reproductive behavior. In: Nelson, R. J., ed. An introduction to behavioral endocrinology. Sunderland: Sinauer Associates; 1995:231–288.
52. Newman, S. W. The medial extended amygdala in male reproductive behavior. Ann. N.Y. Acad. Sci. 877:242–257; 1999.
53. Nishizuka, M.; Arai, Y. Sexual dimorphism in synaptic organization in the amygdala and its dependence on neonatal hormone environment. Brain Res. 212:31–38; 1981.
54. Nishizuka, M.; Arai, Y. Male–female differences in the intra-amygdaloid input to the medial amygdala. Exp. Brain Res. 52:328–332; 1983.
55. Nishizuka, M.; Arai, Y. Regional difference in sexually dimorphic synaptic organization of the medial amygdala. Exp. Brain Res. 49:462–465; 1983.
56. Österlund, M.; Kuiper, G. G.; Gustafsson, J.-A.; Hurd, Y. L. Differential distribution and regulation of estrogen receptor-alpha and -beta mRNA within the female rat brain. Mol. Brain Res. 54:175–180; 1998.
57. Paxinos, G.; Watson, C. The rat brain in stereotaxic coordinates, 2nd ed. San Diego: Academic Press; 1986.
58. Paxinos, G.; Watson, C. The rat brain in stereotaxic coordinates, 4th ed. San Diego: Academic Press; 1998.
59. Petito, C. K.; Morgello, S.; Felix, J. C.; Lesser, M. L. The two patterns of reactive astrocytosis in postischemic rat brain. J. Cer. Blood Flow Metab. 10:850–859; 1990.
60. Pfaus, J. G.; Marcangione, C.; Smith, W. J.; Manitt, C.; Abillamaa, H. Differential induction of Fos in the female rat brain following different amounts of vaginocervical stimulation: Modulation by steroid hormones. Brain Res. 741:314–330; 1996.
61. Pilegaard, K.; Ladefoged, O. Total number of astrocytes in the molecular layer of dentate gyrus of rats at different ages. Analyt. Quantitat. Cytol. Histol. 18:274–285; 1996.
62. Pilgrim, Ch.; Reisert, I. Differences between male and female brains—Developmental mechanisms and implications. Horm. Metab. Res. 24:353–359; 1992.
63. Pitkänen, A. Connectivity of the rat amygdaloid complex. In: Aggleton, J. P., ed. The amygdala: A functional analysis. Oxford: Oxford University Press; 2000:31–115.
64. Rasia-Filho, A. A.; Londero, R. G.; Achaval, M. On some functional activities of the amygdala: An overview. J. Psych. Neurosci. 25:14–23; 2000.
65. Rasia-Filho, A.; Londero, R. G.; Achaval, M. Effects of gonadal hormones on the morphology of neurons from the medial amygdaloid nucleus of rats. Brain Res. Bull. 48:173–183; 1999.
66. Rasia-Filho, A. A.; Peres, T. M. S.; Cubilla-Gutierrez, F. H.; Lucion, A. B. Effect of estradiol implanted in the corticomedial amygdala on the sexual behavior of castrated male rats. Braz. J. Med. Biol. Res. 24:1041–1049; 1991.
67. Rhodes, M. E.; O'Toole, S. M.; Czambel, R. K.; Rubin, R. T. Male–female differences in rat hypothalamic–pituitary–adrenal axis responses to nicotine stimulation. Brain Res. Bull. 54:681–688; 2001.
68. Rhodes, M. E.; O'Toole, S. M.; Wright, S. L.; Czambel, R. K.; Rubin, R. T. Sexual diergism in rat hypothalamic–pituitary–adrenal axis responses to cholinergic stimulation and antagonism. Brain Res. Bull. 54:101–113; 2001.
69. Rocha, E.; Rodnight, R. Chronic administration of lithium chloride increases immunodetectable glial fibrillary acidic protein in the rat hippocampus. J. Neurochem. 63:1582–1584; 1994.
70. Rocha, E.; Achaval, M.; Santos, P.; Rodnight, R. Lithium chloride causes glioses and modifies the morphology of hippocampal astrocytes in rats. Neuroreport 9:3971–3974; 1998.
71. Sheehan, T. P.; Cirrito, J.; Numan, M. J.; Numan, M. Using c-fos immunohistochemistry to identify forebrain regions that may inhibit maternal behavior in rats. Behav. Neurosci. 114:337–352; 2000.
72. Sheridan, P. J. The nucleus interstitialis stria terminalis and the nucleus amygdaloideus medialis: Prime targets for androgen in the rat forebrain. Endocrinology 104:130–136; 1979.
73. Simerly, R. B. Organization and regulation of sexually dimorphic neuroendocrine pathways. Behav. Brain Res. 92:195–203; 1998.
74. Simerly, R. B.; Chang, C.; Muramatsu, M.; Swanson, L. W. Distribution of androgen and estrogen receptor mRNA-containing cells in the rat brain: An *in situ* hybridization study. J. Comp. Neurol. 294:76–95; 1990.
75. Sterneberger, L. A. Immunohistochemistry. Chichester: Wiley; 1979.
76. Steward, O.; Torre, E. R.; Tomasulo, R.; Lothman, E. Neuronal activity up-regulates astroglial gene expression. Proc. Natl. Acad. Sci. U.S.A. 88:6819–6923; 1991.
77. Stone, D. J.; Song, Y.; Anderson, C. P.; Krohn, K. K.; Finch, C. E.; Rozovsky, I. Bidirectional transcription regulation of glial fibrillary acidic protein by estradiol *in vivo* and *in vitro*. Endocrinology 139:3202–3209; 1998.
78. Swanson, L. W.; Petrovich, G. D. What is the amygdala? Trends Neurosci. 21:323–331; 1998.
79. Vinader-Caerols, C.; Collado, P.; Segovia, S.; Guillamón, A. Estradiol masculinizes the posteromedial cortical nucleus of the amygdala in the rat. Brain Res. Bull. 53:269–273; 2000.
80. Winsky, L.; Kuznicki, J. Antibody recognition of calcium-binding proteins depends on their calcium-binding status. J. Neurochem. 66:764–771; 1996.
81. Wofchuk, S. T.; Rodnight, R. Glutamate stimulates the phosphorylation of glial fibrillary acidic protein in slices of immature rat hippocampus via a metabotropic receptor. Neurochem. Int. 24:517–523; 1994.
82. Wood, R. I.; Newman, S. W. Hormonal influence on neurons of the mating behavior pathway in male hamsters. In: Micevych, P. E.; Hammer, R. P., Jr., eds. Neurobiological effects of sex steroid hormones. New York: Cambridge University Press; 1995:3–39.

ELSEVIER

Comparative Biochemistry and Physiology Part B 131 (2002) 807–814

CBP

www.elsevier.com/locate/cbpc

Sciatic nerve transection decrease substance P immunoreactivity in the lumbosacral spinal cord of the frog (*Rana catesbeiana*)

Wania A. Partata[a,*], Josi F. Cerveira[a], Léder L. Xavier[b], Giordano G. Viola[b], Matilde Achaval[b]

[a]*Departamento de Fisiologia, Laboratório de Neurobiologia Comparada, Instituto de Ciências Básicas da Saúde, Universidade Federal do Rio Grande do Sul, Rua Sarmento Leite, 500, 90050-170, Porto Alegre, RS, Brazil*
[b]*Departamento de Ciências Morfológicas, Laboratório de Histofisiologia Comparada, Instituto de Ciências Básicas da Saúde, Universidade Federal do Rio Grande do Sul, Rua Sarmento Leite, 500, 90050-170, Porto Alegre, RS, Brazil*

Received 29 March 2001; received in revised form 25 January 2002; accepted 29 January 2002

Abstract

Using immunohistochemistry and optical densitometry, substance P (SP) was investigated in the lumbar spinal cord of the frog *Rana catesbeiana* after sciatic nerve transection. In control animals, there was a high density of SP fibers in the Lissauer's tract and in the mediolateral band of the dorsal gray matter. Other SP immunoreactive fibers were observed in the dorsal part of the lateral funiculus and in the ventral horn. No SP label was found in any cell bodies. After axotomy, SP immunoreactive fibers decreased in the Lissauer's tract on the same side of the lesion. The other regions remained labeled. The changes were observed at 3 days following axonal injury and persisted at 5, 8 and 15 days. At 20 days, there was no significant difference between the axotomized side and the control one, thus indicating a recovery of the SP expression. These results indicate that the frog may be used as a model to study the effects of peripheral axotomy, contributing to elucidate the SP actions in the pain neuropath.

Keywords: Substance P; Lumbosacral spinal cord; Frog; Immunohistochemistry; Axotomy; Sciatic nerve; Densitometry; Pain

1. Introduction

Substance P (SP) is a neuropeptide prominently expressed in small sensory primary afferents that is involved in the modulation of pain-related information in the spinal dorsal horn (Rang et al., 1994). Its chemical structure is highly conserved in non-mammalian species, being found also in frogs (Lorez and Kemali, 1981). In the spinal cord of these animals the SP is mainly located in substantia gelatinosa, suggesting some role in nociceptive process. Although the spinal cord of frogs has been frequently used in physiological and pharmacological studies (Stevens and Pezalla, 1983, 1984; Pezalla and Stevens, 1984), no reported was found on the effect of peripheral axotomy on SP immunoreactivity. In rats it was observed that the peripheral nerve section leads to a marked quantitative decrease of SP, which is partially or completely restored after a variable time (Tessler et al., 1985; Himes and Tessler, 1989; Wang et al., 1991). Thus, the main goal of the present study is to provide detailed information on the effect of peripheral axotomy on SP immunoreactivity in the frog *Rana catesbeiana.* The comparison of the present results with those obtained in other vertebrates will undoubtedly increase our knowledge of

*Corresponding author. Tel.: +55-51-316-3320; fax: +55-51-316-3166.
E-mail address: achaval@ufrgs.br (W.A. Partata).

1096-4959/02/$ - see front matter
PII: S1096-4959(02)00041-6

the evolution of the brain neurochemistry in vertebrates, and it might give a phylogenetic basis for better understanding the functions of SP in the spinal cord of the frogs and mammals.

2. Materials and methods

2.1. Animals

Experiments were conducted on frogs *Rana catesbeiana*, adult, both sex, weighing 30–60 g. These animals were obtained from Javapark Comércio de Alimentos LTDA (Porto Alegre, RS) at all seasons of the year. Upon arrival, frogs were housed in cages through which water at 22–26 °C was frequently flushed, and fed ad libitum with specific ration. Experimental procedures were approved by the authorities of the Instituto Brasileiro de Meio Ambiente e dos Recursos Renoviveis (IBAMA) (License 031/95 DEVIS). Under anesthesia (lidocaine—0.1 ml/100 g body wt.) and sterile conditions, the right sciatic nerve was exposed and transected approximately 5-mm distal to the sciatic notch. Groups of three animals were killed after 0, 3, 5, 8, 15, and 20 days.

2.2. Immunohistochemical procedure

The operated and control frogs were descerebrated at different survival times and, after a brief saline flush, were intracardically perfused with 4% paraformaldehyde in 0.1 M phosphate buffer (pH 7.4). The lumbar spinal cord was quickly dissected out, immersed in the same fixative solution for 4 h and then cryoprotected in 15 and 30% sucrose solutions in phosphate buffer at 4°C. Coronal serial sections (50 μm) were obtained on cryostat and collected in cold phosphate buffered saline (PBS). The sections were then treated with 3% hydrogen peroxide in 10% methanol for 30 min, washed with PBS for a further 30 min and incubated for 30 min in 3% normal goat serum in PBS containing 0.4% Triton X-100 (PBS-T). The sections were incubated overnight with gentle agitation at 4°C in a polyclonal antibody to rabbit SP (a gift from Dr Joaquín Del Rio—Pharmacological Department, Faculty of Medicine, Navarra University, Spain), diluted 1:800 in PBS-T. The primary antibody was then removed and the sections washed in PBS-T for 30 min. Then the sections were immersed in a secondary antibody (anti-lgG, Sigma), diluted 1:50 in PBS-T, for 2 h at room temperature with gentle agitation. After washing with PBS-T for 30 min a soluble complex of horseradish peroxidase rabbit anti-horseradish peroxidase diluted 1:500 was applied for 2 h at room temperature. The samples were then washed in PBS, incubated in a solution of 3,3′-diaminobenzidine tetrahydrochoride (60 mg/100 ml, Sigma) and 0.005% v/v hydrogen peroxide in PBS. The sections were washed, mounted onto gelatinized slides and coverslipped with Entellan (Merck). Specific immunostaining was abolished when the primary antibody was omitted from the staining sequence. The intact contralateral spinal segments were used as a control.

Sections were examined and photographed with Nikon Optiphot-2 microscope equipped with a Nikon FX-35DX camera.

2.3. Optical densitometry

In order to measure the intensity of reaction product of SP immunohistochemistry (semiquantitative analysis), a Nikon Eclipse E 600 (40OX) microscope coupled to a Pro-Series High Performance CCD camera and Image Pro Plus Software 4.1 (Media Cybernetics, USA) was employed. Immunoreactive regions of the lumbar spinal cord were selected, the blood vessels and other artifacts were avoided. At least five readings were taken, per animal. Selected areas were converted into black and white digital images (0–255 gray levels) and the optical density was measured. Background staining was determined and used to correct the optical density measurements. All lighting conditions and magnifications were held constant for the different sections. The animals with different times of survival could not be compared, because the immunohistochemistry was performed on different days. Statistical analysis was carried out using a paired Student's *t*-test. A *p*-value of 0.01 or less was considered significant. The statistical analysis was made using SPSS 7.0 software.

The formula of optical density used was:

$$\begin{aligned}\text{OPTICAL DENSITY}_{(X,Y)} &= -\log\big[(\text{BACKGROUND}_{(X,Y)} - \text{BLACK}) \\ &\quad - (\text{INTENSITY}_{(X,Y)} \\ &\quad - \text{BLACKY})/\big((\text{INCII})\text{ENT} - \text{BLACK}\big)\big]\end{aligned}$$

Where: $\text{Background}_{(X,Y)}$ is the intensity of background at pixel; $\text{Intensity}_{(X,Y)}$ is the intensity at pixel; Black is the intensity generated when no

light passes through the material, in this case 5, 32 (0–255); and Incident is the intensity if the incidental light in this case 250, 41 (0–255).

The results obtained represent the mean of all pixels in the selected area. The estimation of surface density (a precise and unbiased, stereological method) (Cruz-Orive, 1997) could not be used, because this approach requests the use of vertical sections and it is impossible to determine the localization of the dorsal horn in vertical sections.

3. Results

SP immunoreactivity was only detected in varicose fibers and dot-like structures without intervaricose connections. These structures (termed fibers below) are nerve terminals according to Ljungdahl et al. (1978). These structures appear as distinct dark brown particles and/or 'strings of beads' (Fig. 1B–D).

Control sections did not reveal any immunoreactivity. In control animals, SP immunoreactivity was found in the dorsal and ventral horns of the lumbar spinal cord. A similar density of fiber clusters was found in both sides of the spinal cord (Fig. 1A). In the dorsal horn, the SP fibers entered the dorsal root. The strongest positive fibers were located in the Lissauer's tract (Fig. 1A,B). Other SP immunoreactive fibers were identified in the dorsal part of the lateral funiculus. The density of these fibers in the lateral funiculus decreased in a dorsal to ventral direction. Medially, these fibers were continuous with a concentration of SP fibers located at the base of the dorsal horn, between the dorsal and ventral terminal fields (Fig. 1A). This cluster of fibers, referred to as the mediolateral band, showed the highest density of SP immunoreactivity in the dorsal gray matter. These fibers seemed to cross the midline of the spinal cord and continue to the contralateral side. A few SP fibers were observed in substantia gelatinosa (Fig. 1C). No SP label was found in any cell body. SP immunoreactivity varicosities were scattered in the ventral horn and some of them abutted on motoneurons, which did not show immunoreaction (data not shown).

After the sciatic nerve section, there was a reduction in SP immunoreactive fibers in the dorsal horn of the lumbar spinal cord on the same side as the lesion (Fig. 2). The depletion of immunostaining was observed in the small fibers of the Lissauer's tract and in fibers located in the dorsal part of the lateral funiculus. The other fibers were still labeled, with a similar reaction to the control side. These changes already appeared at 3 days following nerve transection. These data persisted at 5, 8 (Fig. 2B), and 15 days (Fig. 2C). But no difference from contralateral side were found at 20 days after sciatic nerve transection (Fig. 2D). In experimental frogs the pattern of the immunoreaction in the ipsilateral side was virtually identical to that of the contralateral side. This immunohistochemical data was confirmed by optical density (Fig. 3).

4. Discussion

SP immunoreactivity of the frog lumbar spinal cord is higher in gray matter than in white matter. The dorsal horn develops more SP immunoreactivity than the ventral one. This data is in agreement with previous studies in other vertebrates (Lavalley and Ho, 1983; Reiner et al., 1984; Nakaya et al., 1994) and in frogs (Inagaki et al., 1981; Lorez and Kemali, 1981; Adli et al., 1988). However, in a recent study in frog spinal cord, the SP immunoreactive fibers was also found in the entire lateral and (adjacent) ventral funiculus, and in sparse cell bodies of the dorsal horn, intermediate and central gray matter (Lorez and Kemali, 1981). In contrast to these results, other studies showed no SP cells in frog spinal cord (Inagaki et al., 1981; Adli et al., 1988), as in the present study. At the moment it is impossible to explain this difference. However, it could be emphasized that our description of the SP immunoreactivity distribution is in general agreement with a study of *Rana catesbeiana* (Inagaki et al., 1981). It should be mentioned that in the latter work the term 'substantia gelatinosa' was misused to describe the dorsal part of the lateral funiculus (including Lissauer's tract).

The main finding of the present study is the decrease in SP immunoreactivity after sciatic nerve transection. However, this immunoreactivity was recovered along the temporal course of transection, as was observed in the rat (Tessler et al., 1985; Himes and Tessler, 1989; Wang et al., 1991). In this animal the SP changes appear to be a more general event in nerve de- and regeneration. In a previous study with a model of chronic constriction injury in rats, it was suggested that the decreased level of SP in the dorsal horn could be involved

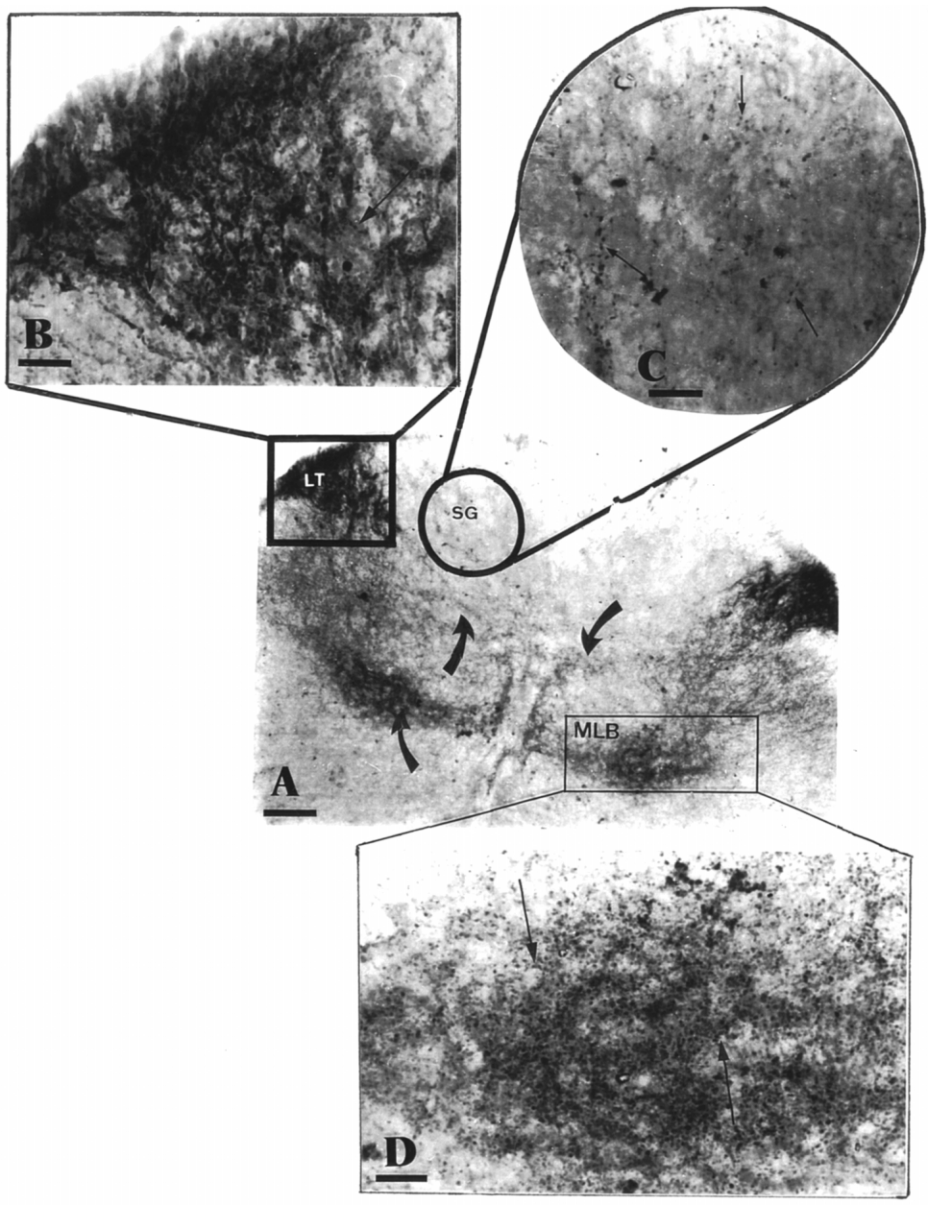

Fig. 1. SP immunoreactivity in the frog lumbosacral spinal cord (A). Note the abundant fibers in framed regions which correspond to Lissauer's tract (LT) and mediolateral band (MLB). The encircled region indicates the substantia gelatinosa (SG) and the curved arrows indicate the fibers that seem to cross the midline. The photomicrographs B–D are higher magnification of the framed and encircle regions in A. Note the varicose fibers and dot-like structures termed fibers here (arrows). Bar = 200 μm (A), 80 μm (B–D).

in the increased sensibility of the second-order neurons to incoming signals (Sommer and Myers, 1995). According to these authors, such mechanism might underlie altered central processing which has been observed in patients with neuropathic pain. The spinal cord of the frog is remarkably similar to that of mammals in terms of both general layout and some details (Cruce, 1974; Jhaveri and Frank, 1983; Székely and Antal, 1984; Rosenthal and Cruce, 1985). These similarities may suggest that the SP decrease in frogs could play the same role as that observed in mammals.

While SP fibers in the dorsal horn of amniotes are more dense in the superficial laminae (Hökfelt et al., 1976; Ljungdahl et al., 1978; Seybold and Elde, 1980; Charnay et al., 1981; Wolters et al.,

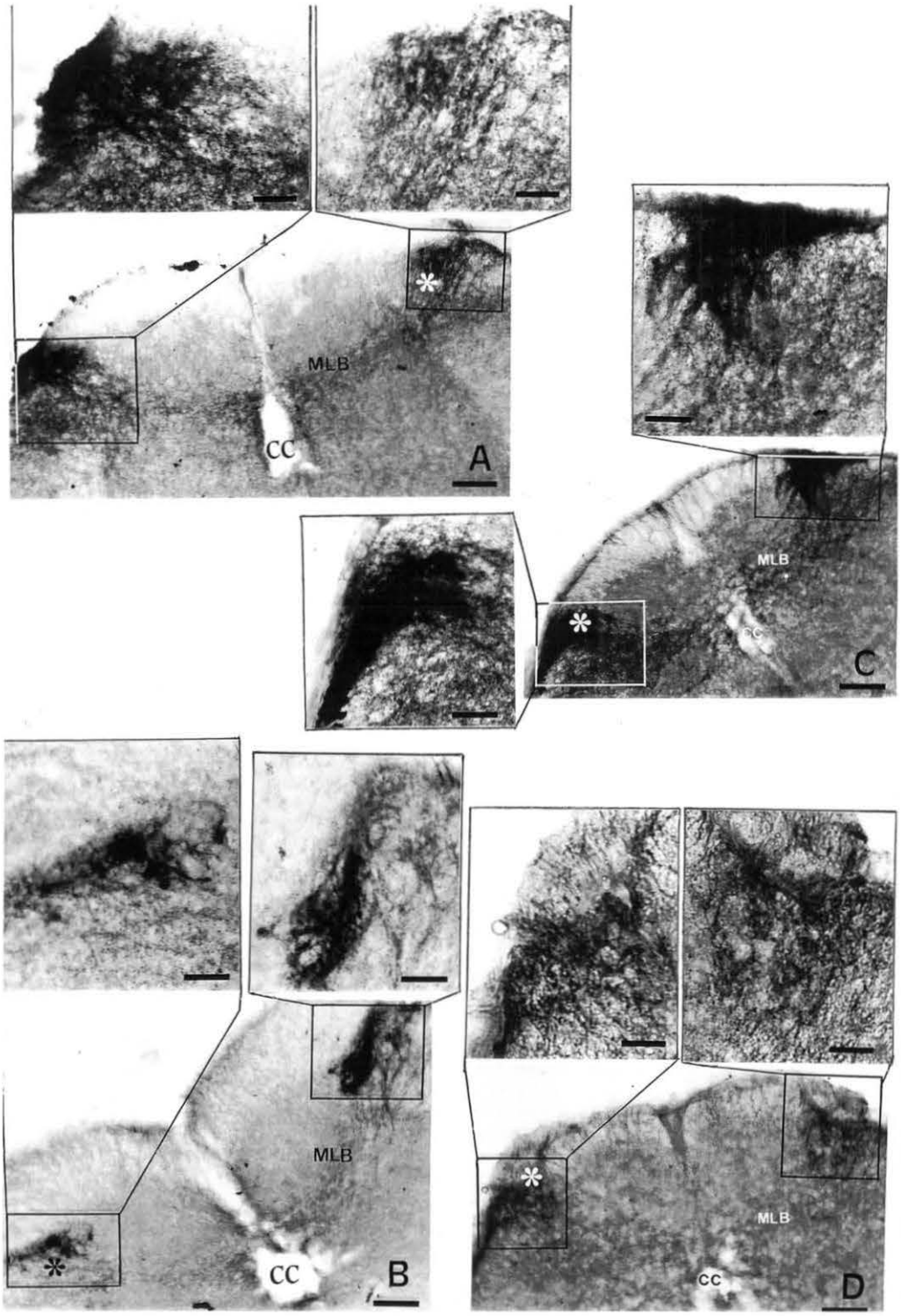

Fig. 2. SP immunoreactivity in the frog lumbosacral spinal cord 3 (A), 8 (B), 15 (C) and 20 (D) days after transection of the sciatic nerve. The ipsilateral side of the lesion is indicated by asterisks. The framed regions showed here are a higher magnification of the Lissauer's tract. MLB, mediolateral band; CC, central canal. Bar = 200 μm (A–D), 40 μm (in framed regions).

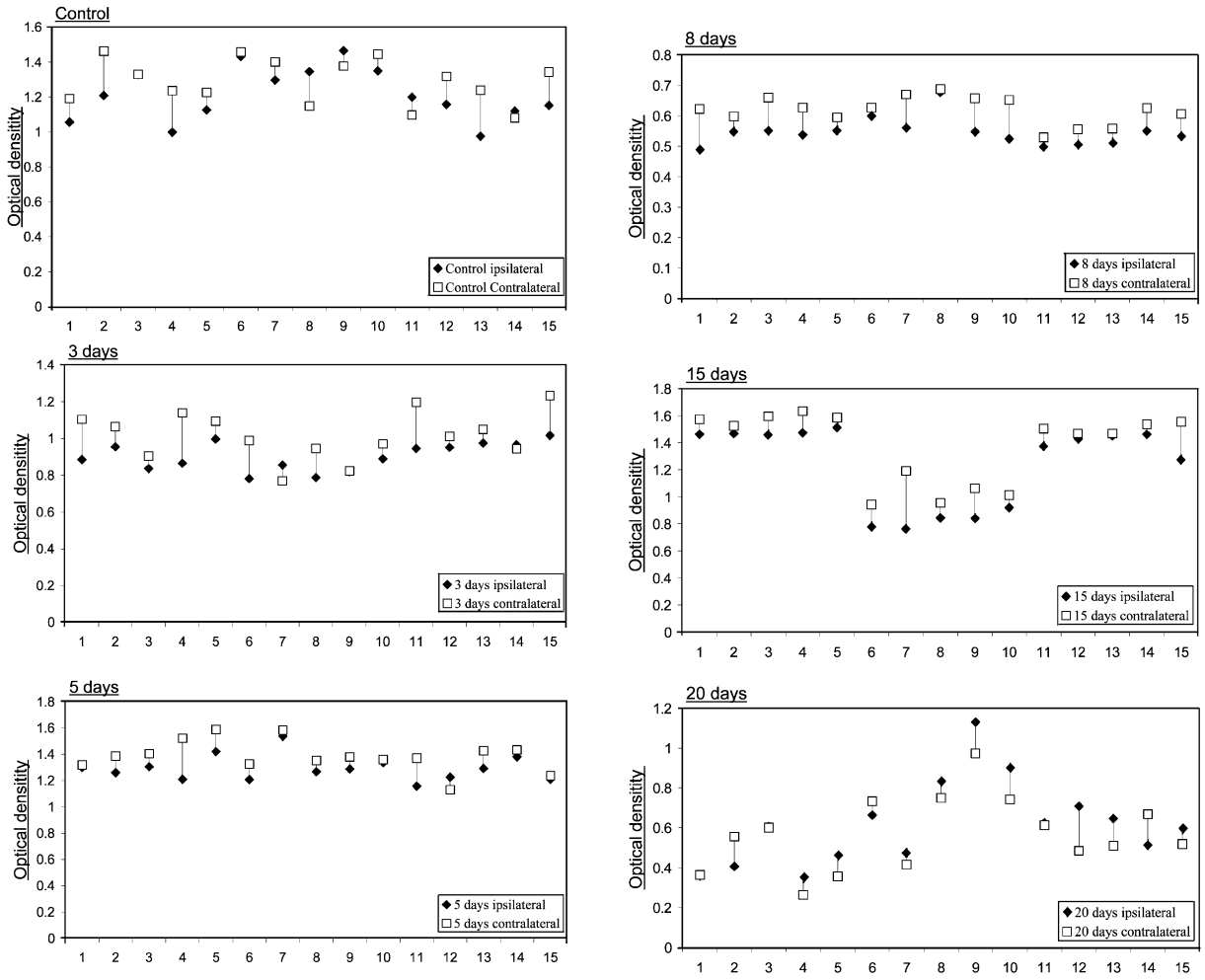

Fig. 3. Optical densitometric measurements of SP immunoreactivity in lumbar spinal cord of the frog in different days of survival after denervation: control, 3, 5, 8, 15 and 20 days. The optical density is represented on the *y*-axis and the different measurements (measure for each section) are represented on the *x*-axis. A significant reduction of SP is detected in the ipsilateral side in the days 3, 5, 8, 15 ($p < 0.01$).

1986), the upper part of the frog dorsal gray matter (which corresponds to laminae I and II of amniotes) showed few SP fibers. SP immunoreactive fibers were concentrated in the mediolateral band, a region poor in primary fiber terminals (Adli et al., 1988). This puzzling situation is quite different from that found in amniotes, which suggests a different role to SP in frogs following nerve transection. However, it is accepted that the dorsal part of the frog lateral funiculus include the Lissauer's tract (Adli et al., 1988), as with amniotes. Thus, it may be that the few SP immunoreactive fibers in frog substantia gelatinosa could partially originate from the dorsal roots. Mammalian dorsal roots and root ganglia contain SP cells and fibers (Takahashi and Otsuka, 1975; Hökfelt et al., 1976; Jessell et al., 1979; Seybold and Elde, 1980; Charnay et al., 1981; Leah et al., 1985). If it is the case, SP may have a role in the processing of frog sensory information, and its decrease might reflect the involvement of this neuropeptide in the pathogenesis of neuropathic pain in these animals.

In the present study the SP recovery is faster in the frog than in the rat. In these mammals, measurements of the density of SP immunoreactivity at the light microscopic level showed a significant reduction at 4 days, which reached a minimum of 35% of control values 10 days following deafferentation. Immunoreactivity returned to 75% of the control values 60 days following the lesion (Wang

et al., 1991). In frogs, this rapid response could be due to the sprouting of the intraspinal undamaged projections. In mammals, light microscopic immunocytochemistry has shown sprouting by selected undamaged intraspinal projections, including those that express the SP (Croul et al., 1995). The evidence remains inconclusive in relation to the significance of the findings. Further studies on the relationship between SP immunohistochemistry and electron microscopic characterization in frog spinal cord after nerve deafferentation are necessary in order to clarify the subject. In rats, quantitative immunoelectron microscopy shows a recovery of SP-containing terminals beginning within 10 days, which is virtually complete after approximately 60 days following deafferentation (Zhang et al., 1993).

It is early to speculate whether the SP actions are similar in frogs and in mammals, and it is evident that to understand the significance and real role of this neuropeptide in the frog spinal cord, multiple approaches, including biochemical, cytochemical, other immunocytochemical, molecular and other physiological procedures will be necessary. Some of these studies are currently taking place in our laboratory. Nevertheless, the similar response of both the frog and rat demonstrated here must be taken into account. Despite the difference observed in this immunohistochemical map, the present study indicates that the frog may be used as a model to study the effects of peripheral axotomy, which mimic the clinical conditions of pain neuropathy. This model can also contribute to elucidating the SP actions in this situation.

Acknowledgments

The authors would like to thank Dr Maria Marques for her comments on this manuscript. This study was supported by Conselho Nacional de Desenvolvimento Científico e Tecnológico (CNPq) and Fundação de Amparo a Pesquisa do Rio Grande do Sul (FAPERGS).

References

Adli, D.S.H., Rosenthal, B.M., Yuen, G.L., Ho, R.H., Cruce, W.L.R., 1988. Immunohistochemical localization of substance P, somatostatin, enkephalin, and serotonin in the spinal cord of the northern leopard frog, *Rana pipiens*. J. Comp. Neurol. 275, 106–116.

Charnay, Y., Paulin, C., Chayvialle, J.A., Dubois, P.M., 1981. Distribution of substance P-like immunoreactivity in the spinal cord and dorsal root ganglia of the human foetus and infant. Neuroscience 6, 713–723.

Croul, S., Svertiuk, A., Radzievsky, A., Murray, M., 1995. Modulation of neurotransmitter receptor following unilateral L1–S2 deafferentation: NK1, NK2, NMDA, and 5HT1a receptor binding autoradiography. J. Comp. Neurol. 361, 633–644.

Cruce, W.L.R., 1974. The anatomical organization of hindlimb motoneurons in the lumbar spinal cord of the frog, *Rana catesbeiana*. J. Comp. Neurol. 153, 59–76.

Cruz-Orive, L.M., 1997. Stereology of single objects. J. Microsci. 186, 93–107.

Himes, B.T., Tessler, A., 1989. Death of some dorsal root ganglion neurons and plasticity of others following sciatic nerve section in adult and neonatal rats. J. Comp. Neurol. 284, 215–230.

Hökfelt, T., Elde, R., Johansson, O., Luft, R., Nilsson, G., Arimura, A., 1976. Immunohistochemical evidence for separate populations of somatostatin-containing and substance P-containing primary afferent neurons in the rat. Neuroscience 1, 131–136.

Inagaki, S., Senba, E., Shiosaka, S., et al., 1981. Regional distribution of substance P-like immunoreactivity in the frog brain and spinal cord: immunohistochemical analysis. J. Comp. Neurol. 201, 243–254.

Jessell, T., Tsunoo, A., Kanazawa, I., Otsuka, M., 1979. Substance P: depletion in the dorsal horn of the rat spinal cord after section of the peripheral process of primary sensory neurons. Brain Res. 168, 247–259.

Jhaveri, S., Frank, E., 1983. Central projections of the brachial nerve in bullfrogs: muscle and cutaneous afferents project to different regions of the spinal cord. J. Comp. Neurol. 221, 304–312.

Lavalley, A.L., Ho, R.H., 1983. Substance, somatostatin, and methionine enkaphalin immunoreactivity elements in the spinal cord of the domestic fowl, *Gallus domesticus*. J. Comp. Neurol. 213, 406–413.

Leah, J.D., Cameron, A.A., Kelley, W.L., Snow, P.J., 1985. Coexistence of peptide immunoreactivity in sensory neurons of the cat. Neuroscience 16, 683–690.

Ljungdahl, A., Hökfelt, T., Nilsson, G., 1978. Distribution of substance P-like immunoreactivity in the central nervous system of the rat-I. Cell bodies and nerve terminals. Neuroscience 3, 861–943.

Lorez, H.P., Kemali, M., 1981. Substance P-, met-enkephalin- and somatostatin-like immunoreactivity distribution in the frog spinal cord. Neurosci. Lett. 26, 119–124.

Nakaya, Y., Kaneko, T., Shigemoto, R., Nakanish, S., Mizuno, N., 1994. Immunohistochemical localization of substance P receptor in the central nervous system of the adult rat. J. Comp. Neurol. 347, 249–274.

Pezalla, P.D., Stevens, C.W., 1984. Behavioral effects of morphine, levorphanol, dextrorphan and naloxone in the frog *Rana pipiens*. Pharmacol. Biochem. Behav. 21, 213–217.

Rang, H.P., Bevan, S., Dray, A., 1994. Nociceptive peripheral neurons: cellular properties. In: Wall, P.D., Melzack, R. (Eds.), Textbook of Pain, Churchill Livingstone, New York pp. 57–78.

Reiner, A., Krause, J.E., Keyser, K.T., Eldred, W.D., McKelvy, J.F., 1984. The distribution of substance P in turtle nervous system: a radioimmunoassay and immunohistochemical study. J. Comp. Neurol. 226, 50–75.

Rosenthal, B.M., Cruce, W.L.R., 1985. Distribution and ultrastructure of primary afferent axons in Lissauer's tract in the northern leopard frog (*Rana pipiens*). Brain Behav. Evol. 27, 195–214.

Seybold, V., Elde, R., 1980. Immunohistochemical studies of peptidergic neurons in the dorsal horn of the spinal cord. J. Histochem. Cytochem. 28, 367–370.

Sommer, C., Myers, R.R., 1995. Neurotransmitters in the spinal cord dorsal horn in a model of painful neuropathy and in nerve crush. Acta Neuropathol. 90, 478–485.

Stevens, C.W., Pezalla, P.D., 1983. A spinal site mediates opiate analgesia in frogs. Life Sci. 33, 2097–2103.

Stevens, C.W., Pezalla, P.D., 1984. Naloxone blocks the analgesic action of levorphanol but not of dextrorphan in the leopard frog. Brain Res. 301, 171–174.

Székely, G., Antal, M., 1984. Segregation of muscle and cutaneous afferent fibre terminals in the brachial spinal cord of the frog. J. Hirforsch. 25, 671–675.

Takahashi, T., Otsuka, M., 1975. Regional distribution of substance P in the spinal cord and nerve roots of the cat and the effect of dorsal root section. Brain Res. 87, 1–11.

Tessler, A., Himes, B.T., Krieger, N.R., Murray, M., Golberger, M.E., 1985. Sciatic nerve transection produces death of dorsal root ganglion cells and reversible loss of substance P in spinal cord. Brain Res. 332, 209–218.

Wang, S.D., Goldberger, M.E., Murray, M., 1991. Plasticity of spinal systems after unilateral lumbosacral dorsal rhizotomy in the adult rat. J. Comp. Neurol. 304, 555–568.

Wolters, J.G., ten Donkelaar, H.J., Verhofstad, A.A.J., 1986. Distribution of some peptides (substance P, [leu]enkephalin, [met]enkephalin) in the brain stem and spinal cord of a lizard, *Varanus exanthematicus*. Neuroscience 18, 917–946.

Zhang, B., Goldberger, M.E., Murray, M., 1993. Proliferation of SP and 5HT containing terminals in lamina II of the rat spinal cord following dorsal rhizotomy: quantitative EM-immunocytochemical studies. Exp. Neurol. 123, 51–64.

Brazilian Journal of Medical and Biological Research (2003) 36: 515-520
ISSN 0100-879X Short Communication

Substance P immunoreactivity in the lumbar spinal cord of the turtle *Trachemys dorbigni* following peripheral nerve injury

W.A. Partata[1], A.M.R. Krepsky[1], L.L. Xavier[2], M. Marques[1] and M. Achaval[2]

Departamentos de [1]Fisiologia and [2]Ciências Morfológicas, Instituto de Ciências Básicas da Saúde, Universidade Federal do Rio Grande do Sul, Porto Alegre, RS, Brasil

Abstract

Immunoreactive substance P was investigated in turtle lumbar spinal cord after sciatic nerve transection. In control animals immunoreactive fibers were densest in synaptic field Ia, where the longest axons invaded synaptic field III. Positive neuronal bodies were identified in the lateral column of the dorsal horn and substance P immunoreactive varicosities were observed in the ventral horn, in close relationship with presumed motoneurons. Other varicosities appeared in the lateral and anterior funiculi. After axotomy, substance P immunoreactive fibers were reduced slightly on the side of the lesion, which was located in long fibers that invaded synaptic field III and in the varicosities of the lateral and anterior funiculus. The changes were observed at 7 days after axonal injury and persisted at 15, 30, 60 and 90 days after the lesion. These findings show that turtles should be considered as a model to study the role of substance P in peripheral axonal injury, since the distribution and temporal changes of substance P were similar to those found in mammals.

Correspondence
W.A. Partata
Departamento de Fisiologia
ICBS, UFRGS
Rua Sarmento Leite, 500
90050-170 Porto Alegre, RS
Brasil
Fax: +55-51-316-3166
E-mail: partataw@excite.com

Research supported by CAPES, CNPq and FINEP (No. 66.91.0509.00).

Received September 25, 2001
Accepted January 6, 2003

Key words
- Substance P immunoreactivity
- Axonal injury
- Spinal cord
- Turtle
- *Trachemys dorbigni*

Peripheral nerve injury may result in significant changes in neuropeptide production and the development of neuropathic pain behavior (1). In rats, peripheral nerve sectioning leads to a marked quantitative decrease in the nerve of substance P, a peptide of 11 amino acids that is present in small primary afferents and plays an important role in pain sensation (2,3).

The chemical structure of substance P is highly conserved in non-mammalian species, and is also found in turtles, animals considered phylogenetically related to the extinct theropsids from which mammals arose (4). Previous studies demonstrated substance P immunoreactivity in the turtle central nervous system (5,6); however, the effects of peripheral axotomy on substance P distribution have not been studied. Therefore, the aim of this study was to determine the effects of sciatic nerve transection on substance P immunoreactive fibers in the lumbar spinal cord of the turtle *Trachemys dorbigni*.

Under ether-induced anesthesia (7), the right sciatic nerve was exposed and transected approximately 5 mm distal to the sciatic notch. In this nerve transection, a 2-mm segment of the nerve was removed to ensure that the transection was complete. Groups of three turtles of both sexes, weighing 300-400

g, were sacrificed 7, 15, 30, 60 and 90 days later. On the final day of the experiment, both operated and control turtles were anesthetized (25 mg/kg Thionembutal, intraperitoneally) and perfused through the heart with cold saline solution followed by 4% paraformaldehyde in 0.1 M sodium phosphate buffer, pH 7.4. The lumbar spinal cord was quickly dissected out, immersed in the same fixative for 2 h and then cryoprotected in 15 and 30% sucrose solutions in phosphate buffer at 4ºC. Coronal serial sections (50 µm) were obtained with a cryostat (Leitz) and collected in cold phosphate-buffered saline (PBS). The sections were then treated with 3% hydrogen peroxide in 10% methanol for 30 min, washed with PBS for a further 30 min and incubated for 30 min in 3% normal goat serum in PBS containing 0.4% Triton X-100 (PBS-T). A polyclonal antibody to rabbit substance P (a gift from Dr. Joaquín Del Río, Department of Pharmacology, Navarra University, Spain), whose specificity has been described in a previous report (8), diluted 1:800 in PBS-T, was applied to the sections which were incubated overnight with gentle shaking at 4ºC. The primary antibody was then removed and the sections were washed in PBS-T for 30 min and were then immersed in secondary antibody (anti-IgG; Sigma, St. Louis, MO, USA), diluted 1:50 in PBS-T, for 2 h at room temperature with gentle shaking. After washing with PBS-T for 30 min, a soluble complex of horseradish peroxidase rabbit anti-horseradish peroxidase (Sigma) diluted 1:500 was applied for 2 h at room temperature. The samples were then washed in PBS, incubated in a solution of 3,3-diaminobenzidine tetrahydrochloride (60 mg/100 ml; Sigma) and 0.005% (v/v) hydrogen peroxide in PBS. The sections were washed, mounted onto gelatinized slides and coverslipped with Entellan. Specific immunostaining was abolished when the primary antibody was omitted in the staining sequence. The intact contralateral spinal segments were used as control. Sections were examined and photographed with a Nikon Optiphot-2 microscope equipped with a Nikon FX-3 5DX camera.

A Nikon Eclipse E 600 (400X) microscope coupled to a pro-series high performance CCD camera and image Pro Plus software 4.1 (Media Cybernetics, Silver Spring, MD, USA) was used to measure the intensity of the reaction product of substance P immunohistochemistry (semiquantitative analysis). Synaptic subfield Ia was delimited, the obtained images were digitized and converted to 8-bit gray scale (0-255 gray levels) and the regional absorbance was measured. Obvious blood vessels and other artifacts were not considered. The readings were performed on the left and right side of the lumbar spinal cord and at least five readings were obtained. Background staining from a non-reactive tissue was determined and used to correct the absorbance measurements. All lighting conditions and magnifications were held constant.

During the analysis, the investigator was unaware of the experimental groups from which the slices were obtained. The absorbance (A) measurement formula used was the following:

$$A_{(x,y)} = 100 - \{[(background_{(x,y)} - black) - (intensity_{(x,y)} - black)/(incident - black)]/255\} \times 100$$

where $background_{(x,y)}$ is the background intensity at $pixel_{(x,y)}$, and $intensity_{(x,y)}$ is the intensity at $pixel_{(x,y)}$, black is the intensity generated when no light goes through the material, and incident is the intensity of the incident light. The results reported represent the mean of all pixels in the selected area on a 100% scale. In the present study, the thickness of the sections (50 µm) used did not lead to immunohistochemical over-reactions or saturation of absorbance. Other anatomical areas located in the lumbar spinal cord could not be selected because these areas did not present well-defined limits. The animals with different survival times could not be

compared because the immunohistochemistry was performed on different days. Statistical analysis was carried out using the paired Student *t*-test. The mean diameter of immunostained cell bodies was measured semi-automatically using the same software employed to determine absorbance.

Commonly accepted cytoarchitectonic divisions derived from investigations on mammals proved inadequate when exploring the dorsal gray of the turtle. Thus, for the dorsal horn description we followed the pattern described for turtles by Trujillo-Cenóz et al. (9), which suggests the occurrence of four axonal populations in the turtle dorsal horn. According to these investigators, synaptic field Ia is probably analogous to Lissauer's tract in mammals, while synaptic field II is perhaps homologous to the substantia gelatinosa.

Substance P immunoreactivity was detected in varicose fibers and dot-like structures without intervaricose connections. These structures (termed fibers below) are believed to be mostly nerve terminals according to Ljungdahl et al. (10). They appear as distinct dark brown particles and/or "strings of beads". Control sections did not present immunoreactivity.

In control animals, substance P immunoreactivity was found in the dorsal and ventral horns of the lumbar spinal cord, which was higher in gray matter than in white matter. A similar density of fiber clusters was observed on both sides of the spinal cord. The dorsal horn developed more substance P immunoreactivity than the ventral horn. In the dorsal horn, dense immunoreactive fibers were identified in synaptic field Ia (Figure 1, top, A and B), with the longest axons invading synaptic field III, which exhibited some positive fibers. Furthermore, some long positive fibers were detected crossing the midline of the spinal cord and entering the contralateral side (Figure 1, top, D). The synaptic fields Ib and II were unstained. A dense collection of positive fibers was identified in the ventromedial dorsal horn. Immunostaining of neuronal cell bodies (20.08 $\pm$ 0.72 µm in diameter) occurred in the lateral column of the dorsal horn (Figure 1, top, C). Substance P immunoreactive varicosities were scattered in the ventral horn and some of them appeared to abut motoneurons, which showed no immunoreactivity (Figure 1, top, E). Other positive varicosities were found in the lateral and dorsal funiculi (data not shown). These data agree with previous investigations that reported the presence of substance P in the nervous system of the turtle *Chrysemys picta picta* (5). However, our results seem to be higher than those found in a previous study in the dorsal horn of *Chrysemys d'orbigny* (6). These investigators only reported the presence of substance P immunoreactivity in synaptic field Ia, which invaded synaptic field III, and in the ventral horn limit. There is no report of positive immunoreactive fibers in the lateral and dorsal funiculi. Nevertheless, it is known that this neuropeptide has been detected in these regions in mammals (11,12), frogs (13,14), and domestic fowl (15). In addition, these studies demonstrated the presence of substance P immunoreactivity in the ventral horn of these animals, as found in turtles. The same studies do not refer to the presence of substance P immunoreactivity in cell bodies of the spinal cord, except for frogs (14). It is possible that the presence of immunoreactive cell bodies in *Trachemys dorbigni* spinal cord resulted from the different postperfusion immersion procedure employed. The duration of this step has a greater effect on perinuclear immunoreactivity than colchicine treatment (5). In the present study the postperfusion immersion time was shorter than that used by Reiner et al. (5). Further studies about this question are necessary.

Transection of the sciatic nerve resulted in small changes in the pattern of substance P distribution in the turtle dorsal horn. These modifications were located on the same side as the lesion. They consisted of a small

decrease in the long immunoreactive fibers that penetrated synaptic field III (Figure 1, bottom) and in the varicosities of the lateral and anterior funiculi. These changes were already present by 7 days after nerve transection (Figure 1, bottom, A), and persisted unchanged at 15, 30, 60 and 90 days following the lesion (Figure 1, bottom, B-D). The synaptic field Ia showed the same staining pattern on the ipsilateral and contralateral side of the spinal cord (Figure 1, bottom, A-D), which was confirmed by optical densitometry (Figure 2).

In mammals, peripheral nerve section also leads to a marked quantitative decrease of substance P in the dorsal horn (11,16). Data from quantitative immunoelectron microscopy and receptor binding experiments showed that this change resulted from the degeneration of dorsal root afferents (17,18). In turtles, the dorsal root terminals were found in synaptic fields Ia, Ib, II and III, with some long fibers projecting to the contralateral dorsal horn (9). These findings support the view that the changes described here correspond to degeneration of dorsal root afferents located in synaptic field III. However, there is a striking similarity between the immunoreactive patterns of the ipsilateral and contralateral synaptic fields Ia. However, a recent study has revealed that the synaptic arrays in the peripheral synaptic fields (Ia, Ib and II) are complex, whereas they are simple in deeper regions of the

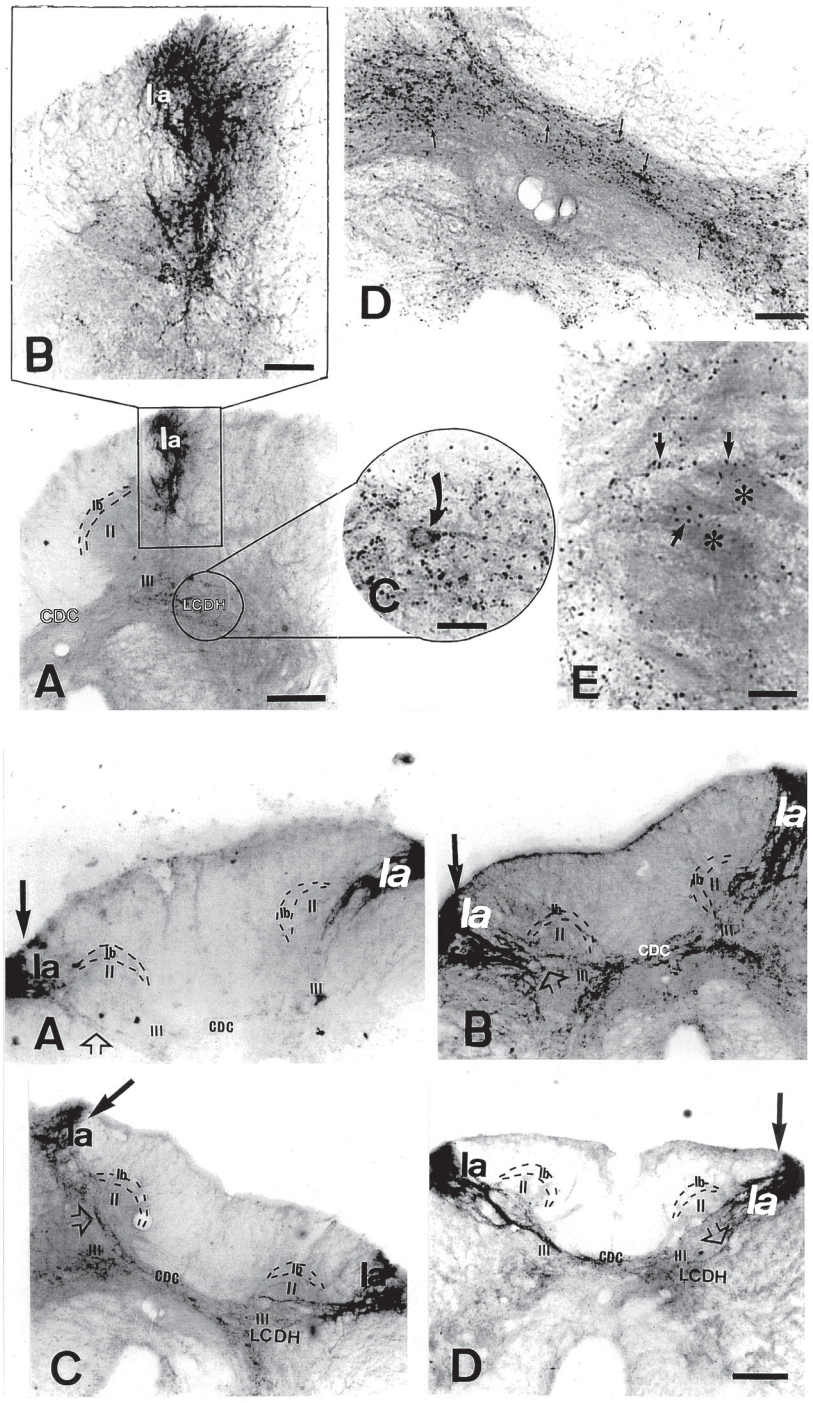

Figure 1. *Top*, Distribution of substance P immunoreactivity in the spinal cord of control turtles. *A*, Intense immunoreactive fibers in synaptic field Ia. From this area the positive fibers project to deeper dorsal horn regions until they reach synaptic field III. Note the lack of reactivity in synaptic fields II and Ib. However, observe the presence of immuneroactivity in the lateral column of the dorsal horn (LCDH). CDC: dorsal commissure. Scale bar: 300 µm. *B*, High magnification of the region analyzed in *A*. Scale bar: 100 µm. *C*, High magnification of the encircled region shown in *A*. Immunoreactive neuron of the LCDH (arrow). Scale bar: 50 µm. *D*, Immunoreactive fibers (arrows) in the dorsal commissure. Scale bar: 100 µm. *E*, Immunoreactive fibers (arrows) in the ventral horn. Note that these fibers appear to abut motoneurons (asterisks). Scale bar: 50 µm. *Bottom*, Substance P immunoreactivity in the spinal cord of the turtles 7 (A), 15 (B), 30 (C) and 90 (D) days following peripheral nerve transection. The arrows indicate the side of the lesion. Note the decrease in substance P immunoreactivity in the long fibers on the lesion side (open arrow). Scale bar: 300 µm.

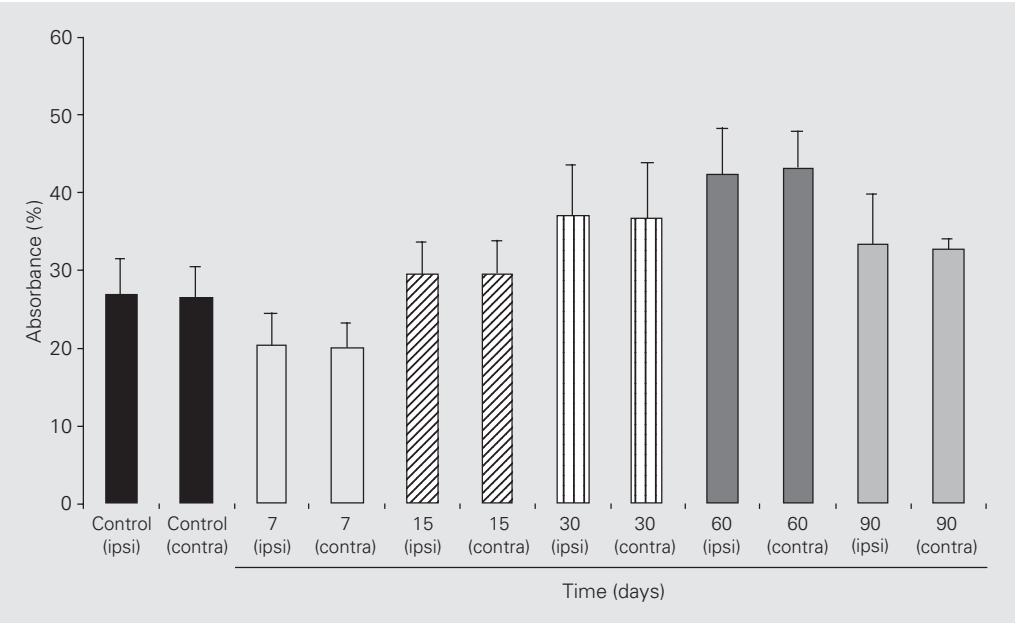

Figure 2. Absorbance of substance P immunoreactivity, obtained from synaptic subfield Ia. No statistical difference was found between the ipsilateral (ipsi) and contralateral (contra) sides in any of the groups studied (a P value of 0.05 or less being considered significant). All statistical analyses were performed using the Student *t*-test and the SPSS 7.0 statistical package software. The results are reported as means ± SD.

dorsal horn (synaptic field III), consisting of typical synaptic boutons contacting either dendrites or neuronal somata (9). Therefore, it seems reasonable to speculate on whether the initial changes following deafferentation begin in the more simple synaptic arrays and extend to the complex synaptic field later, after 90 days. If this occurs, the pattern of change in the turtle is slower than in the rat, since in the latter the density of substance P immunoreactivity showed a significant reduction at 4 days, which reached almost complete terminal restoration at 2 months following deafferentation (19). Nevertheless, if this is true, this slow rate of change in the turtle may permit researchers to follow step by step the modifications resulting from peripheral nerve section. This characteristic makes the turtle an excellent model for the investigation of the anaerobic process, that may be common to all vertebrate brains, since the sequence of mammal changes occurs so rapidly that is difficult to follow it (20). However, it is possible that the difference between turtle and rat could be due to a lack of recovery in the turtle, since the observations did not continue beyond 90 days.

It is difficult, at this time, to say that the changes only resulted from primary afferent degeneration. Further experiments using electron microscopy and anterograde and retrograde tracers will be necessary. In addition, it is early to speculate whether the actions of substance P are similar in turtles and mammals, and it is evident that to understand the significance and real role of this neuropeptide in the turtle spinal cord, multiple approaches, including biochemical, cytochemical, other immunohistochemical, molecular and other physiological procedures will be necessary. However, the observations reported here suggest that the similarity is probable. Actually, interest in more simple, experimentally resistant biological material is increasing. Within this context, the turtle should not be ignored as a model for the study of substance P actions and could offer new insights into nociception, since this neuropeptide is involved in the modulation of pain-related information in mammals.

Acknowledgments

We would like to thank Christiane de Queiroz Lopes and Eudira da Luz Amaral for technical assistance.

References

1. Fields HL (1994). Peripheral neuropathic pain: An approach to management. In: Wall PD & Melzack R (Editors), *Textbook of Pain*. Churchill Livingstone, New York, NY, USA.
2. Tessler A, Himes BT, Krieger NR, Murray M & Goldberger ME (1985). Sciatic nerve transection produces death of dorsal root ganglion cells and reversible loss of substance P in spinal cord. *Brain Research*, 332: 209-218.
3. Wang SD, Goldberger ME & Murray M (1991). Plasticity of spinal systems after unilateral lumbosacral dorsal rhizotomy in the adult rat. *Journal of Comparative Neurology*, 304: 555-568.
4. Northcutt RG (1970). *The Telencephalon of the Western Painted Turtle* (*Chrysemys picta bellis*). University of Illinois Press, Urbana, Chicago, London.
5. Reiner A, Krause JE, Keyser KT, Eldred WD & McKelvy JF (1984). The distribution of substance P in turtle nervous system: A radioimmunoassay and immunohistochemical study. *Journal of Comparative Neurology*, 226: 50-75.
6. Luthman J, Fernández A, Radmilovich M & Trujillo-Cenóz O (1991). Immunohistochemical studies on the spinal dorsal horn of the turtle *Chrysemys d'orbigny*. *Tissue and Cell*, 23: 515-523.
7. Belló AA & Belló-Klein A (1991). A technique to anesthetize turtles with ether. *Physiology and Behavior*, 50: 847-848.
8. De Felipe MC, Molinero MT & Del Río J (1989). Long-lasting neurochemical and functional changes in rats induced by neonatal administration of substance P antiserum. *Brain Research*, 485: 301-308.
9. Trujillo-Cenóz O, Fernández A & Radmilovich M (1990). Fine structure and synaptic connections of the spinal dorsal root terminals in the turtle *Chrysemys d'orbigny*. *Tissue and Cell*, 22: 811-826.
10. Ljungdahl A, Hökfelt T & Nilsson G (1978). Distribution of substance P-like immunoreactivity in the central nervous system of the rat. I. Cell bodies and nerve terminals. *Neuroscience*, 3: 861-944.
11. De Ceballos ML, Jenner P & Marsden CD (1999). Increased (met)enkephalin and decreased substance P in spinal cord following thermal injury to one limb. *Neuroscience*, 36: 731-736.
12. Aronin N, Difiglia M & Leeman SE (1983). Substance P. In: Krieger DT, Brownstein MJ & Martin JB (Editors), *Brain Peptides*. Wiley, New York, NY, USA.
13. Inagaki S, Senba E, Shiosaka S, Takagi H, Kawai Y, Takatsuki K, Sakanaka M, Matsuzaki T & Tohyama M (1981). Regional distribution of substance P-like immunoreactivity in the frog brain and spinal cord: Immunohistochemical analysis. *Journal of Comparative Neurology*, 201: 243-254.
14. Lorez HP & Kemali M (1981). Substance P-, met-enkephalin- and somatostatin-like immunoreactivity distribution in the frog spinal cord. *Neuroscience Letters*, 26: 119-124.
15. Lavalley AL & Ho RH (1983). Substance P, somatostatin, and methionine enkephalin immunoreactivity elements in the spinal cord of the domestic fowl, *Gallus domesticus*. *Journal of Comparative Neurology*, 213: 406-413.
16. Jessell T, Tsunoo A, Kanazawa I & Otsuka M (1979). Substance P: Depletion in the dorsal horn of the rat spinal cord after section of the peripheral processes of primary sensory neurons. *Brain Research*, 168: 247-259.
17. Murray M & Goldberger ME (1986). Replacement of synaptic terminals in lamina II and Clarke's nucleus after unilateral lumbosacral dorsal rhizotomy in adult cats. *Journal of Neuroscience*, 16: 3205-3217.
18. Croul S, Svertink A, Radzievsky A & Murray M (1995). Modulation of neurotransmitter receptors following unilateral L1-S2 deafferentation: NK1, NK3, NMDA, and 5HT1a receptor binding autoradiography. *Journal of Comparative Neurology*, 361: 633-644.
19. Zhang B, Goldberger ME & Murray M (1993). Proliferation of SP and 5HT containing terminals in lamina II of rat spinal cord following dorsal rhizotomy: Quantitative EM-immunocytochemical studies. *Experimental Neurology*, 123: 51-64.
20. Lutz PL (1992). Mechanisms for anoxic survival in the vertebrate brain. *Annual Review of Physiology*, 54: 601-618.

Available online at www.sciencedirect.com
SCIENCE DIRECT
Brain Research 986 (2003) 200–205
BRAIN RESEARCH
www.elsevier.com/locate/brainres

Short communication

Failure of estrogen to protect the substantia nigra pars compacta of female rats from lesion induced by 6-hydroxydopamine

Anete Curte Ferraz[a,*], Léder Leal Xavier[b], Sílvia Hernandes[a], Martha Sulzbach[a], Giordano Gubert Viola[b], Janete A. Anselmo-Franci[c], Matilde Achaval[b], Claudio Da Cunha[a]

[a]*Laboratório de Fisiologia e Farmacologia do Sistema Nervoso Central, Departamento de Fisiologia e Farmacologia, Universidade Federal do Paraná, C.P. 19.031, 81.531-990 Curitiba, PR, Brazil*
[b]*Laboratório de Histofisiologia Comparada, Departamento de Ciências Morfológicas, Instituto de Ciências Básicas da Saúde, Universidade Federal do Rio Grande do Sul, Rua Sarmento Leite 500, 90.050-170 Porto Alegre, RS, Brazil*
[c]*Faculdade de Odontologia Ribeirão Preto, Departamento de Morfologia, Estomatologia e Fisiologia, Av. Café s/n[0], 14.040-904 Ribeirão Preto, SP, Brazil*

Accepted 9 June 2003

Abstract

The immunostaining for tyrosine hydroxylase (TH) in the substantia nigra pars compacta (SNpc) and in the ventral tegmental area (VTA) after intranigral infusion of 6-hydroxydopamine (6-OHDA, 6 μg/side) was analyzed in ovariectomized adult female Wistar rats. Estrogen replacement for 52 days (400-μg 17-β-estradiol capsules) did not prevent the loss of TH-immunoreactive cells induced by 6-OHDA in the SNpc. This result indicates that the neuroprotective effect of dopaminergic mesencephalic cells is not observed with long-term estrogen replacement.

Theme: Disorders of the nervous system

Topic: Degenerative disease: Parkinson's

Keywords: Neuroprotection; 6-Hydroxydopamine; Parkinson's disease; Estrogen; Substantia nigra pars compacta

Mesencephalic dopaminergic cells are among the elements of basal ganglia most vulnerable to neurodegeneration [1,3]. Parkinson's disease (PD) results from the degeneration of these dopaminergic neurons in the substantia nigra pars compacta (SNpc) and, to a lesser extent, in the retrorubral field and ventral tegmental area (VTA) [5,6,15,17,19]. This disease causes progressive impairment of motor, autonomic, cognitive and mood functions [27]. PD affects ~1% of the population under 50 years of age and several studies have reported that males are more affected than females [11,13,14,22].

Increasing evidence supports a neuroprotective role for estrogen in neurodegenerative disease (e.g. Alzheimer and PD), stroke, and seizure-induced hippocampal cell loss [16,20,29]. The neuroprotective role of estrogen in PD is partly supported by animal studies showing that high estrogen levels observed in females can protect mesencephalic dopaminergic cells from degeneration. The neuroprotective action of estrogen against 1-methyl-4-phenyl-1,2,3,6-tetrahydropyridine (MPTP) has being consistently reported in various studies on mice [7,10,12,13,18], but fewer studies have reported the effect of estrogen on 6-hydroxydopamine (6-OHDA)-induced DA depletion in female rats [9,23]. In view of the importance of this subject for planning estrogen replacement therapy for women after menopause and also for the search for neuroprotective treatment for PD, we decided to further study the effect of estrogen replacement on the survival of dopaminergic mesencephalic cells insulted with 6-OHDA in ovariectomized rats.

A total of 24 adult female Wistar rats from our own breeding stock weighing 220–250 g at the beginning of the

*Corresponding author. Tel.: +55-41-361-1722; fax: +55-41-361-1722.
E-mail address: anete@ufpr.br (A.C. Ferraz).

0006-8993/03/$ – see front matter
doi:10.1016/S0006-8993(03)03198-6

experiments were used. The animals were maintained in a temperature-controlled room (22±2 °C) on a 12/12-h light cycle (lights on at 7:00 a.m.) and had free access to food and water. All efforts were made to minimize animal suffering and both Brazilian laws and the recommendations of the National Institute of Health guide for experimental animal care were strictly followed.

Ovariectomy, estrogen replacement and substantia nigra lesion were planned to determine if high circulating estrogen concentrations would protect against dopaminergic mesencephalic cell lesion according to the experimental groups described in Table 1.

The ovaries of the rats were bilaterally removed under ethyl-ether anesthesia and a 15-mm-long Silastic capsule (Down Corning, Midland, MI) was implanted subcutaneously close to the region of the removed ovaries. The capsules implanted in 12 rats contained 400 μg/8 μl of 17-β estradiol (Sigma, St. Louis, MO) diluted with corn oil; capsules implanted in 12 other rats (controls) contained only corn oil. Plasma estradiol concentration was monitored using blood samples collected from the rat tails 10 and 52 days after ovariectomy and capsule implantation. A vaginal smear was collected and analyzed every week after capsule implantation to determine the efficiency of estradiol treatment.

The experimental schedule for the groups is presented in Table 1. At 7 days after ovariectomy and capsule implantation, two groups of four rats each with and without estrogen replacement, respectively, received atropine sulfate (0.4 mg/kg, i.p.) to suppress salivation, and penicillin G-procain (20,000 U in 0.1 ml, i.m.), and were anesthetized with 40 mg/kg sodium thiopental (i.p.). 6-OHDA HCl (Sigma, 6 μg in 2 μl of artificial cerebrospinal fluid (aCSF), 0.33 μl/min) was bilaterally infused into the SNpc through a 30-gauge needle. Two other groups of four rats each, with and without estrogen replacement, respectively, were sham-operated, i.e. submitted to the same procedure, but 2 μl of aCSF was infused into the SNpc instead of 6-OHDA. Two other groups of four rats each were not submitted to stereotaxic surgery and are referred to as non-operated groups with and without estrogen replacement, respectively. The coordinates for the injections were: anteroposterior (AP) −5.0 mm from bregma, mediolateral (ML) ±2.1 mm from midline, dorsoventral (DV) −7.7 mm from skull, adapted from Paxinos and Watson [25]. The composition of aCSF was as follows: 8.66 g NaCl, 0.250 mg KCl, 0.76 g $CaCl_2 \cdot 2H_2O$, and 0.173 g $MgCl_2 \cdot 6H_2O$.

Table 1
Experimental schedule of the groups

Experimental group	Intranigral 6-OHDA treatment	Hormonal treatment
C	Non-operated control	Oil
C/E	Non-operated	Estradiol
S	Sham-operated	Oil
S/E	Sham-operated	Estradiol
6-OHDA	Lesioned	Oil
6-OHDA/E	Lesioned	Estradiol

Ovariectomy and subcutaneous implant of a capsule with 17-β-estradiol were performed 7 days before intranigral treatment. Animals received intranigral 6-OHDA infusion and were sacrificed for nigral tyrosine hydroxylase immunostaining analysis 52 days after ovariectomy, respectively. C, control group; E, estrogen treatment; S, sham-operated group; 6-OHDA, 6-hydroxydopamine treatment.

At 52 days after ovariectomy, under deep anesthesia (200 mg/kg sodium thiopental), the animals were transcardially perfused with saline solution followed by a solution of 4% paraformaldehyde in 0.1 M phosphate buffer, pH 7.4 (PB). After perfusion, the brains were removed from the skulls, post-fixed in the same solution at room temperature for 2 h and cryoprotected by immersion in 30% sucrose solution in PB at 4 °C until they sank. For each brain, serial coronal sections (50 μm) were obtained using a cryostat (Leitz, Digital 1702) at −20 °C and collected in PB. For immunohistochemistry, the free-floating sections were pretreated with 10% methanol diluted in 3% hydrogen peroxidase for 30 min, carefully washed and blocked with 3% normal goat serum (NGS) in 0.1 M phosphate buffer, 0.9% NaCl, pH 7.4 (PBS) containing 0.3% Triton X-100 (PBS-Tx, Sigma) for 30 min and incubated with monoclonal tyrosine hydroxylase (TH) antibody raised in mice (Sigma) diluted 1:750 with 3% NGS in PBS-Tx for 48 h at 4 °C. After washing several times with PBS-Tx, tissue sections were incubated with a biotinylated secondary antibody (Dako, Carpinteria, CA) diluted 1:200 in PBS-Tx at room temperature for 2 h. Sections were washed again in PBS and incubated with peroxidase-conjugated streptavidin (Dako) diluted 1:100 in PBS for 90 min at room temperature. The immunohistochemical reaction was developed by incubating the sections in a medium containing 0.06% 3,3 diaminobenzidine (DAB, Sigma) dissolved in PBS for 10 min, and then in the same solution containing 1 μM of 3% H_2O_2 per ml of DAB medium for 10 min. Next, the sections were rinsed with PBS, dehydrated with ethanol, cleared with xylene, and covered with Permount and coverslips. Control sections were prepared by omitting the primary antibody and replacing it with PBS. The brains of the animals were fixed and postfixed for the same time in identical solutions and rigorously processed at the same time, and the sections were incubated in an identical medium for the same period of time. This precaution was taken to avoid overreaction, differences in chromogen reaction, saturation of optical density, and changes in background levels. Coronal sections of substantia nigra were selected for this immunohistochemical study. These areas were identified according to the atlas of Paxinos and Watson [25] and the readings were made between the coordinates interaural 4.2 mm, bregma −4.8 mm and interaural −2.7 mm, bregma −6.3 mm. The intensity of the reaction product of TH was measured semi-quantitatively using a Nikon Eclipse E-600

(50×) microscope coupled to a Pro-Series High Performance CCD camera and Image Pro Plus Software 4.1 (Media Cybernetics, Carlsbad, CA). Data were obtained and the selected areas were converted to an 8-bit gray scale (0–255 gray levels). The measurements were made by placing a 19,600-μm^2 sampling box, area of interest (AOI), on the SNpc and VTA. Obvious blood vessels and other artifacts were avoided. The readings were performed in both hemispheres and at least 30 readings per animal were obtained. The size and shape of the AOI were determined in order to avoid the borders of the SNpc and VTA and to collect a significant number of pixels from this area. All lighting conditions and magnifications were held constant. Moreover, the investigator was unaware of the experimental groups from which the slices were obtained. The staining generated from a non-reactive tissue was measured and the mean obtained, which represents the background staining, was used to set the gray scale [24,26]. The algorithm of optical density used in the present study is based on the following formula [24]:

$$OD_{(x,y)} = -\log[(background_{(x,y)} - black) - (Intensity_{(x,y)} - black)/(INCIDENT - BLACK)]$$

where *OD* is optical density, $background_{(x,y)}$ is the mean intensity of background staining, $Intensity_{(x,y)}$ is the intensity at $pixel_{(x,y)}$, *black* is the intensity generated when no light goes through the material, and *INCIDENT* is the intensity of the incident light. The optical density measured in different sections was averaged by rat. The number of tyrosine hydroxylase immunoreactive neurons (TH-IR) per mm^2 in the SNpc and in the VTA was estimated using the same software employed to measure the optical density. Briefly, a square of known area (0.012 mm^2) was overlaid on the analyzed regions. The TH-IR neurons located inside this square or intersected by the lower and/or right edge of the square were counted. The neurons that were intersected by the upper and/or left edge of the square were not counted. At least ten sections were analyzed in each brain.

Data were analyzed by two- or three-way ANOVA taking the estrogen and 6-OHDA treatments as dependent variables and the day of the sample collection as repeated measures. Differences between groups were further analyzed by the post hoc Scheffé test.

The plasma concentrations of 17-β-estradiol in ovariectomized rats implanted or not with the capsule are presented in Table 2. The animals implanted with capsules presented higher plasma 17-β-estradiol concentration 10 days after capsule implantation compared to the concentration observed 52 days after capsule implantation ($F(1,18)=21.21$; $P=0.0002$). Nevertheless, even on the 52nd day, the plasma 17-β-estradiol concentration was higher than in control animals with oil capsule implantation ($F(1,18)=64.65$); $P<0.0001$). The effectiveness of estradiol treatment was also confirmed by analysis of vaginal smears that showed corneified cells typical of the estrous phase throughout the study period.

Table 2
Plasma 17-β-estradiol concentration in ovariectomized rats treated or not with this hormone

Experimental group	17-β-Estradiol (pg/ml)	
	Day 10	Day 52
C	12.8±0.7	13.9±1.8
C/E	104.6±19.5[a]	48.1±16.3[a]
S	10.5±1.5	10.8±1.2
S/E	107.0±22.9[b]	22.4±22.5[b]
6-OHDA	8.3±1.1	11.7±1.9
6-OHDA/E	88.6±23.1[c]	31.0±3.5[c]

Blood samples were collected 10 and 52 days after ovariectomy and capsule implant. Values are expressed as mean±S.E.M.; Day 10 and Day 52 refer to days after subcutaneous estrogen capsule implantation. C, control group; E, estrogen treatment; S, sham-operated group; 6-OHDA, 6-hydroxydopamine treatment.

[a] $P\leq0.05$ compared to control group without estradiol treatment, Scheffé test after three-way ANOVA.

[b] $P\leq0.05$ compared to control group without estradiol treatment, Scheffé test after three-way ANOVA.

[c] $P\leq0.05$ compared to control group without estradiol treatment, Scheffé test after three-way ANOVA.

The effect of treatment of the rats with 6-OHDA and estrogen on SNpc lesion is presented in Figs. 1 and 2. Two-way ANOVA showed that the 6-OHDA treatment caused a significant decrease in the optical density of TH immunostaining in the SNpc ($F(2,16)=35.24$; $P\leq0.001$), and in the TH-immunostained neuronal density in the SNpc ($F(2,16)=111.54$; $P\leq0.001$). Furthermore, estrogen treatment did not protect SNpc neurons from the 6-OHDA-induced lesion (TH immunostaining in the SNpc: $F(1,16)=0.59$; $P=0.45$ and TH-immunostained neuronal density in the SNpc: $F(1,16)=0.20$; $P=0.65$). Neither 6-OHDA nor estrogen treatments affected the optical density (6-OHDA treatment: $F(2,16)=2.75$; $P=0.09$ and estrogen treatment: $F(1,16)=0.68$; $P=0.42$) or the neuronal density (6-OHDA treatment: $F(2,16)=2.07$; $P=0.15$ and estrogen treatment: $F(1,16)=1.07$; $P=0.31$) of TH immunostained tissue in the VTA.

The present results suggest that estrogen does not decrease the neurotoxicity of 6-OHDA on SNpc neurons, at least under the conditions used in our study. Two other studies by Dluzen et al. [9] and Murray et al. [23] suggested that estrogen presents a protective effect against the decrease in striatal DA depletion induced by 6-OHDA. The former study showed a modest, but significant, effect of estrogen replacement in ovariectomized rats lesioned with an intrastriatal infusion of 6-OHDA. The latter study showed a more consistent protective effect of estrogen against DA depletion after the infusion of 6-OHDA into the medial forebrain bundle of ovariectomized rats. The contradictory results obtained in the present study and these other two studies may be due to the methodological differences between them. One of these differences was the

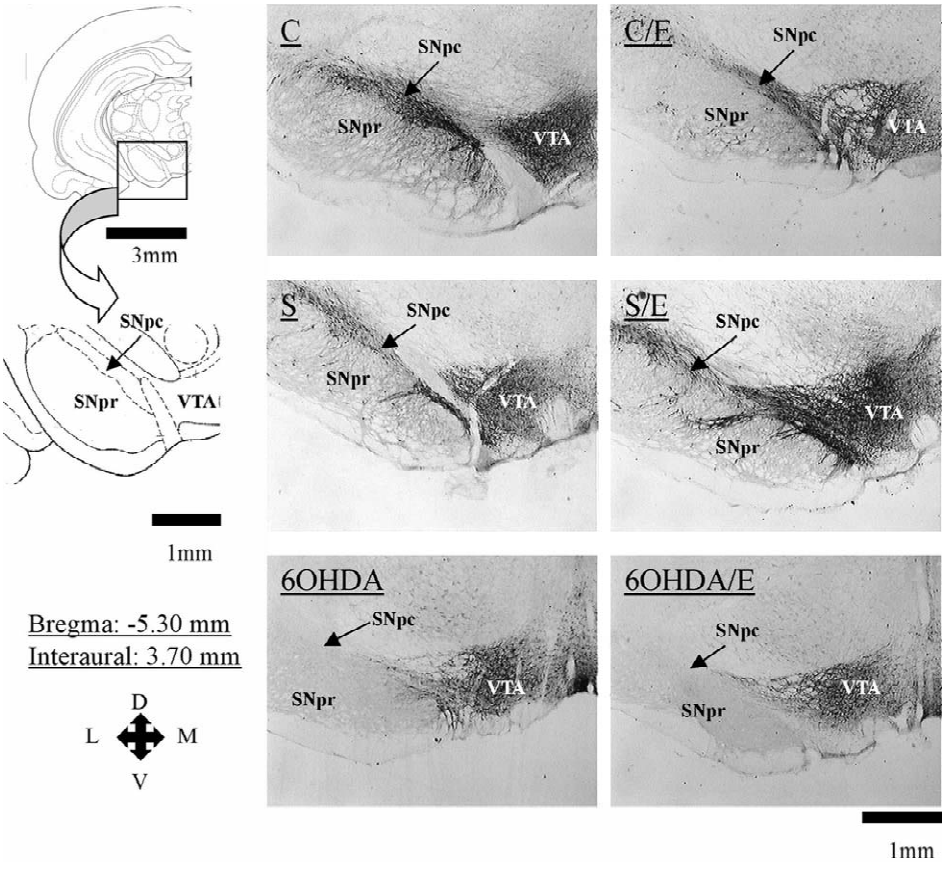

Fig. 1. Digitized images of substantia nigra and ventral tegmental area after different treatments. Note the decreased TH immunoreactivity found in SNpc, but not in VTA, in the animals treated with 6-OHDA. C, control group; E, estrogen treatment; 6-OHDA, 6-hydroxydopamine treatment; S, sham-operated group; SNpc, substantia nigra-pars compacta; SNpr, pars reticulata; VTA, ventral tegmental area. The schematic drawings were modified from the atlas of Paxinos and Watson [25].

site of 6-OHDA administration (SNpc, striatum and medial forebrain bundle). Another difference was the dose of 6-OHDA that varied from 1 to 18 μg. It is important to note that in the study by Murray et al. [23], the protective effect of estrogen replacement was observed only for doses of 6-OHDA lower than 3 μg. The dose used in the present study (6 μg/side) was reported to be resistant to the neuroprotective effect of estrogen by Murray et al. [23]. We can also emphasize that these two previous studies did not investigate cell survival but only the physiological capacity of the remaining neurons to produce/release DA since they reported higher striatal DA concentrations in estrogen-treated rats, while our study investigated the density of TH-immunoreactive neurons. It is possible that the same number of surviving cells present different concentration of DA after estrogen replacement. Thus, it is important to note that most of the studies reporting a neuroprotective effect of estrogen on mesencephalic dopaminergic cells in mice also reported a decreased DA release induced by MPP^+ [2,7,8], but did not estimate dopaminergic cell survival. Similarly, Callier et al. [4] did not find a neuroprotective effect of estrogen against MPP^+ insult at a concentration at which the hormone is specific for dopaminergic cells in primary culture.

However, the most important difference between the present study and the studies by Dluzen [9] and Murray et al. [23] was that they sacrificed the animals 7–10 days after the 6-OHDA insult while we tested SNpc neuron survival 45 days after intranigral 6-OHDA infusion. It is possible that estrogen replacement protected some injured dopaminergic cells from death for a limited period of time (at least 10 days) but that these cells may die later on. On this basis, it is interesting to note that estrogen concentration was higher 3 days after 6-OHDA infusion than 45 days later. Since PD presents long-term development and the hormonal treatment lasts many years from menopause to the end of life, its effectiveness for long-term neuroprotection of the SNpc neurons is questionable.

Our results showed that even 52 days after capsule implantation, plasma estrogen concentrations were higher compared to the control rats implanted with oil capsules and within the physiological concentration range for a cycling rat, which does not reach levels higher than 50 pg/ml [28]. However, a few days after capsule implanta-

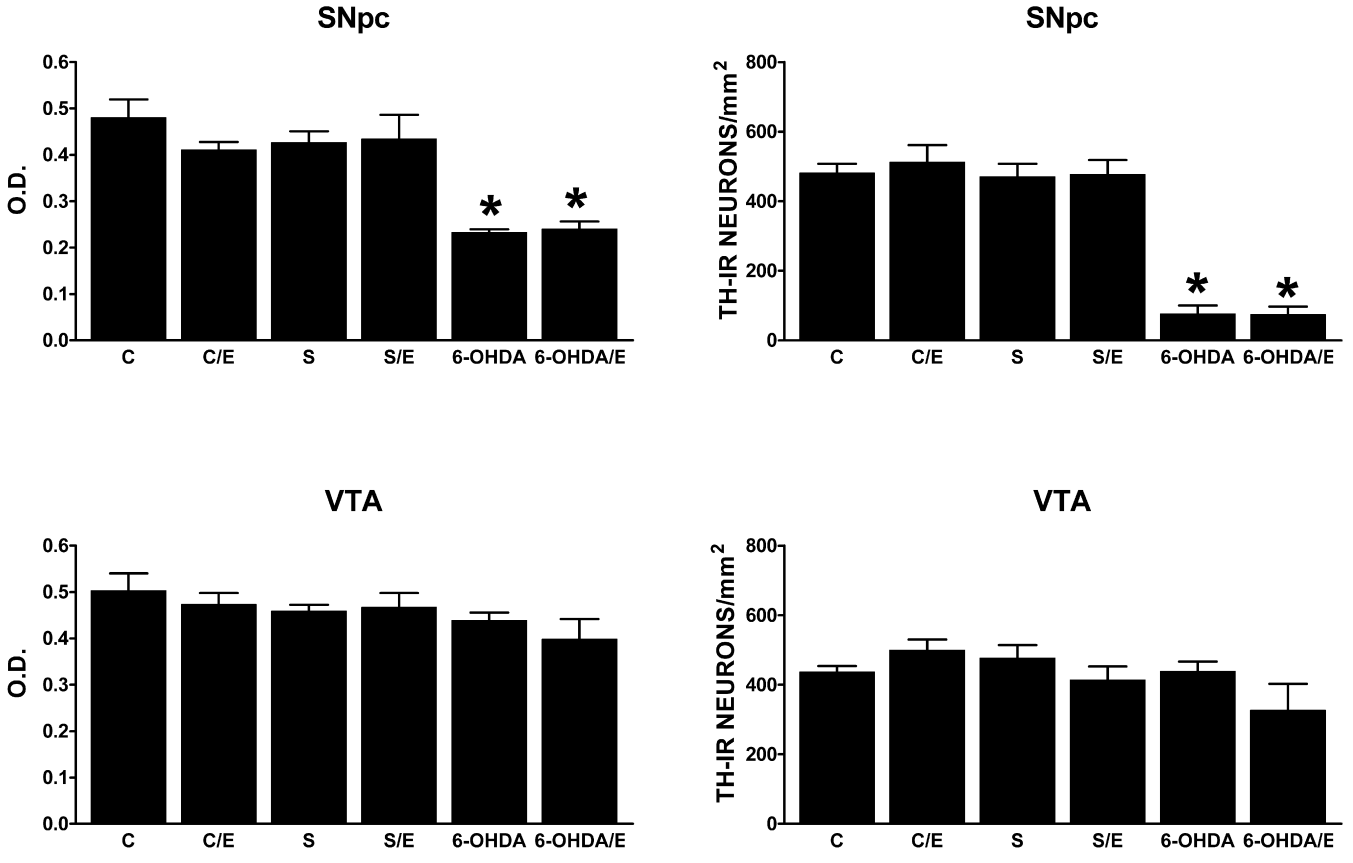

Fig. 2. Effects of 6-OHDA and estrogen treatments on optical density measurements (OD) and neuronal density of tyrosine hydroxylase immunoreactive neurons (TH-IR) in the substantia nigra pars compacta (SNpc) and tegmental ventral area (VTA) of ovariectomized rats. Values are expressed as means±S.E.M. C, control group; E, estrogen treatment; 6-OHDA, 6-hydroxydopamine treatment; S, sham-operated group. *$P<0.05$ compared to the C, C/E, S or S/E groups, Scheffé test after two-way ANOVA.

tion, the 17-β-estradiol concentration in plasma was higher than 100 pg/ml. A study by Leranth and coworkers [21] reported a neuroprotective effect of 80–90 pg/ml 17-β-estradiol concentration in plasma in female monkeys. Since in the other studies plasma estradiol concentrations were not measured and the neuroprotective effect was reported a few days after capsule implantation, the time when our data showed the highest plasma estradiol levels, it is possible that supraphysiological plasma estrogen concentrations are necessary for an effective neuroprotective effect on SNpc cells. If this is the case, one should be aware of the fact that potentially risky higher doses of estrogen replacement therapy would be necessary to prevent or treat PD in postmenopausal women.

In summary, the present study shows that long-term estrogen replacement treatment of ovariectomized rats did not protect SNpc neurons from an insult with 6-OHDA and indicates that the potential neuroprotective effect of estrogen may occur only under special circumstances. Therefore the potential neuroprotective effect of estrogen on SNpc cells should be considered more carefully when planning estrogen replacement therapy with the objective of preventing or slowing down the progress of PD.

Acknowledgements

This research was partly supported by CNPq and CAPES.

References

[1] T. Araki, T. Kumagai, K. Tanaka, M. Matsubara, H. Kato, Y. Itoyama, Y. Imai, Neuroprotective effect of riluzole in MPTP-treated mice, Brain Res. 918 (2002) 176–181.
[2] M. Arvin, L. Fedorkova, K.A. Disshon, D.E. Dluzen, R.E. Leipheimer, Estrogen modulates responses of striatal dopamine neurons to MPP^+: evaluations using in vitro and in vivo techniques, Brain Res. 872 (2000) 160–171.
[3] F. Blandini, G. Nappi, C. Tassorelli, E. Martignoni, Functional changes of the basal ganglia circuitry in Parkinson's disease, Prog. Neurobiol. 62 (2000) 63–88.
[4] S. Callier, M. Le Saux, A.M. Lhiaubet, P. Di Paolo, W. Rostène, D. Pelaprat, Evaluation of the protective effect of oestradiol against toxicity induced by 6-hydroxydopamine and 1-methyl-4-phenylpyridinium ion (MPP^+) towards dopaminergic mesencephalic neurons in primary culture, J. Neurochem. 80 (2002) 307–316.
[5] P. Damier, E.C. Hirsch, Y. Agid, A.M. Graybiel, The substantia nigra of the human brain II. Nigrosomes and the nigral matrix, a

compartmental organization based on calbindin D28k immunohistochemistry, Brain 122 (1999) 1421–1436.
[6] P. Damier, E.C. Hirsch, Y. Agid, A.M. Graybiel, The substantia nigra of the human brain II. Patterns of loss of dopamine-containing neurons in Parkinson's disease, Brain 122 (1999) 1437–1448.
[7] K.A. Disshon, D.E. Dluzen, Estrogen as a modulator of MPTP-induced neurotoxicity: effects upon striatal dopamine release, Brain Res. 764 (1997) 9–16.
[8] K.A. Disshon, D.E. Dluzen, Estrogen reduces acute striatal dopamine responses in vivo to the neurotoxin MPP^+ in females, but not male rats, Brain Res. 868 (2000) 95–104.
[9] D. Dluzen, Estrogen decreases corpus striatal neurotoxicity in response to 6-hydroxydopamine, Brain Res. 767 (1997) 340–344.
[10] D.E. Dluzen, Neuroprotective effects of estrogen upon the nigrostriatal dopaminergic system, J. Neurocytol. 29 (2000) 387–399.
[11] D.E. Dluzen, J.L. McDermott, Gender differences in neurotoxicity of the nigrostriatal dopaminergic system: implications for Parkinson's disease, J. Gend. Specific Med. 3 (2000) 36–42.
[12] D.E. Dluzen, J.L. McDermott, B. Liu, Estrogen as a neuroprotective against MPTP-induced neurotoxicity in C57/B1 mice, Neurotoxicol. Teratol. 18 (1996) 603–606.
[13] D.E. Dluzen, K.A. Disshon, J. McDermott, Estrogen as a modulator of striatal dopaminergic neurotoxicity, in: J. Marwah, H. Teitelbaum (Eds.), Recent Advances in Neurodegenerative Disorders, Prominent Press, Scottsdale, 1998, pp. 149–192.
[14] R.C. Duvoisin, Parkinson's Disease, 3rd Edition, Raven Press, New York, 1991.
[15] J.M. Fearnley, A.J. Lees, Ageing and Parkinson's disease: substantia nigra regional selectivity, Brain 114 (1991) 2283–2301.
[16] A.S. Galanopoulou, E.M. Alm, J. Velíimagek, Estradiol reduces seizure-induced hippocampal injury in ovariectomized female but not in male rats, Neurosci. Lett. 342 (2003) 201–205.
[17] D.C. German, K. Manaye, W.K. Smith, D.J. Woodward, C.B. Saper, Midbrain dopaminergic cell loss in Parkinson's disease: computer visualization, Ann. Neurol. 26 (1989) 507–514.
[18] M. Grandbois, M. Morissette, S. Callier, T. Di Paolo, Ovarian steroids and raloxifene prevent MPTP-induced dopamine depletion in mice, Neuroreport 11 (2000) 343–346.
[19] G.M. Halliday, D.A. McRitchie, H.R. Cartwright, R.S. Pamphlett, M.A. Hely, J.G.L. Morris, Midbrain neuropathology in idiopathic Parkinson's disease and diffuse Lewy body disease, J. Clin. Neurosci. 3 (1996) 52–60.
[20] P.D. Hurn, I.M. Macrae, Estrogen as a neuroprotectant in stroke, J. Cereb. Blood Flow Metab. 20 (2000) 631–652.
[21] C. Leranth, R.H. Roth, J.D. Elswoth, F. Naftolin, T.L. Horvath, D.E. Redmond Jr., Estrogen is essential for maintaining nigrostriatal dopamine neurons in primates: implications for Parkinson's disease and memory, J. Neurosci. 20 (2000) 8604–8609.
[22] R. Mayeux, J. Denaro, N. Hermenegildo, K. Marder, M.X. Tang, L.J. Cote, Y. Stern, A population-based investigation of Parkinson's disease with and without dementia. Relationship to age and gender, Arch. Neurol. 49 (1992) 492–497.
[23] H.E. Murray, A.V. Pillai, S.R. McArthur, N. Razvi, K.P. Datla, D.T. Dexter, G.E. Gillies, Dose- and sex-dependent effects of the neurotoxin 6-hydroxydopamine on the nigrostriatal dopaminergic pathway of adult rats: differential actions of estrogen in males and females, Neuroscience 116 (2003) 213–222.
[24] W.A. Partata, J.F. Cerveira, L.L. Xavier, G.G. Viola, M. Achaval, Sciatic nerve transection decreases substance P immunoreactivity in the lumbosacral spinal cord of the frog (*Rana catesbeiana*), Comp. Biochem. Physiol. A 131 (2002) 807–814.
[25] G. Paxinos, C. Watson, The Rat Brain in Stereotaxic Coordinates, Academic Press, San Diego, 1997.
[26] A.A. Rasia-Filho, L.L. Xavier, N. Santos, G. Gehlen, M. Achaval, Glial fibrillary acidic protein immunodetection and immunoreactivity in the anterior and posterior medial amygdala of male and female rats, Brain Res. Bull. 58 (2002) 67–75.
[27] L.M. Shulman, Is there a connection between estrogen and Parkinson's disease?, Parkinsonism Relat. Disord. 8 (2002) 289–295.
[28] M.S. Smith, M.C. Freeman, J.D. Neill, The control of progesterone secretion during the estrous cycle and early pseudopregnancy in the rat: prolactin, gonadotropin and ovarian steroids associated with rescue of the corpus luteum of pseudopregnancy, Endocrinology 96 (1975) 219–226.
[29] P.M. Wise, Estrogens and neuroprotection, Trends Endocrinol. Metab. 13 (2002) 229–230.

Receiving Editor
Dr Takeshi Kaneko
Department of Morphological Brain Science
Graduate School of Medicine
Kyoto University
e-mail: kaneko@mbs.med.kyoto-u.ac.jp

Preconditioning changes cytochrome oxidase activity and hippocampal volume after global cerebral ischemia

Léder Leal Xavier[1,2] , Pedro Rosa Neto[1,2] , Giordano Gubert Viola[2], Paulo Worm[1] , Carlos Alexandre Netto[1], Matilde Achaval[2]

Departments of [1]Biochemistry and [2]Morphological Sciences, Basic Health Sciences Institute of the Federal University of Rio Grande do Sul. Porto Alegre, Rio Grande do Sul, Brazil.

22 Pages; 1 Table; 3 Figures

*Corresponding Author:
Matilde Achaval
Laboratório de Histofisiologia Comparada
Departamento de Ciências Morfológicas
Instituto de Ciências Básicas da Saúde
Universidade Federal do Rio Grande do Sul
Rua Sarmento Leite 500
90050-170
Porto Alegre, RS, Brazil.
Telephone: +55-51-3316-36-24
Fax: +55-51-3316-30-92
E-mail: achaval@ufrgs.br

Abstract

Preconditioning by a sublethal ischemic event attenuates hippocampal cell death and neurochemical outcomes occurring after a prolonged, lethal, ischemic event in rodents. We tested whether one aspect of brain energy metabolism, i.e., cytochrome oxidase activity, would change after different periods of transient forebrain ischemia and reperfusion and if ischemic preconditioning attenuates these effects. Rats were divided into four experimental groups: a) control; b) receiving 2 minutes of ischemia, sublethal ischemia; c) receiving 10 minutes of ischemia, lethal ischemia and d) preconditioned, animals submitted to a 10 min ischemic episode 24 hours after the 2 min ischemic event. Animals were sacrificed immediately, 24 hours, 48 hours or 7 days after the event and histochemistry for cytochrome oxidase was run, followed by a semi-quantitative densitometric analysis. The stereological volume estimation of the CA1 and dentate gyrus fields of hippocampus of rats submitted to the same periods of ischemia and reperfused for 30 days was also obtained, in order to relate tissue loss with changes in enzyme activity.

Our results were: a) both sublethal and lethal ischemic events increase cytochrome oxidase activity in strata oriens, pyramidale and radiale, this effect was reversed by the ischemic preconditioning, b) there was an increase in cytochrome oxidase activity in all hippocampal subfields 24 hours after lethal ischemia, that was not reduced by ischemic preconditioning c) there are no differences in cytochrome oxidase activity between control and ischemic groups seven days after the event. In the stereological study, a significant decrease of CA1 volume after lethal ischemia was observed and that was prevented by ischemic preconditioning. We suggest that the maintenance of cytochrome oxidase activity caused by the preconditioning episode could be related to the CA1 neuronal survival caused by this event.

Keywords: Ischemia; Ischemic Preconditioning; Hippocampus; Cytochrome Oxidase; Stereology

1.Introduction

Transient global cerebral ischemia is an important cause of neurological impairment and neuronal death (Pulsinelli and Duffy, 1983). Some brain regions are more susceptible to neuronal damage than others; a phenomenon called "selective vulnerability" (Schimidt-Kaster and Freund, 1991). Although the CA1 hippocampal subfield is particularly sensitive to cerebral ischemia, presenting a characteristic pattern of neuronal death, the dentate gyrus is well preserved after a transient ischemic event (Kirino, 1982; Pulsinelli et al., 1982; Schimidt-Kaster and Freund, 1991).

Cellular and molecular mechanisms involved in cell death due to cerebral ischemia and the neurochemical basis of selective vulnerability are not completely understood. The elevation in extracellular levels of excitatory amino acids such as glutamate and aspartate, a disturbance in calcium homeostasis, the activation of calcium dependent enzymes, increases in oxygen free radical formation, activation of specific genes and a specific increase in protein synthesis are probably involved in the neuronal death after ischemia (Dienel et al., 1980; Rothman and Olney, 1986; Silver and Erecinska, 1992; Kogure and Kato, 1993).

Previous studies showed that rodents made tolerant to brain ischemia, i.e., receiving a sublethal ischemic episode 24h before a lethal ischemic insult, exhibit a significant attenuation of neuronal damage observed in hippocampus (Kirino et al., 1991). Although the mechanisms underlying neuronal survival promoted by ischemic preconditioning remain to be determined, a few molecular events have been suggest to participate: the upregulation of neuroprotective genes; the changes in protein synthesis; the inhibition of post-ischemic activation of N-methyl-D-aspartate (NMDA) glutamate receptors; the A1 adenosine receptor activation and, more recently, the decrease in mitocondrial activity (Nagagomi et al., 1993; Heurteaux, et al., 1995; Kato et al., 1995; Kawai et al., 1998; Wiegand et al., 1999; Currie et al., 2000; Maruoka et al., 2002; Truettner et al., 2002).

Cytochrome oxidase (CO) (Ferrocytochrome C: oxygen oxidoreductase EC1.9.3.1) is at the end of the mitochondrial respiratory chain; along with other chain enzymes it is responsible for pumping protons from the mitochondrial matrix to the intermembrane space, generating an electrochemical proton gradient across the inner mitochondrial membrane which drives ATP synthase for ATP production in all animal brain cells (Gonzáles-Lima and Garrosa, 1991; Hevner et al., 1995; Vander-Heiden et al., 1997; Kadenbach et al., 2000). The levels of CO activity, as assessed by densitometry of histochemical preparation (Gonzáles-Lima and Garrosa, 1991; Hevner et al., 1995), has been proposed to be a sensitive index of mitochondrial activity, both in the resting state (Wong-Riley, 1989; Harley and Bielajew, 1992) and in different metabolic situations (Wong-Riley et al, 1997).

The present work was designed to test whether an ischemic event is able to promote changes in hippocampal CO activity and if this effect would be attenuated by the preconditioning episode. In addition we obtained an unbiased volume estimation of CA1 and dentate gyrus in animals submitted to the same periods of ischemia and reperfused for 30 days.

2. Materials and Methods

Animals

100 male adult Wistar rats weighing between 180 and 260 g were used in the present study. The animals were kept under a constant 12:12h light–dark cycle at a room temperature of 22± 1^{0}C and maintained with food and water a*d libitum*. All efforts were made to minimize animal suffering and to reduce the number of the animals needed. The Brazilian Laws and the National Institute of Health Guide for Animal Care and Use of Laboratory Animals were strictly followed.

Experimental groups

For CO histochemistry, the animals were divided into 4 groups: control, (20); animals receiving 2 minutes of ischemia, or sublethal ischemia, (20); animals submitted to 10 minutes of ischemia, lethal ischemia, (20) and animals with 2 minutes of ischemia followed by 24 hours of reperfusion and a 10 minutes event, named ischemic preconditioned (20). All ischemic groups were subdivided into 4 subgroups according to the reperfusion time (5 animals each): Immediately reperfused, (1 or 2 minutes) (0h), 24 hours (24h), 48 hours (48h), and 7 days (7d) of reperfusion. As for the stereological evaluation, animals were divided into the same 4 experimental groups, but sacrificed 30 days after the event. There were at least 5 animals per group.

Animal treatments

Transient forebrain ischemia was produced using the 4-vessel occlusion method (Pulsinelli and Brierley, 1979), with minor modifications (Valentim et al., 2001). Briefly, animals were anaesthetized with halothane mixed with breathing air and an occluding device (a loop of silicone tubing) was loosely placed around each carotid artery to allow subsequent occlusion of these vessels with minimal mechanical disturbances. The animals were then placed on a stereotaxic frame and the vertebral arteries were eletrocoagulated.

One day after surgery, a severe forebrain ischemia was produced by occluding both common carotid arteries. Animals that did not lose the righting reflex or that convulsed during the ischemic episode were not used in the experiments (Valentim et al., 2001). The control group was composed of naive, untouched animals.

Cytochrome oxidase histochemistry

Cytochrome oxidase activity was detected according to the method previously described by Wong-Riley (Wong-Riley, 1979). Under a deep chloral hydrate (35%) anesthesia (1ml /kg, i.p), the animals were transcardially perfused with cold saline solution followed by a solution of 4%

paraformaldehyde and 0.2% glutaraldehyde (Sigma) in 0.1 M phosphate buffer, pH 7.4 (PB), using a peristaltic pump (20 ml/ min). Their brains were then removed from their skulls, postfixed in a solution containing 4% paraformaldehyde in phosphate buffer (PB) at 4°C for 2 h and cryoprotected by immersion in 30% sucrose solution in PB, at 4°C overnight with continuous agitation. For each brain, serial coronal sections (50 μm) were obtained using a cryostat (Leitz, Digital 1702) at -20^0C and collected in cold (4^0C) PB. Free-floating sections were incubated at 37^0C for 4 hours in the cytochrome oxidase incubation medium, containing 1.54 mM 3.3 diaminobenzidine tetrahydrochloride (Sigma), 26 mM cytochrome c, type III (Sigma) and 0.12 mM sucrose dissolved in 90 ml of PB. After incubation, the sections were washed three times in PB, mounted onto gelatinized slides and then dehydrated in ethanol, cleared with xylene and covered with Permount (Fischer) and coverslips. For control, some sections were incubated without substrate. The histochemical procedure was divided in four different experiments (animals briefly reperfused (0h) and reperfused for 24hours, 48hours and 7 days); for this reason groups processed in different days are not to be compared .

Each experiment was performed under controlled conditions (fixation and postfixation periods), with the same reagent pool and incubation times, in order to avoid procedural biases in the experimental group.

Evaluation of cytochrome oxidase activity

The evaluation of cytochrome oxidase activity was made by regional densitometry (Gonzáles-Lima and Garrosa, 1991; Hevner et al., 1995; Ferraz et al., 2003). To measure reaction product intensity of CO histochemistry (semi-quantitative analysis) a Nikon Eclipse E-600 coupled to an Image Pro-Plus Software 4.1 (Media Cybernetics, USA) was used. After microscopic analysis of sections at a final magnification of 500 X, images of different regions of the hippocampus were obtained with a high resolution CCD camera (Pro-Series High Performance), microscopic fields

obtained were converted into black and white digital images and the optical density was measured. Optical densitometric readings were obtained from *strata oriens, pyramidal, radial* and *lacunosum-moleculare* of hippocampal formation from both hemispheres. These areas were identified according to the atlas of Paxinos and Watson (1998) between -1.8 mm and -4.52 mm coordinates from bregma. The readings were obtained by placing a 67 μm^2 sampling box over the analyzed region. Four readings were made for each region in every brain, consequently 20 samples *per* group *per* region were acquired. All lighting conditions and magnifications were held constant between sections and areas; additionally the investigator was unaware of the experimental groups from which the analyzed sections were obtained. The optical density was calculated using the following formula:

$OD_{(x,y)} = -\log [(INTENSITY_{(x,y)}-BLACK)/(INCIDENT-BLACK)]$

Where: OD = Optical Density; $INTENSITY_{(x,y)}$ is the intensity at pixel $_{(x,y)}$; BLACK is the intensity generated when no light goes through the material; INCIDENT is the intensity of the incident light. Results obtained represent the mean of all pixels in the selected area.

Volume estimation

After reperfusion, the animals were anaesthetized with sodium pentobarbital (60 mg /kg, i.p), transcardially perfused with saline solution followed by 10% formalin solution and the brains were removed, postfixed for 30 days in the same fixative solution and sectioned in the coronal plane at 100 μm thickness in a vibratome (Leica).

Tissue was stained using the Hematoxylin–Eosin method; the volume of CA1 and dentate gyrus regions were estimated by the application of Cavalieri design in combination with the point counting method (Gundersen and Jensen, 1987; Cruz-Orive, 1997). According to the Cavalieri principle the volume of an object may be estimated by cutting it into equally spaced sections. Thus, the images of hippocampal sections were digitized in the same software employed for OD

calculation. In each hippocampus, the first section analyzed was chosen using a random number table, the area of this section was estimated using a point counting method, where, a systematic array of test points was randomly placed on the digitized images and all points hitting the CA1 subfield and dentate gyrus were counted. This procedure was repeated into other equally spaced sections.

The volumes of CA1 and dentate gyrus were then calculated using the following formula: $\mathbf{V = t.\ a/p.\Sigma p}$

Where: V= volume estimated; t= distance between two measures; a/p= area of point; Σp= sum of the points counted. The error prediction of the volume estimation is expressed as a coefficient of error $CE^2(V_{est})$. The coefficient of error was calculated using this equation.

$CE^2(V_{est}) = CE^2(V_{sections}) + CE^2(V_{point\ counting})$

Where $CE^2(V_{sections})$ is the contribution of the variability among sections and whereas $CE^2(V_{point\ counting})$ is the mean variability generated by the point counting method (Garcia-Finãna et al., 2003).

A more detailed description of CE calculation is available elsewhere (Garcia-Finãna et al., 2003). To calculate CA1 and dentate gyrus volume, an area/point = 44.1 μm^2 and a distance of 300 μm between the sections analyzed was employed. Since the thickness shrinkage factor (Schmitz et al., 2000) could not be calculated, our data are not expressed in micrometers; the CA1 and dentate gyrus volumes of ischemic animals are expressed as percentage of controls.

Statistical Analyses

Statistical analysis of the optical density and volume estimation were run using one-way analysis of variance, ANOVA, followed by the Tukey Kramer multiple comparisons test, with *p* values of 0.05 or less being considered significant. A statistical package software (SPSS 8.0) was employed.

3. Results

CO activity was present in all hippocampal subfields and dentate gyrus, and was observed both in neuronal cell bodies and in their processes. The CO stained sections showed a good resolution under light microscopy allowing a precise delineation of the anatomical boundaries between the different *strata* of the hippocampus. Activity in the CA2 and CA3 subfields were always significantly higher than that of the CA1 region, this observation was further confirmed by densitometric measurements (data not shown). The ependymal layer did not present any CO reactivity and the enzymatic activity was not detected when the substrate was omitted.

The animals submitted to lethal and sublethal ischemia and briefly reperfused showed a statistically significant increase of CO reactivity in the strata *oriens*, *pyramidale* and *radiale* when compared to control and preconditioned groups (Table 1; Figure 1).

Twenty four hours after the ischemic event the lethal and preconditioned groups displayed a significant increase in the CO reaction in all hippocampal subfields analysed. After 48 hour of reperfusion this increase in CO activity remains only in the *pyramidale* strata (Table1; Figure 1). After 7 days of reperfusion the optical density levels measured in control animals were similar to those measured in the ischemic animals (Table 1; Figure 1).

The morphological changes in CA1 and dentate gyrus volume after different periods of ischemia are shown in figure 6 and illustrated in figure 7. All coefficients of error calculated were below 8%; the average coefficient of error for CA1 volume estimation was 4.86% and for dentate gyrus was 2.89%.

The lethal ischemic group presented a severe CA1 volume reduction (31%), when compared to the other groups $F_{0.05;\,3;\,16} = 3.625$; $p = 0.036$. There was no significant decrease of CA1 volume in the sublethal ischemic group nor in the pre-conditioned animals (Figures 2 and 3).

The lethal ischemic CA1 volume reduction was more pronounced in the caudal and ventral portion of CA1, after bregma - 4.80 mm coordinates, according to the atlas of Paxinos and Watson (1998). No statistically significant difference was detected in the dentate gyrus when comparing lethal ischemic animals to all other groups (Figure 2).

4. Discussion

The neuroprotection mediated by preconditioning has been demonstrated in different models of ischemia (Corbett and Crooks, 1997; Pérez-Pinzon et al., 1997; Wiegand et al., 1999; Maruoka et al., 2002). However, this work is the first stereological study showing that a previous sublethal ischemic episode is able to reduce the CA1 ischemic lesion produced by 10 minutes of global cerebral ischemia and that no change was observed in the dentate gyrus volume under the same experimental conditions.

The hippocampal neuronal loss promoted by lethal ischemic events was described in previous papers, either using non-stereological methods (Kogure and Kato, 1993) or precise stereological tools (Herguido et al., 1999; Larsson et al., 2001). Herguido and co-workers (1999), by means of the optical fracionator, showed neuronal loss averaging 39% in CA1 subfield in animals submitted to 10 minutes of global ischemia, this result is similar to the data obtained in our work. The more pronounced CA1 reduction in the ventral-caudal portion of the hippocampus that we report, is probably associated with the heterogeneity of vascular network along the septotemporal axis of the hippocampus (Grivas et al., 2003).

As shown in Table 1 and in Figure 1. CO activity increased immediately after both sub-lethal and the lethal ischemic events, one effect cancelled by preconditioning. A rapid impairment of energy production is promoted by global cerebral ischemia, resulting in ATP depletion due to glucose, phosphocreatine, glycogen and oxygen deprivation (Pulsinelli and Duffy, 1983; Nowak et

al., 1985). Increases in the ATP/ADP ratio are able to promote an allosteric inhibition of CO activity due to a reversible cAMP dependent phosphorylation of this enzyme, this effect is reversed by Ca^{++} activated protein phosphatase (Bender and Kadenbach., 2000; Kadenbach et al., 2000). Immediately after the ischemic insult, the ATP/ADP ratio is decreased and the intracellular levels of calcium are increased by activation of NMDA glutamate receptors (Nowak et al., 1985; Silver and Erecinska, 1992). Therefore, the decrease in ATP levels and the increase in neurotransmitter release and intracellular calcium levels could explain the enhanced CO activity found in the *strata oriens, pyramidale* and *radiale* immediately after ischemia in sub-lethal and lethal ischemic groups. This increase was not observed in the *stratum lacunosum molecular* nor in the molecular layer of dentate gyrus of animals immediately reperfused, and it may be associated with the "pathway differences", as the dentate gyrus mainly receives innervation from the enthorrinal cortex through the perforant pathway (Amaral and Witter, 1995).

Correlations between the decrease in mitochondrial activity and neuronal survival were previously described using chemical preconditioning with 3-nitropropionic acid (3-NPA) (Wiegand et al., 1999; Maruoka et al., 2002). In our work, this reduction of mitochondrial activity is represented by the attenuation of CO activity increase, induced by the preconditioning episode, in *strata oriens, pyramidale* and *radiale* immediately after ischemia, We suggest that is probably associated with: 1-the inhibition of postischemic activation of NMDA receptors; 2- the upregulation of [(3)H] muscimol binding to γ aminobutyric acid A (GABA A) receptor; and 3-the reduced intracellular calcium elevation promoted by ischemic preconditioning in the hippocampal CA1 neurons (Silver and Ericinska., 1992; Kogure and Kato., 1993; Sommer et al., 2002).

An increase in ATP levels is required for the gene expression (transcription and translation) and for the protein synthesis (Katayama and Welsh, 1989). The increase in CO activity found 24 hours after the ischemic event in preconditioned animals can also be related to increases in genic

transcription and protein synthesis such as the heat shock proteins; HSP 60, HSP 70 and HSP 72, or increases in expression of the anti-apoptotic factors, Bcl-2 and Bclx-1-mRNA (Chen et al., 1997; Abe et al., 1998; Martin et al, 1998; Currie et al., 2000; Truettner et al., 2002).

On the other hand, astrocytes appear to play an important role in neuronal healing and reorganization in the adult hippocampus some days after the lethal ischemic event, with an extensive glial proliferation and a massive glial reactivity coupled to an increase in astrocyte glucose utilization (Beck et al., 1990; Gage et al., 1990; Rischke and Krieglstein, 1991). Thus, this increase in the energy demand of these glial cells could also be responsible for the increase in CO activity (Mjaatvedt and Wong-Riley, 1988), affecting the density of CO reaction in the *stratum pyramidale* 48 hours after the insult in ischemic groups.

In conclusion, we have mapped CO activity in the hippocampal subfields after different periods of ischemia and reperfusion, as well as confirmed that the CA1 neuronal damage is attenuated by the preconditioning episode. Our most important finding was that the preconditioning event is able to counteract the increase of CO activity induced by the sublethal and lethal ischemic events in the *strata oriens, pyramidale* and *radiale* immediately after ischemia, but not after other reperfusion times. We suggest this rapid respiratory chain inhibition could be a common feature of different preconditioning techniques (Wiegand et al., 1999; Maruoka et al., 2002), and that it might be used to develop new pharmacological strategies to minimize the effects of lethal ischemic event.

Acknowledgements

The authors wish to express their gratitude to thank Dr Marta Garcia-Fiñana and Dr Luis M. Cruz-Orive (Department of Mathematics, Statistics and Computation, University of Cantabria, Spain) for their help during the entire work. This investigation was supported by grants from Brazilian funding agencies CNPq, CAPES, FAPERGS, PRONEX, FINEP.

References

Abe, K., Kawagoe, J., Aoki, M., Kogure, K., Itoyama, Y., 1998. Stress protein induction after brain ischemia. Cell. Mol. Neurobiol. 18, 709-719.

Amaral, D. G., Witter, M.P., 1995. Hippocampal formation. In: Paxinos, G., The Rat Nervous System. Academic Press, Sidney, pp. 443-493.

Aoki, M., Abe, K., Kawagoe, J., Nakamura, S., Kogure, K, 1993. The Preconditioned hippocampus accelerats HSP70 heat-shock gene expression following transient ischemia in the gerbil. Neurosci. Lett. 155, 7-10.

Beck, T., Wree, A., Schleicher., 1990. A. Glucose utilization in rat hipoccampus after long-term recovery from ischemia. J. Cereb. Blood Flow Metab. 10, 542-549.

Bender, E., Kadenbach, B., 2000. The allosteric ATP-inhibition of cytochrome c oxidase activity is reversibly switched on by cAMP-dependent phosphorylation. FEBS Lett. 466, 130-134.

Benveniste, H., Drejer, J., Schousboe, A., Diemer, R.H., 1984. Elevation of the extracellular concentrations of glutamate and aspartate in the rat hippocampus during transient cerebral ischemia monitored by intracerebral microdialysis. J. Neurochem. 43, 1369-1374.

Benveniste, H., Jorgensen, M. B., Sandberg, M., Christensen, T., Hagberg, H., Diemer, N. H.,1989. Ischemic damage in hippocampal CA1 is dependent on glutamate release and intact innervation from CA3. J. Cereb. Blood Flow Metab. 9, 629-39.

Chen, J., Graham, S.H., Nakayama, M., Zhu, R.L., Jin, K., Stetler, R.A., Simon, R.P.,1997. Apoptosis repressor genes bcl-2 and bcl-x-long are expressed in the rat brain following global ischemia. J. Neurochem. 67, 64-71.

Choi, J., 1997. The excitotoxic concept. In: Welch, K.M.A., Caplan, L.R., Reis, D.J., Siesjö, B.K., Weir, B., Primer on Cerebrovascular Diseases. Academic Press, New York, pp.167-190.

Corbett, D., Crooks, P., 1997. Ischemic preconditioning: a long term survival study using behavioural and histological endpoints. Brain Res. 760, 129-136.

Cruz-Orive, L. M., 1997. Stereology of single objects. J. Microsc. 163, 102-113.

Currie, R.W., Ellison, J.A., White, R.F., Feuerstein, G.Z., Wang, X.K., Barone, F.C., 2000. Benign focal ischemic preconditioning induces neuronal Hsp70 and prolonged astrogliosis with expression of Hsp27. Brain Res. 863, 169-181.

Dave, K.R., Saul, I., Busto, R., Ginsberg, M.D., Sick, T.J., Perez-Pinzon, M.A., 2001. Ischemic preconditioning preserves mitochondrial function after global cerebral ischemia in rat hippocampus. J. Cereb. Blood Flow Metab. 21, 1401-1410.

Dienel, G.A., Pulsinelli, W.A., Duffy, T.E., 1980. Regional protein synthesis in rat brain following acute hemispheric ischemia. J. Neurochem. 35, 1216-1228.

Ferraz, A.C., Xavier, L.L., Hernandes, S., Sulzbach, M., Viola, G.G., Anselmo- Franci, J.A., Achaval, M., Cunha, C., 2003. Failure of estrogen to protect the substantia nigra pars compacta of female rats from lesion induced by 6-hydroxidopamine. Brain Res. 986, 200-205.

Gage, F.H., Buzsaki, G., Armstrong, D.M.,1990. NGF-dependent sprouting in the hippocampus. Prog. Brain Res. 83, 357-370.

Garcia-Fiñana, M., Cruz-Orive, L.M., Mackay, C.E., Pakkenberg, B., Roberts, N., 2003. Comparison of MR imaging against physical sectioning to estimate the volume of human cerebral compartments. NeuroImage. 18, 505-516.

Graham, S.H., Shiraishi, H., Panter, S.S., Simon, R.P., Faden, A.I., 1990. Changes in extracellular amino acid neurotransmitters produced by focal ischemia. Neurosci. Lett. 110, 124-130.

Graham, S.H., Chen, J. Programmed cell death in cerebral ischemia., 2001 J. Cereb. Blood Flow Metab. 21, 99-109.

Grivas, I., Michaloudi, H., Batzios, Ch., Chiotelli,M,, Papatheodoropoulos, C., Kostopoulos, G., Papadopoulos, G.C., 2003. Vascular network of the rat hippocampus is not homogeneous along the septotemporal axis. Brain Res. 971, 245-249.

González-Lima, F., Garrosa, M., 1991. Quantitative histochemistry of cytochrome oxidase in rat brain. Neurosci. Lett. 123, 251-253.

Gundersen, H.J.G., Jensen, E.B.,1987. The efficiency of sytematic sampling in stereology and its prediction. J. Microsc. 147, 229-263.

Harley, C. A., Bielajew, C. H., 1992. A comparison of glycogen phosphorylase a and cytochrome oxidase histochemical staining in rat brain. J. Comp. Neurol. 322, 377-389.

Herguido, M.J., Carceller, F., Roda, J.M., Avendano, C., 1999. Hippocampal cell loss in transient global cerebral ischemia in rats: A critical assessment. Neuroscience. 93, 71-81.

Heurteaux, C., Lauritzen, I., Widmann, C., Lazdunski, M.,1995. Essential role of adenosine, adenosine A1 receptors, and ATP-sensitive K^+ channels in cerebral ischemic preconditioning. Proc Natl Acad Sci U.S.A. 92, 4666-4670.

Hevner, R. F., Liu, S., Wong-Riley, M. T. T., 1995. A metabolic map of cytochrome oxidase in the rat brain: histochemical, densitometric and biochemical studies. Neuroscience. 65, 313-342.

Kadenbach, B., Hüttemann, M., Arnold, S., Lee, I., Bender, E., 2000. Mitochondrial energy metabolism is regulated via nuclear coded subunits of cytochrome c oxidase. Free Rad. Biol. Med,. 29, 211-221.

Katayama, Y., Welsh, F., 1989. A. Effect of dichloroacetate on regional energy metabolites and pyruvate dehydrogenase activity during ischemia and reperfusion in gerbil brain. J. Neurochem. 52, 1817-1822.

Kato, H., Kogure, K., Nakata, N., Araki, T., Itoyama, Y., 1995. Facilitated recovery from suppression of protein synthesis in the gerbil brain with ischemic tolerance. Brain Res. Bull. 36, 205-208.

Kawai, K., Nakagomi, T., Kirino, T., Tamura, A., Kawai, N., 1998. Preconditioning in vivo inhibits anoxic long-term potentiation and functionally protects CA1 neurons in the gerbil. J. Cereb. Blood Flow Metab. 18, 288-296.

Kirino, T., 1982. Delayed neuronal death in the gerbil hippocampus following ischemia. Brain Res. 239, 57-69.

Kirino, T., Tsujita, Y., Tamura, A., 1991. Induced tolerance to ischemia in gerbil hippocampal neurons. J. Cerebr. Blood Flow Metab. 11, 299-307.

Kogure, K., Kato, H., 1993. Altered gene expression in cerebral ischemia. Stroke. 24, 2121-2127.

Larsson, E., Lindvall, O., Kokaia, Z., 2001. Stereological assessment of vulnerability of immunocytochemically identified striatal and hippocampal neurons after global cerebral ischemia in rats. Brain Res. 913, 117-132.

Marini, A.A., Paul, S.M., 1992. N-methyl-D-aspartate receptor-mediated neuroprotection in cerebellar granule cells require new RNA and protein synthesis. Proc. Natl. Acad. Sci. USA. 89, 6555-6559.

Martin, L.J., Al-Abdulla, N.A., Brambrink, A.M., Kirsch, J.R., Sieber, F.E., Portera-Cailiau, C., 1998. Neurodegeneration in excitoxicity, global cerebral ischemia and target deprivation: A perspective on the contributions of apoptosis and necrosis. Brain. Res. Bull. 46, 281-3098.

Maruoka, N., Murata, T., Omata, N., Fujibayashi, Y., Yonekura, Y., Wada, Y., 2002. Hypoxic tolerance induction in rat brain slices following 3-nitropropionic acid treatment as revealed by dynamic changes in glucose metabolism. Neurosci. Lett. 319, 83-86.

Mjaatvedt, A. E., Wong Riley, M. T., 1988. Relationship between synaptogenesis and cytochrome oxidase activity in Purkinje cells of the developing rat cerebellum. J. Comp. Neurol. 277, 155-182.

Nagagomi, T., Kirino, T., Kenemitsu. H., Tsujita, Y., Tamura, A., 1993. Early recovery of protein synthesis following ischemia in hippocampal neurons with induced tolerance in the gerbil. Acta Neuropathol. 86, 10-15.

Nicotera, P., Leist, M., 1997. Energy suply and shape of death in neurons and lymphoid cells. Cell Death and Differentation. 4, 435-442.

Nowak, T. S . JR., Fried, R. L., Lust, W.D., Passonneau, J. V., 1985. Changes in brain energy metabolism and protein synthesis following transient bilateral ischemia in gerbil. J. Neurochem. 44, 487-494.

Paxinos, G., Watson, C., 1998. The Rat Brain in Stereotaxic Coordinates, 4th ed. Academic Press, San Diego.

Pérez-Pinzon, M.A., Xu, G.P., Dietrich, W.D., Rosenthal, M., Sick, T.J., 1997. Rapid preconditioning protects rats against ischemic neuronal damage after 3 hours but not 7 days of reperfusion following global cerebral ischemia. J. Cereb. Blood Flow Metab. 17, 175-182.

Pulsinelli, W. A., Brierley, J. B., 1979. A new model of bilateral hemispheric ischemia in the unanesthetized rat. Stroke. 10, 267-272.

Pulsinelli, W. A., Brierley, J. B., Plum, F., 1982. Temporal profile of neuronal damage in a model of transient forebrain ischemia. Ann. Neurol. 11, 491-498.

Pulsinelli, W.A., Duffy, T.E., 1983. Regional energy balance in rat brain after transient forebrain ischemia. J. Neurochem. 40, 1500-1503.

Rischke, R., Krieglstein, J., 1991. Postischemic neuronal damage causes astroglial activation and increase in local cerebral glucose utilization of rat hippocampus. J. Cerebr. Blood Flow Metab. 11, 106-113.

Rothman, S., Olney, J., 1986. Glutamate and pathophysiology of hipoxic-ischemic brain damage. Ann. Neurol. 19, 105-111.

Schmidt-Kaster, R., Freund, T.F., 1991. Selective vulnerability of the hippocampus in brain ischemia. Neuroscience. 40, 599-636.

Schmitz, C., Dafotakis, M., Heinsen, H., Mugrauer, K., Niesel, A, Popken, G. J., Stephan, M., Van de Berg, W.D.J., Hörsten, S.V., Korr, H., 2000. Use of cryostat sections from snap-frozen nervous tissue for combining stereological estimates with histological cellular, or molecular analyses on adjacent sections. J. Chem. Neuroanat. 20, 21-29.

Silver, I.A., Erecinska, M., 1992. Ion homeostasis in rat brain in vivo: intra and extracellular [Ca^{++}] and [H^{+}] in the hippocampus during recovery from short term transient ischemia. J Cerebr. Blood Flow Metab. 12, 759-772.

Sims, N.R., Anderson, M.F., 2002. Mitochondrial contributions to tissue damage in stroke. Neurochem Internat. 40, 511-526.

Sommer, C., Fahrner, A., Kiessling, M., 2002. [(3)] Muscimol binding to gamma aminobutyric acid (A) receptors is upregulated in CA1 neurons of the gerbil hippocampus in the ischemia tolerant state. Stroke. 33, 1698-1705.

Truettner, J., Busto, R,, Zhao, W., Ginsberg, M.D., Pérez-Pinzon, M.A., 2002. Effect of ischemic preconditioning on the expression of putative neuroprotective genes in the rat brain. Mol. Brain Res. 103, 106-115.

Valentim, L.M., Geyer, A.B., Tavares, A., Cimarosti, H., Worm, P.V., Rodnight, R., Netto, C.A., Salbego, C.G., 2001. Effects of global cerebral ischemia and preconditioning on heat shock protein 27 immunocontent and phosphorylation in rat hippocampus. Neuroscience. 107, 43-49.

Vander Heiden, M.G., Chandel, N.S., Williamson, E.K., Schumacker, P.T., Thompson, C.B., 1997. Bcl-xL regulates the membrane potential and volume homeostasis of mitochondria. Cell. 91, 627-637.

Wiegand, F., Liao, W., Bush, C., Castell, S., Knapp, F., Lindauer, U., Megow, D., Meisel, A., Redetzky, A., Ruscher, K., Trendelenburg, G., Victorov, I., Riepe, M., Diener, H.C., Dirnagl, U., 1999. Respiratory chain inhibition induces tolerance to focal cerebral ischemia, J. Cerebr. Blood Flow Metab. 19, 1229-1237.

Wong-Riley, M., 1979. Changes in the visual system of monocularly sutured or enucleated cats demonstrable with cytochrome oxidase histochemistry. Brain Res. 171, 11-28 .

Wong-Riley, M. T., 1989. Cytochrome oxidase: an endogenous metabolic marker for neuronal activity. TINS. 12, 94-101.

Wong-Riley, M., Antuono, P., Ho, K., Egan, R., Hevner, R., Liebl, W., Huang, Z., Rachel, R., Jones, J., 1997.Cytochrome oxidase in Alzheimer's Disease: biochemical, histochemical and immunohistochemical analyses of the visual and other systems. Vision Res. 37, 3593-3608.

Zhou, M., Demo, S.D., McClure, T.N., Crea, R., Bitler, C.M., 1998. A novel splice variant of cell death-promoting protein BAX. J. Biol. Chem. 273, 11930-11936.

Table 1

Stratum		0 hour					24 hours				
		C	2min	10 min	2+10 min	F	C	2min	10 min	2+10 min	F
Oriens	Mean	0.89	1.02***	1.03***	0.83	22.83	0.34	0.51[a]	0.84[ab]	0.86[ab]	93.09
	±Sd	0.09	0.07	0.07	0.30		0.10	0.14	0.11	0.10	
Pyramidale	Mean	0.92	1.04**	1.06**	0.91	9.79	0.68	0.71	0.91***	0.87***	28.67
	±Sd	0.09	0.08	0.04	0.17		0.01	0.09	0.09	0.09	
Radiale	Mean	0.70	0.90***	0.86***	0.57	22.89	0.34	0.40	0.78**	0.64**	8.43
	±Sd	0.12	0.09	0.06	0.13		0.13	0.05	0.03	0.03	
Lac Mol	Mean	0.60	0.69	0.68	0.58	2.72	0.65	0.76[a]	0.88[ab]	0.94[ab]	30.76
	±Sd	0.04	0.05	0.03	0.13		0.04	0.09	0.08	0.06	
		48 hours					7 days				
		C	2min	10 min	2+10 min	F	C	2min	10 min	2+10 min	F
Oriens	Mean	0.62	0.68	0.70	0.55	0.04	0.58	0.68	0.69	0.51	1.07
	±Sd	0.11	0.15	0.15	0.18		0.18	0.18	0.22	0.17	
Pyramidale	Mean	0.17	0.34***	0.39***	0.38***	48.84	0.68	0.73	0.78	0.61	1.03
	±Sd	0.06	0.06	0.08	0.07		0.15	0.15	0.20	0.13	
Radiale	Mean	0.38	0.50	0.44	0.35	1.04	0.31	0.41	0.36	0.31	0.39
	±Sd	0.13	0.16	0.15	0.14		0.16	0.13	0.22	0.16	
Lac Mol	Mean	0.87	0.91	0.86	0.77	2.06	0.70	0.76	0.79	0.68	0.76
	±Sd	0.04	0.09	0.09	0.13		0.17	0.14	0.14	0.13	

Optical densitometric measurements of CO reactivity in the *strata oriens, pyramidale, radiale and lacunosum-moleculare (Lac Mol)* in controls (C), sublethal ischemic animals (2min), lethal ischemic animals (10 min) and preconditioned animals (2+10 min) after different times of reperfusion (immediately reperfused (0 hour), 24 hours, 48 hours and 7 days); F= $F_{0.05;3;16}$; (n=5). All values are expressed as mean + SD. *** P<0.001; **P <0.01 relative to control group; "a" P <0.01 relative to control group "ab"; P <0.01 relative to control and sublethal groups

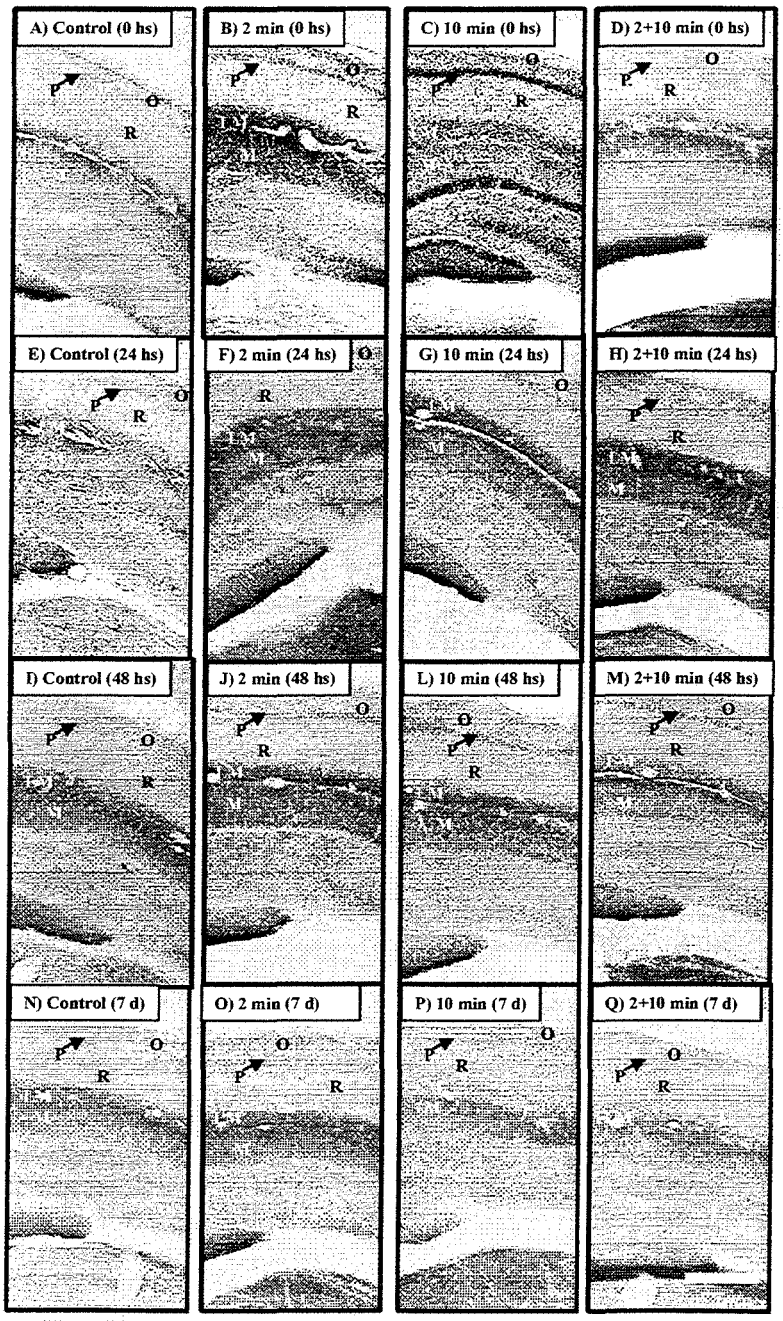

Fig. 1. Digitized images of coronal sections obtained from hippocampal formation, *strata oriens* (O); *pyramidale* (P); *radiale* (R); *lacunosum-moleculare* (LM) and molecular layer of the dentate gyrus (M), showing the changes in cytochrome oxidase (CO) activity induced by different periods of ischemia and reperfusion. Note an increase in CO activity in the *strata oriens, pyramidale* and *radiale* in the sublethal and lethal ischemic groups immediately reperfused (B and C) when compared to controls and preconditioned animals submitted to the same periods of reperfusion (A and D). Note also an increase in CO activity in all subfields of hippocampal formation 24 hours after the ischemic event in all ischemic groups (F,G,H) and the increased CO reaction in the *stratum pyramidale* of ischemic animals 48 hours after the event (J,L,M). Images were obtained from a dorsal view of the hippocampus between bregma -1.8 mm and bregma -4.52 mm coordinates (Paxinos and Watson, 1998). Scale bar = 1mm.

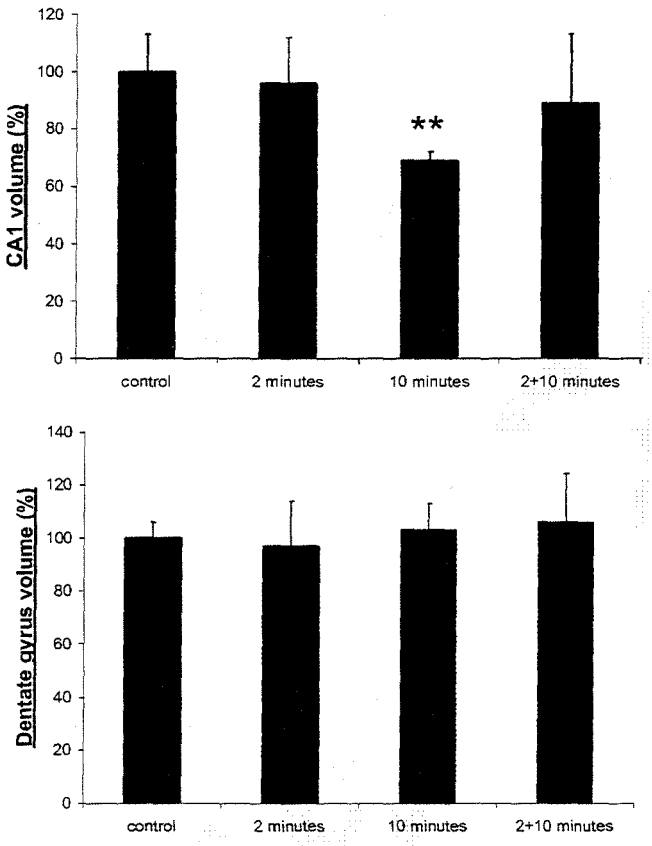

Fig. 2. Estimation of CA1 and dentate gyrus volume (expressed in percentage of control volume). Note the decrease of CA1 volume after a lethal ischemic event (10 minutes of ischemia) when compared to the other groups *($P<0.05$). The dentate gyrus volume was not significantly modified by these periods of ischemia and reperfusion. Data are mean $\pm$ SD.

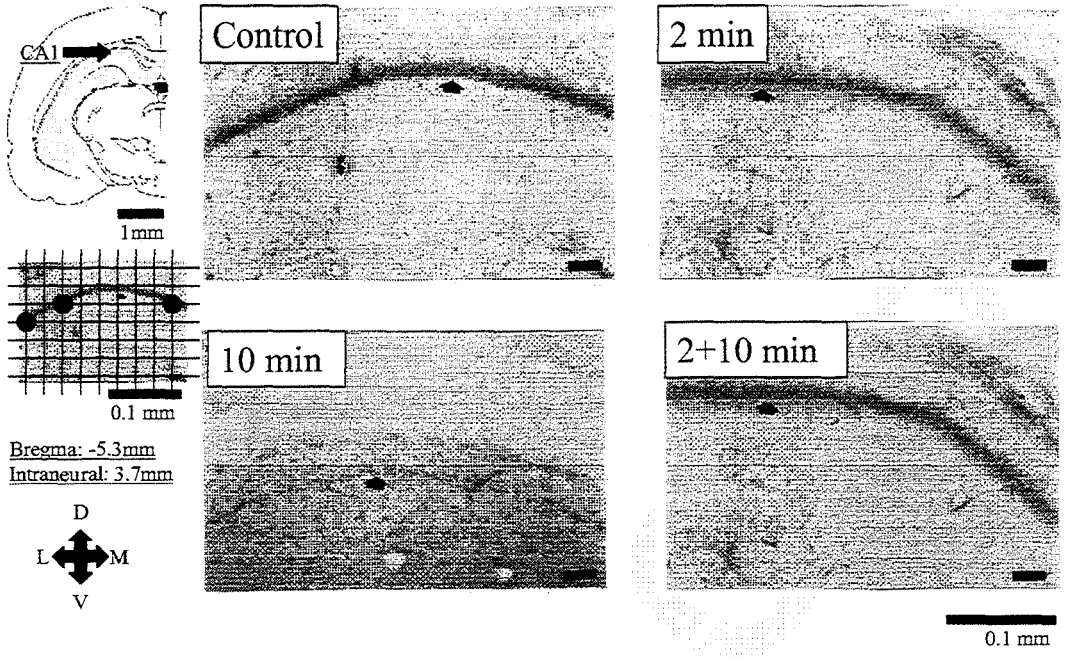

Fig. 3. Digitized images obtained from coronal sections of the hippocampal formation, note the reduction in the height of CA1 subfield in the lethal ischemic animal (10 min), when compared to control, sublethal ischemic (2 min) and preconditioned animals (2+10 min). Images were obtained from a dorsal view of the hippocampus (Paxinos and Watson, 1998).

A simple and fast densitometric method to analyze tyrosine hydroxylase immunoreactivity in the substantia nigra pars compacta and in the ventral tegmental area.

Léder Leal Xavier[1,2], Giordano Gubert Viola[2], Anete Curte Ferraz[3], Claudio Da Cunha[3], Carlos Alexandre Netto[1], Matilde Achaval[2*]

Departments of [1]Biochemistry and [2]Morphological Sciences, Health Basic Sciences Institute of the Federal University of Rio Grande do Sul. Porto Alegre, Rio Grande do Sul, Brazil.
[3]Department of Physiology and Pharmacology, Federal University of Paraná. Curitiba, Paraná, Brazil.

16 pages; 2 figures.

* Correspondence to:
Matilde Achaval
Laboratório de Histofisiologia Comparada
Departamento de Ciências Morfológicas
Instituto de Ciências Básicas da Saúde
Universidade Federal do Rio Grande do Sul
Rua Sarmento Leite 500
90050-170
Porto Alegre, RS, Brazil.
Telephone: +55-51-3316-36-24
Fax: +55-51-3316-30-92
E-mail: achaval@ufrgs.br

Acknowledgements: This research was supported by FAPERGS, CNPq and CAPES.

Abstract

Parkinson's disease is a progressive dyskinetic disorder caused by degeneration of mesencephalic dopaminergic neurons in the substantia nigra pars compacta (SNpc) and, to a lesser extent, in the ventral tegmental area (VTA). Tyrosine hydroxylase (TH) is a rate-limiting enzyme for dopamine synthesis, therefore immunohistochemistry for TH can be used as an important marker of dopaminergic cell loss in these regions. Traditionally, the product of immunohistochemical experiments are semiquantitatively evaluated by densitometry. However a great problem found in these previous articles is the lack of a clear explanation about the algorithms and macros employed. In this work we describe an easy, fast and precise protocol to analyze TH immunoreactivity in SNPc and VTA using a popular image analysis software package (Image Pro-Plus). We believe that this protocol will facilitate the evaluation of TH immunoreactivity after different experimental Parkinson's disease treatment.

Theme: Disorders of the nervous system

Topic: Degenerative disease: Parkinson's

Keywords: Image analysis, Densitometry, Parkinson's disease; Substantia nigra pars compacta, Ventral tegmental area.

1. Type of research

Parkinson's disease, or paralysis agitans, is a disorder promoted by degeneration of dopaminergic nigrostriatal system characterized by hypokinetic features as akinesia and bradikinesia and hyperkinetic features as rigidity and tremor [1,8]. This dopaminergic degeneration is traditionally assessed by tyrosine hydroxilase (TH) immunohistochemistry [1,8].

This protocol was initially developed to evaluate immunohistochemistry for tyrosine hydroxilase (TH) in the substantia nigra pars compacta (SNpc) and in the ventral tegmental area (VTA) after different Parkinson's disease treatments, but it could also be used for any type of research that require a semi quantitative evaluation of histochemical and immunohistochemical procedures in different regions of nervous system.

2. Time required

- Treatment with 6-hydroxydopamine (6-OHDA), a potent neurotoxic agent: 45 days
- Transcardial perfusion followed by post fixation and crioprotection: 24 hours
- Brain sectioning: 4 hours (30 minutes each brain)
- Immunohistochemistry procedure: The time required for the whole immunohistochemistry procedure is about 3 days, divided in:
- Incubation with the primary antibody 48 hours
- Incubation with the secondary antibody 2 hours
- Incubation with the revelation system (3.3' Diaminobenzidine tetrahydrochloride (DAB) and H_2O_2): 20 minutes (10 minutes each)
- All washing steps: 2 hours
- Section mounting on glass slide procedure: 4 hours, 30 minutes per brain, dependent on number of sections)
- Drying of slides: 24 hours

•Dehydrating, clearing and coverslipping slides: 2 hours

•Drying coverslipped slides: 3 days

•Creating, measuring and editing areas of interest (AOI) and macros: 2 hours

•Capturing and converting images using macros : 8 hours, (480 images, 1 minute per image)

•Measuring optical density using macros: 8 hours, (480 images, 1 minute per image)

•Statistical analysis: 1 hour

In fact, the time required to complete whole protocol is about 2 months, but it can be modified according with the treatment employed. In fact, the time employed for the image analysis is about 2 days.

3. Materials

3.1 Animals

To demonstrate our protocol eight female adult Wistar rats weighing between 220-250 were used. The animals were kept under a constant 12:12h light–dark cycle (lights on at 7:00 a.m.) at a room temperature of 22 ± 2^{0}C and maintained with food and water a*d libitum*. All efforts were made to minimize animal suffering and to reduce the number of the animals needed. The Brazilian Laws and the National Institute of Health Guide for Animal Care and Use of Laboratory Animals were strictly followed.

3.2 Special equipment

• Interactive Image Analysis System (Image Pro-Plus, version 4.1, Media Cybernetics, MA, USA installed on a Pentium II PC)

•Videocamera (Pro-Series High Performance CCD camera, CA, USA) Attached to a light microscope (Nikon Eclipse E-600)

• Statistical packages for the social sciences (SPSS), version 8.0

• Perfusion pump (any supplier)

• Criostat (any supplier)

3.3 Chemicals and reagents

• Drugs: 6-hydrodopamine (6OHDA) (Sigma-Aldrich); Sodium Thiopental (any supplier)

•Antibodies: monoclonal tyrosine hydroxylase antibody (Sigma-Aldrich); Secondary antibody biotinylated (Dako corporation, Carpinteria, CA).

•Peroxidase conjugated streptavidin (Dako corporation, Carpinteria, CA).

•3.3' Diaminobenzidine tetrahydrochloride (DAB) and all other chemicals were purchased from Sigma-Aldrich

All solutions described in this protocol were made in fresh double distilled and deionized water.

4.0 Detailed procedure

4.1 Drug treatment

The animals were divided 2 groups (4 animals each): control and animals submitted to intranigral infusion of neurotoxin 6-hydroxydopamine (6-OHDA, 6 μg/side). Treated animals were anesthetized with sodium thiopental (200 mg/kg) and 6-OHDA HCl (Sigma, 6 μg in 2 μl of artificial cerebrospinal fluid (aCSF), 0.33 μl/min) was bilaterally infused into the SNpc through a 30-gauge needle. The coordinates for the injections were: anteroposterior (AP), -5.0 mm from bregma, mediolateral (ML) $\pm$ 2.1 mm from midline, dorsoventral (DV), -7.7 mm from skull, adapted from Paxinos and Watson [15]. The composition of aCSF was as follows: 8.66 g NaCl, 0.250 mg KCl, 0.76 g $CaCl_2 \cdot 2H_2O$, and 0.173g $MgCl_2 \cdot 6H_2O$

4.2 Fixation, post-fixation and crioprotection

Fourty-five days after infusion, under deep anesthesia (200 mg/kg sodium thiopental), the animals were transcardially perfused with saline solution followed by a solution of 4% paraformaldehyde in 0.1 M phosphate buffer, pH 7.4 (PB). After perfusion the brains were removed from the skulls, post-fixed in the same solution at room temperature for 2 h and cryoprotected by immersion in 30% sucrose solution in PB at 4°C until they sank.

4.3 Tyrosine hydroxylase immunohistochemistry

For each brain, serial coronal sections (50 μm) were obtained using a cryostat (Leitz, Digital 1702) at -20^{0}C and collected in PB. The free-floating sections were pretreated with 10% methanol diluted in 3% hydrogen peroxidase for 30 min, carefully washed and blocked with 3% normal goat serum (NGS) in 0.1 M phosphate buffer, 0.9% NaCl, pH 7.4 (PBS) containing 0.3% Triton X-100 for 30 min and incubated with monoclonal tyrosine hydroxylase antibody raised in mice diluted 1:750 with 3% NGS in PBS-Tx for 48 h at 4°C. After washing several times with PBS-Tx, tissue sections were incubated with a secondary antibody biotinylated diluted 1:200 in PBS-Tx at room temperature for 2 h. Sections were washed again in PBS and incubated with peroxidase-conjugated streptavidin diluted 1:100 in PBS for 90 min at room temperature.

The immunohistochemical reaction was developed by incubating the sections in a medium containing 0.06% 3,3 diaminobenzidine dissolved in PBS for 10 min, and then in the same solution containing 1 μM of 3% H_2O_2 per ml of DAB medium for 10 min. Next, the sections were rinsed with PBS, dehydrated with ethanol, cleared with xylene, and covered with Permount and coverslips. Control sections were prepared by omitting the primary antibody and replacing it with PBS.

The brains of the animals were fixed and postfixed for the same time in identical solutions and rigorously processed at the same time, and the sections were incubated in the same medium for the same period of time. This precaution was taken to avoid overreaction, differences in chromogen reaction, saturation of optical density or changes in background staining levels.

Note that DAB may be carcinogenic and for this reason the revelation procedure should be performed with special care and gloves. Afterwards all glasswork and other equipment that have been in contact with DAB solutions should be treated, for at least 24 hours, with 10% sodium hypocloride solution and washed in excess water. In case of contact, immediately flush skin with water.

4.4 Image Analysis

The coronal sections of substantia nigra and ventral tegmental area (VTA) were selected for this protocol. These areas were identified according to the atlas of Paxinos and Watson and the readings were made between the coordinates interaural 4.2 mm, bregma – 4.8 mm and interaural –2.7 mm, bregma – 6.3 mm. The intensity of the reaction product of TH was measured semi-quantitatively using a Nikon Eclipse E-600 (50X) microscope coupled to a Pro-Series High Performance CCD camera and Image Pro Plus Software 4.1 (Media Cybernetics, CA, USA). This procedure can be divided into six different steps: 1-Creating and measuring the Area of Interest (AOI); 2-Calibrating the Optical density; 3-Acquiring, converting and saving images; 4-Performing the background correction; 5-Setting of the AOI in the acquired image to measure the optical density; 6-Creating macros

1-Creating and measuring the Area of Interest (AOI)

To create and save an appropriate AOI; Select: New AOI command. The AOI created can be measured using the measure commands calibrated by an image of micrometer object captured with the same magnifications. The size and shape of the AOI should be determined in order to avoid the borders of the SNpc and VTA and to collect a significant number of pixels from this area. For our work, we create a square AOI and it was named ODTH.

2-Calibrating the optical density

To calibrate optical density select: Measure/Calibration/Intensity calibration; click in the Std Optical Density and click in OK.

3-Acquiring, converting and saving images

To acquire images the some previous steps are necessary:

Turn on microscope lamp and leave on for at least 15 minutes to stabilize illumination. Select in the main menu: Acquire/Video/Digital/Start and adjust the illumination using a proper Koehler alignment [2] . Adjust the level of light source to a point that permits image capture without oversaturating the CCD camera, if necessary, neutral filters can be used [2].

After these procedures select an image of SNPc and/or VTA and click in SNAP, return to the main menu and select:Edit/Convert to/Gray scale 8; return newly to the main menu and select: File/Save.

4-Performing the background correction

To perform the background correction a background image should be captured and opened during the process, in our protocol this image was named background. The background image was generated with the slide removed from the microscope stage. For this procedure the following steps are necessary; select: Background operations/background correction. Click in the the black level to define the black. Black is the mean intensity generated when no light goes through the material, in our case 5.3 (0-255); click in OK.

The optical density should be measured only in the image generated after the background correction. The algorithm employed in the background correction is based on the following formula:

$$CI_{x,y} = [(I_{x,y} - BL / BI_{x,y} - BL) \times (N-BL)] + BL$$

where: $CI_{x,y}$ =New pixel in the corrected image; $I_{x,y}$ = Pixel value of the original image at location (x,y); $BI_{x,y}$ = Pixel value of the background image at location (x,y); M = Average pixel value of the background image; BL = Level of black

5-Setting of the AOI in the acquired image to measure the optical density.

To set the AOI and measure the optical density the following steps are necessary. Select:Edit/AOI; click in the ODTH and click OK and set the AOI into the SNpc or VTA, In this procedure obvious blood vessels and other artifacts should be avoided.

To measure the optical density select:Measure/Histogram. The result obtained represent the mean of all pixels in the AOI and it should be transposed to statistical package .

In our work the readings were performed in both hemispheres and at least 30 readings per animal were obtained. All lighting conditions and magnifications were held constant. Moreover, the investigator was unaware of the experimental groups from which the slices were obtained. The optical density was calculated using the following formula:

$OD_{(x,y)} = -\log [(INTENSITY_{(x,y)}-BLACK)/(INCIDENT-BLACK)]$

Where: OD = Optical Density; $INTENSITY_{(x,y)}$ is the intensity at pixel $_{(x,y)}$; BLACK is the intensity generated when no light goes through the material; INCIDENT is the intensity of the incident light.

6-Creating Macros

The time required to perform the measurements of optical density can be greatly reduced by macros. In our study we created three macros using Auto Pro, a Visual Basic programming language for IPP 4.1. The macros 1, 2 and 3 reduce the time required to perform steps 3, 4 and 5 respectively. The macros created are described below.

Macro 1 (Press ctrl G)

```
Sub graysave()
'<c>G
ret=IpAcqShow(ACQ_SNAP, 1)
ret=IpAcqSnap(ACQ_CURRENT)
ret=IpWsConvertToGray()
ret=IpWsSave()
End Sub
```

Macro 2 (Press ctrl B)

```
Sub background correction()
'<c>B
ret=IpOpBkgndCorrect(1,5.3,1)
End Sub
```

Macro 3 (Press ctrl A)

```
Sub set AOI()
'<c>A
ret= IpAoiManager(AOISET,"ODTH")
End Sub
```

4.5 Statistical Analysis

A Student *t* test comparing controls and 6OHDA treated animals was performed using statistical packages for the social sciences (SPSS, 8.0). The level of significance was set as $p < 0.05$.

5. Results

Images of TH immunorectivity in SNPc and VTA in controls and 6OHDA treated animals are shown in the figure 1. Data about the optical density measurements in this regions are shown in the figure 2.

6. Discussion

The results found in our work were previously described [9] and the present investigation only confirms the neurotoxicity of 6OHDA on SNPc neurons but not in VTA, this difference is probably related to the precision in the infusion procedure [9].

This protocol was initially created to analyze TH immunoreactivity in SNPc and VTA, but it may be adjusted to analyze others histochemistries and immunohistochemistries reactions from any part of nervous system.

Immunoreactivity differences could be generally promoted, in general, for four reasons: 1- changes in the total number of cells; 2- changes in the total number of immunoreactive cells; 3- changes in the immunostained area; 4-changes in intracellular immunoreactivity [3,4,5,6,17].

These changes in the intensity of immunoreaction can be analyzed qualitatively by human judgment, semi quantitatively by densitometry or quantitatively by stereology [3,4,5,6,9,10,13,14,16,17]. In fact, semi quantitative analyses by densitometry is much more precise and discriminative than human judgment.

On the other hand, stereological tools as the optical disector and fractionator [7,10,14,18] are the golden pattern to evaluate the total number of cells in three dimensions, but some problems are found in the use of this techniques: 1- The time and experience required; 2-Some regions of central nervous system don't have well defined limits; 3-Changes in intracellular immunoreactivity could not be measured by stereology [4,10].

For these reasons, evaluations of histochemistries and immunohistochemisties experiments are classically done by densitometry [3,4,5,6,9,16,17,19,20,21,22]. Our protocol is the first detailed description of a fast and precise densitometric method to evaluate TH immunreactivity in SNPc and VTA using Image Pro Plus software. We believe that this protocol will facilitate the evaluation of TH immunoreactivity after different experimental Parkinson's disease treatment.

7. Essential references

Original Papers : Refs [1,4,6,19,21]

References

[1] F. Blandini, G. Nappi, C. Tassorelli, E. Martignoni, Functional changes of the basal ganglia circuitry in Parkinson's disease, Prog. Neurobiol. 62 (2000) 63-88.

[2] H.E. Brown, M.M. Garcia, R. Harlan, A two focal plane method for digital quantification of nuclear immunoreactivity in large brain areas using NIH-image software, Brain. Res. Protoc. 2 (1998) 264-272.

[3] J.E. Celis, Cell biology- A laboratory handbook- London: Academic Press. 1998.

[4] P. Chieco, A. Jonker, C.J.F. Van Noorden, Image Cytometry. New York: Springer. 118 p. 2001.

[5] P. Chieco, A. Jonker, C. Melchiorri, G. Vanni, C.J.F. Van Noorden, A user's guide for avoiding errors in absorbance image cytometry: a review with original experimental observations, Histochem. J. 26 (1994) 1-19.

[6] G.R. Contu, J.W. Nelson, Densitometry: modern approaches advance an established technique. Biotechniques., 16 (1994) 322-327.

[7] L.M. Cruz-Orive, Stereology of single objects, J. Microsc. 186 (1997) 93-107.

[8] P. Damier, E.C. Hirsch, Y. Agid, A.M Graybiel, The substantia nigra of the human brain II Patterns of loss of dopaminergic-containing neurons in Parkinson's disease, Brain 122 (1999) 1437-1448.

[9] A.C. Ferraz, L.L. Xavier, S. Hernandez, M. Sulzbach, G.G. Viola, J.A. Anselmo-Franci, J.A, M. Achaval, C. Da Cunha, Failure of estrogen to protect the substancia nigra pars compacta of female rats from lesion induced by 6 hydroxydopamine, Brain Res 986 (2003) 200-205.

[10] C.V. Howard, M.G. Reed, Unbiased stereology. New York: Springer., 246p. 1998.

[11] A.M. Insausti, L.M. Cruz-Orive, I. Jauregui, M. Manrique, R. Insausti. Stereological assessment of the glial reaction to chronic deafferentation of the cochlear nuclei in the macaque monkey (*Macaca fascicularis*), J. Comp. Neurol. 414 (1999) 485-494.

[12] G. Kempermann, H.G. Kunh, F.H.Gage. More hippocampal neurons in adult mice living in a enriched environment, Nature 386 (1997) 493-495.

[13] H. E. Murray, A. V. Pillai, S. R. McArthur, N. Razvi, K. P. Datla, D. T. Dexter, G. E. Gillies, Dose- and sex-dependent effects of the neurotoxin 6-hydroxydopamine on the nigrostriatal dopaminergic pathway of adult rats: Differential actions of estrogen in males and females, Neuroscience 116 (2003) 213-222.

[14] B. Pakkenberg and H.J.G. Gundersen, Total number of neurons and glial cells in human brain nuclei estimated by the disector and fractionator. J. Microsc. 150 (1988) 1-20.

[15] G. Paxinos and C. Watson, The rat brain in stereotaxic coordinates, Academic Press, San Diego, 1997.

[16] W.A. Partata, J.F. Cerveira, L.L. Xavier, G.G. Viola, M. Achaval, Sciatic nerve transection decrease substance P immunoreactivity in the lumbosacral spinal cord of the frog (Rana catesbeiana). Comp Biochem. Physiol. 131 (2002) 807-814.

[17] A .A Rasia-Filho, L.L. Xavier, P. Santos, G. Gehlen, G, M. Achaval, Glial fibrillary acidic protein immunodetection and immunoreactivity in the anterior and posterior medial amygdala of male and female rats. Brain Research Bulletin 58 (2002) 67- 75.

[18] D.C. Sterio, The unbiased estimation of number and sizes of arbitrary particles using the disector. J. Microsc, 134 (1984) 127-136.

[19] M. Tangeng, C. Zhengwei, S.E. Wellman, I.K. Ho, A quantitative histochemistry technique for measuring regional distribution of acetilcholinesterase in the brain using digital scanning densitometry. Anal. Biochem, 296 (2001) 18-28.

[20] R.R.Vaid, B.K. Yee, J.N.P. Rawlins, S. Totterdell, NADPH-diaphorase reactive pyramidal neurons in Ammon's horn and the subiculum of the rat hippocampal formation. Brain. Res, 733 (1996) 31-40. 1996.

[21] C.J.F. Van Noorden, R.G. Butcher, Quantitative enzyme cytochemistry. In: P.J. Stoward.; Pearse, A. G. E. Histochemistry, theoretical and applied, Vol 3: Enzime histochemistry 4th Edn. Churchill Livingstone. Edinburgh. pp 355-432. 1991.

[22] M. Wong-Riley, P. Antuono, K. Ho, R. Egan, R. Hevner, W. Liebl, Z. Huang, R. Rachel, J. Jones, Cytochrome oxidase in Alzheimer's Disease: biochemical, histochemical and immunohistochemical analyses of the visual and other systems. Vision Res, 37 (1997) 3593-3608.

Legends

Figure 1. Digitized images of coronal sections of substantia nigra and ventral tegmental area, in controls and 6 OHDA treated animals showing TH immunoreaction and the shape and relative size of area of interest. Note the decreased TH immunoreactivity found in SNPc, but not in VTA, in the animals treated with 6-OHDA. 6-OHDA, 6-hydroxydopamine treatment; AOI, area of interest, SNpc, Substantia nigra- pars compacta; SNpr- Substantia nigra pars reticulata; VTA, ventral tegmental area. The schematic drawings were modified from the atlas of Paxinos and Watson (1998).

Figure 2. Effects of 6-OHDA on optical density measurements (OD) of tyrosine hydroxylase immunoreactive neurons (TH-IR) in the substantia nigra pars compacta (SNpc) and tegmental ventral area (VTA) in controls and 6-hydroxydopamine (6OHDA) treated animals. Note the decreased optical density in SNPc of the 6-OHDA group. Values are expressed as means and standard deviation. Student *t* test *** $p = 0.0038$.

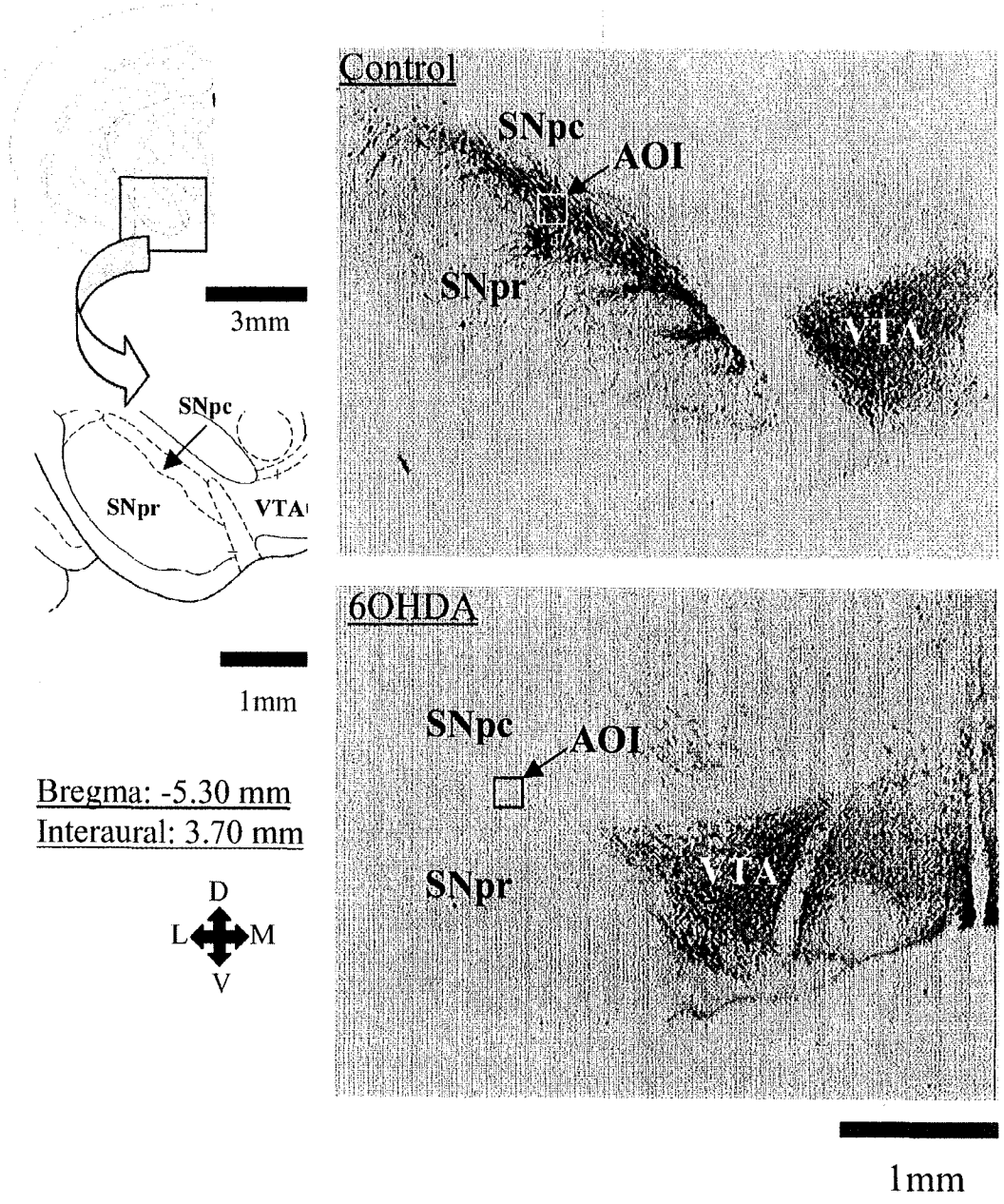
3mm
SNpc
SNpr
VTA
1mm
Bregma: -5.30 mm
Interaural: 3.70 mm
D
L
M
V
Control
SNpc
AOI
SNpr
VTA
6OHDA
SNpc
AOI
SNpr
VTA
1mm

TH immunoreactivity in SNpc and VTA

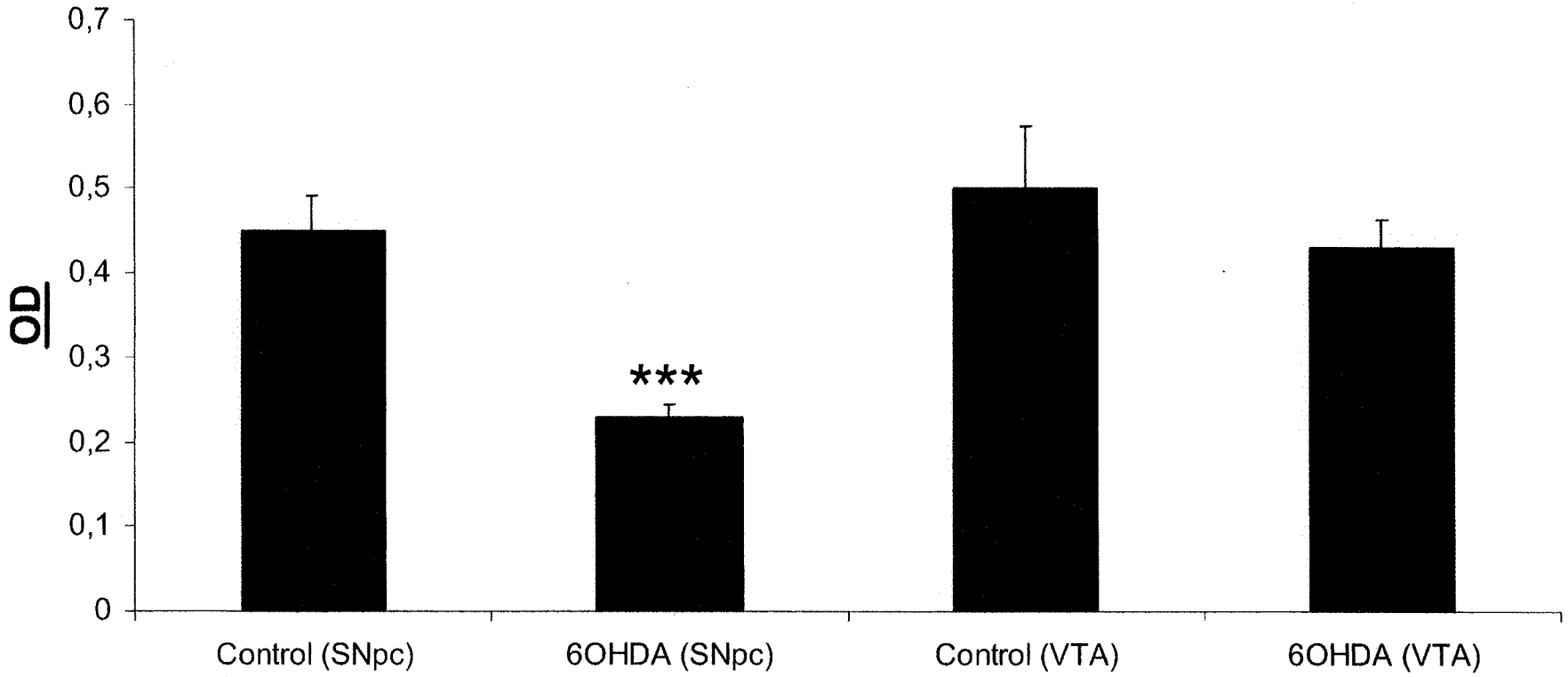

3.7 Protocolo para execução do cálculo de volume e do coeficiente de erro (CE) para o método de Cavalieri associado a técnica de contagem de pontos.

A implementação e a utilização deste protocolo, permite o cálculo do volume e do coeficente de erro gerado pela aplicação do método de Cavalieri associado a técnica de contagem de pontos no software Microsoft Excel.

Este protocolo é uma adaptação do protocolo desenvolvido pelo professor Luis Cruz-Orive no Laboratório de Estereologia da Universidade de Cantabria com a utilização do software S-Plus.

A seguir, apresentamos uma planilha, na qual podemos observar as coordenadas (x,y), onde devem ser inseridas as funções, os textos e os dados.

Planilha

x,y	Função/ Texto /Dados
A1	Estimation of volume from Cavalieri sections
A3	Estimation of strata volume
A5	Stratum
A6	1
A7	2
A8	3
A9	4
A11	T =
A12	A/P
A26	Variance point counting
A34	Kieu Souchet's formula
A36	=(3*(M29-E32)+P29-(4*O29))/(3*(M29-E32)+O29-(4*N29))
A38	q=
A40	q = 0 < 0.25 = formula A
A41	q = 0.25 < 0.75 = formula B
A42	q = 0.75 < 1 = formula C
A44	Formula A-Result
A45	Formula B-Result
A46	Formula C-Result

A49	Var/sec
A50	Nugget
A51	Total
A54	CE2V
A55	Sections
A56	Nugget
A58	CE sect
A59	Cenugg
A61	CE TOT
B5	1
B6	Número de pontos contados na 1ª secção
B7	Número de pontos contados na 7ª secção
B8	Número de pontos contados na 13ª secção
B9	Número de pontos contados na 19ª secção
B28	0,0724
B30	=B28*C28
B32	Variance of section
B38	=(E36*(LOG10(A36))-0,5)
B54	=SOMA(B55:B56)
B55	=B49/(H6*H6)
B56	=B50/(H6*H6)
B58	=100*H55
B59	=100*H56
B61	=100*H54
C4	Section
C5	2
C6	Número de pontos contados na 2ª secção
C7	Número de pontos contados na 8ª secção
C8	Número de pontos contados na 14ª secção
C9	Número de pontos contados na 20ª secção
C18	CE
C28	Valor do coeficiente de forma (shape Z)
C30	=G28*H6
C36	4
C38	0.5-q
C39	1-q
C44	=0,0833-(0,2153*B38)+(0,282*(B38*B38))-(0,289*(B38*B38*B38))
C45	=0,022+0,0627*(0,5-B38)+0,0764*G38+0,059*I38
C46	=0,004167+ (0,01693*D39)+(0,02468*G39)+(0,01895*I39)
C54	%
C55	%
C56	%
D5	3
D6	Número de pontos contados na 3ª secção
D7	Número de pontos contados na 9ª secção

D8	Número de pontos contados na 15ª secção
D9	Número de pontos contados na 21ª secção
D11	Valor da distância entre as medidas (T)
D12	Valor da área ponto (a/p)
D28	number of sections
D30	=RAIZ(C30)
D32	=B30*D30
D36	=LOG10(C36)
D38	=0,5-B38
D39	=1-B38
D54	=(B54/B54)*100
D55	=(B55/B54)*100
D56	=(B56/B54)*100
E5	4
E6	Número de pontos contados na 4ª secção
E7	Número de pontos contados na 10ª secção
E8	Número de pontos contados na 16ª secção
E9	Número de pontos contados na 22ª secção
E32	=B28*C28*(RAIZ(G28*H10))
E36	=POTÊNCIA(D36;-1)
F5	5
F6	Número de pontos contados na 5ª secção
F7	Número de pontos contados na 11ª secção
F8	Número de pontos contados na 17ª secção
F9	Número de pontos contados na 23ª secção
F10	Total
F38	(0.5-q)2
F39	(1-q)2
F54	raiz CEV
F55	raiz sections
F56	raiz nuggets
G5	6
G6	Número de pontos contados na 6ª secção
G7	Número de pontos contados na 12ª secção
G8	Número de pontos contados na 18ª secção
G9	Número de pontos contados na 24ª secção
G28	Número de secções contadas
G38	=D38*D38
G39	=D39*D39
H5	sum pontos
H6	=SOMA(B6:G6)
H7	=SOMA(B7:G7)
H8	=SOMA(B8:G8)
H9	=SOMA(B9:G9)
H10	=SOMA(H6:H9)

H38	(0.5-q)3
H39	(1-q)3
H54	=RAIZ(B54)
H55	=RAIZ(B55)
H56	=RAIZ(B56)
I5	V. Cm3
I6	=D11*D12*H6
I7	=D11*D12*H7
I8	=D11*D12*H8
I9	=D11*D12*H9
I10	=SOMA(I6:I9)
I38	=(D38*D38*D38)
I39	=D39*D39*D39
K5	Section
K6	1
K7	2
K8	3
K9	4
K10	5
K11	6
K12	7
K13	8
K14	9
K15	10
K16	11
K17	12
K18	13
K19	14
K20	15
K21	16
K22	17
K23	18
K24	19
K25	20
K26	21
K27	22
K28	23
K29	Total
L5	Pi
L6	=B6
L7	=C6
L8	=D6
L9	=E6
L10	=F6
L11	=G6

L12	=B7
L13	=C7
L14	=D7
L15	=E7
L16	=F7
L17	=G7
L18	=B8
L19	=C8
L20	=D8
L21	=E8
L22	=F8
L23	=G8
L24	=B9
L25	=C9
L26	=D9
L27	=F9
L28	=G9
L29	=SOMA(L6:L28)
M5	Pi2
M6	=L6*L6
M7	=L7*L7
M8	=L8*L8
M9	=L9*L9
M10	=L10*L10
M11	=L11*L11
M12	=L12*L12
M13	=L13*L13
M14	=L14*L14
M15	=L15*L15
M16	=L16*L16
M17	=L17*L17
M18	=L18*L18
M19	=L19*L19
M20	=L20*L20
M21	=L21*L21
M22	=L22*L22
M23	=L23*L23
M24	=L24*L24
M25	=L25*L25
M26	=L26*L26
M27	=L27*L27
M28	=L28*L28
M29	=SOMA(M6:M28)
M30	C0
N5	Pi. P + 1

N6	=L6*L7
N7	=L7*L8
N8	=L8*L9
N9	=L9*L10
N10	=L10*L11
N11	=L11*L12
N12	=L12*L13
N13	=L13*L14
N14	=L14*L15
N15	=L15*L16
N16	=L16*L17
N17	=L17*L18
N18	=L18*L19
N19	=L19*L20
N20	=L20*L21
N21	=L21*L22
N22	=L22*L23
N23	=L23*L24
N24	=L24*L25
N25	=L25*L26
N26	=L26*L27
N27	=L27*L28
N29	=SOMA(N6:N28)
N30	C1
O5	Pi.Pi +2
O6	=L6*L8
O7	=L7*L9
O8	=L8*L10
O9	=L9*L11
O10	=L10*L12
O11	=L11*L13
O12	=L12*L14
O13	=L13*L15
O14	=L14*L16
O15	=L15*L17
O16	=L16*L18
O17	=L17*L19
O18	=L18*L20
O19	=L19*L21
O20	=L20*L22
O21	=L21*L23
O22	=L22*L24
O23	=L23*L25
O24	=L24*L26
O25	=L25*L27

O26	=L26*L28
O29	=SOMA(O6:O28)
O30	C2
P5	Pi.Pi+4
P6	=L6*L10
P7	=L7*L11
P8	=L8*L12
P9	=L9*L13
P10	=L10*L14
P11	=L11*L15
P12	=L12*L16
P13	=L13*L17
P14	=L14*L18
P15	=L15*L19
P16	=L16*L20
P17	=L17*L21
P18	=L18*L22
P19	=L19*L23
P20	=L20*L24
P21	=L21*L25
P22	=L22*L26
P23	=L23*L27
P24	=L24*L28
P29	=SOMA(P6:P28)
P30	C4

A utilização desta planilha, permite a analise de até vinte e quatro secções por estrutura. Sugere-se que após a implementação, esta planilha deva ser testada com os exemplos 1 e 2, gentilmente fornecidos por E-mail pelo professor Cruz-Orive (um detalhamento do exemplo 1 pode ser obtido no exercício 3.4 do livro "Unbiased Stereology"-Howard e Reed 1998).

Os resultados obtidos com o uso desta planilha, devem ser rigorosamente idênticos aos encontrados pelo protocolo desenvolvido pelo prof Cruz-Orive, indicando assim, que esta foi implementada com sucesso.

Web Mail PUCRS

llxavier@pop3.pucrs.br

Mensagem Nº: 10 de 44

De: Luis Cruz Orive <lcruz@matesco.unican.es>

Para: llxavier@pucrs.br

CC:

Data: Wed, 3 Jul 2002 21:40:59 +0100 (WET DST)

Assunto: **Re: CE**

Querido Leder:

Perdona por la tardanza en contestar. Como te decia, he tenido un Junio muy ocupado.

He decidido darte una caña de pescar (en lugar de un pescado cada vez).
Al final te incluyo el listado de la funcion ce.cav para que lo insertes directamente en Splus.

Ejemplo 1

Ejercicio del 'Stereology Course' que te envié.

```
> Lung.1_c(4,12,13,10,9)    # P(lung) for Stratum 1 of the exercise

> ce.cav(Lung.1, a = 1/1.4^2, T0 = 0.75, shape.z = 4.5)

# a = 1/1.40 cm^2, T0 = 0.75 cm are data from the exercise

# shape.z = mean(B)/sqrt(mean(A)) is supposed to be estimated
  from a few sections. For the exercise we got the value 4.5.

# Splus gives:

$Sum.P:          # Total P
[1] 48

$V:              # est(V) cm^3
[1] 18.36735

$C:                      # constants C0, C1, C2, C4
[1] 510 424 289  36

$q:               # smoothness constant q
[1] 0.4360995

$alpha:           # alpha(q)
```

```
[1] 0.02633392

$ce2.vol:        # ce2(V) between, within (=nugget), and total
[1] 0.001232782 0.002190656 0.003423438

$ce.vol:         # sqrt's of the above
[1] 0.03511099 0.04680445 0.05851015

# You can check that everything coincides with the exercise ANSWERS.

--------

Ejemplo 2
---------

> Hip.1.1_c(2,6,7,11,15,10)  # Your hippocampus I, stratum 1 data.

# PROBLEM. I see you have a= 0.0441 mm^2, T0= 0.3 mm
           but I can't see which shape factor (shape.z) have
           you used! You have to estimate this for each stratum.
           Tentatively I'm taking the value 7.0.

> ce.cav(Hip.1.1, 0.0441, 0.3, 7.0)

$Sum.P:
[1] 51

$V:
[1] 0.67473

$C:
[1] 535 446 295  90

$q:
[1] 0.7248328

$alpha:
[1] 0.01109444

$ce2.vol:
[1] 0.0003813478 0.0034084503 0.0037897981

$ce.vol:
[1] 0.01952813 0.05838193 0.06156134

>

# From the data you sent me, I cannot see many coincidences ...
  (in part this may be due to the fact that you will have used a
  different shape factor)

# If you only want say the total ce, just type:

> ce.cav(Hip.1.1, 0.0441, 0.3, 7.0)$ce.vol[3]
[1] 0.06156134

---------------------

OK Leder, ya me diras si logras implementar la funcion. Si persisten las
dudas, no dudes en decirmelo.

Voy a estar fuera (http://www.neurostereology.info) del 7 al 15.
```

> PS:?Tienes algún palpite sobre quién podrá ganar la Copa?

Creo que la ganará Brasil (...!!) (Enhorabuena!!)

Un abrazo,

Luis

```
> ce.cav_function(z, a, T0, shape.z)
{
        q.cav.e <- function(y, nug)  # Kieu-Souchet formula for q
        {
                ny <- length(y)
                if(ny < 5)
                        return(0)
                else C <- numeric()
                C[1] <- sum(y^2)
                for(k in c(2, 3, 5)) {
                        C[k] <- sum(y[seq(ny - (k - 1))] * y[ - seq(k - 1)])
                }
                num <- 3 * (C[1] - nug) - 4 * C[3] + C[5]
                den <- 3 * (C[1] - nug) - 4 * C[2] + C[3]
                q <- log(num/den)/log(4) - 1/2
                q <- (q + abs(q))/2
                list(q = q, C = C)
        }
        alpha <- function(q)    # Marta's formula, C-O approximation
        {
                if(q <= 0)
                        return(1/12)
                else if(q >= 1)
                        return(1/240)
                else if(q > 0 && q <= 0.25)
                        return(0.0833 - 0.2153 * q + 0.282 * q^2 - 0.289 * q^
                                3)
                else if(q > 0.25 && q <= 0.75)
                        return(0.022 - 0.0627 * (-0.5 + q) + 0.0764 * (-0.5 +
                                q)^2 - 0.059 * (-0.5 + q)^3)
                else return(0.004167 - 0.01693 * (-1. + q) + 0.02468 * (-1. +
                                q)^2 - 0.01895 * (-1. + q)^3)
        }
        nz <- length(z)     # Matheron/Marta/C-O CE predictors
        const <- T0 * a
        Tz <- sum(z)
        Vz <- const * Tz
        nz.pos <- length(z[z > 0.])
        nugz <- (0.0724 * shape.z * sqrt(nz.pos)) * sqrt(Tz)
        C0 <- q.cav.e(z, nugz)$C[1]
        C1 <- q.cav.e(z, nugz)$C[2]
        C2 <- q.cav.e(z, nugz)$C[3]
        C4 <- q.cav.e(z, nugz)$C[5]
        qz <- q.cav.e(z, nugz)$q
        alphaz <- alpha(qz)
        var.V.comp <- c(alphaz * (3. * (C0 - nugz) + C2 - 4. * C1), nugz)
        var.V.comp <- (var.V.comp + abs(var.V.comp))/2
        var.V.comp.fi <- const^2 * var.V.comp
        ce2.V.comp <- var.V.comp/Tz^2
        ce2.V <- sum(ce2.V.comp)
        list(Sum.P = Tz, V = Vz, C = c(C0, C1, C2, C4), q = qz, alpha = alphaz,
                ce2.vol = c(ce2.V.comp, ce2.V), ce.vol = sqrt(c(ce2.V.comp,
                ce2.V)))
```

Luis M. Cruz-Orive
Depto. de Matematicas, Estadistica
y Computacion,
Facultad de Ciencias,
Universidad de Cantabria,
Avda. Los Castros, s/n,
E-39005 Santander

Tel.: 942 20 14 24 (directo)
20 14 20 (secretaria)
Fax: 942 20 14 02

Email: lcruz@matesco.unican.es

Slice	Points hitting transect (P_i)
a	
b	
c	
d	
e	
f	
g	
h	
i	
j	
k	
l	
Sum	$\sum_{i=1}^{12} P_i =$

Estimate of volume of ventricle:

$$\hat{V} = T \cdot a/p \cdot \sum_{i=1}^{12} P_i = [\quad\quad] \cdot [\quad\quad] \cdot [\quad\quad] \text{ mm}^3.$$

Now repeat the exercise using a coarser grid. How do the estimates of ventricular volume compare? What were the respective times taken for estimation with the fine and coarse grids?

Exercise 3.4

(Courtesy of Professor L.M. Cruz-Orive, Santander, Spain)

Aim

The aim of the exercise is to estimate the absolute volume of a rabbit's lung taken from the study reported by Michel and Cruz-Orive (1988).

Background

The lungs were fixed by vascular perfusion and the right lung stratified into four anatomically coherent strata (details in Michel and Cruz-Orive, 1988). Each stratum was then separately embedded in agar and serially sectioned into thin slabs approximately 1.5 mm thick, a constant distance of 7.5 mm apart. The resulting series of sections is shown as tracings in *Figure 3.6*.

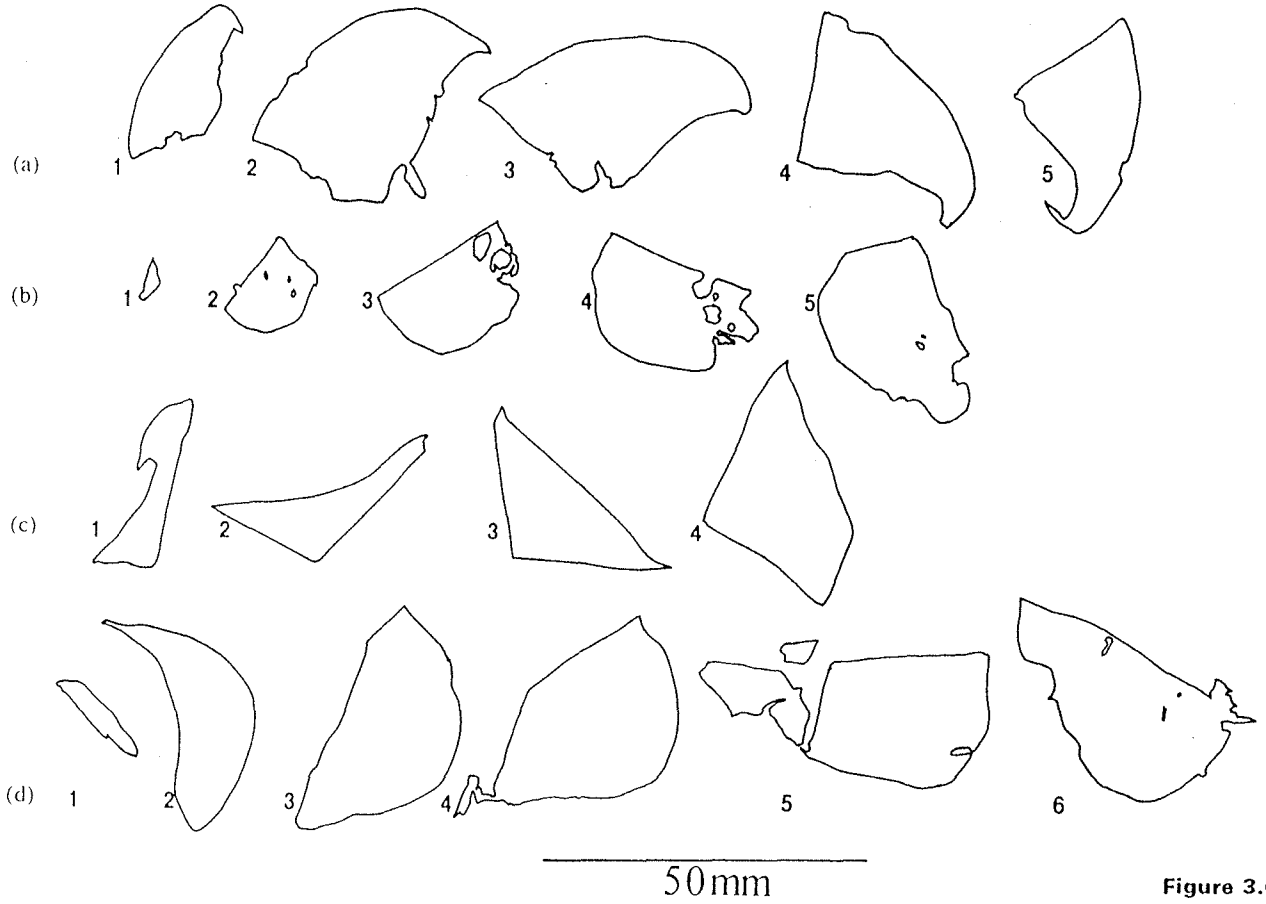

Figure 3.6. See text for details.

Procedure

(i) Calculate the linear magnification, M, of the image.
(ii) Make a copy of point grid P2 (see Appendix B). Calculate the inter-point spacing (Δx) of the point grid.
(iii) Calculate the area per point of the point grid at the level of the lung.
(iv) For each section within each stratum count the number of points hitting the lung transects.

Results

Distance between sections (T) = _____ mm
Magnification, M = _____
Distance between points in grid (Δx) = _____ mm
Area associated with each point (a/p) = _____ mm^2

Stratum	Sections						Total	Volume
	1	2	3	4	5	6	points	of stratum
A								
B								
C								
D								
Total								

Volume of stratum A: $\hat{V}_A = T \cdot a/p \cdot \sum_{i=1}^{5} P_i =$ [ ] · [ ] · [ ] mm^3.

Volume of stratum B: $\hat{V}_B = T \cdot a/p \cdot \sum_{i=1}^{5} P_i =$ [ ] · [ ] · [ ] mm^3.

Volume of stratum C: $\hat{V}_C = T \cdot a/p \cdot \sum_{i=1}^{4} P_i =$ [ ] · [ ] · [ ] mm^3.

Volume of stratum D: $\hat{V}_D = T \cdot a/p \cdot \sum_{i=1}^{6} P_i =$ [ ] · [ ] · [ ] mm^3.

Total volume of lung:

$\hat{V}_{Lung} = \hat{V}_A + \hat{V}_B + \hat{V}_C + \hat{V}_D =$
[ ] + [ ] + [ ] + [ ] mm^3.

Now enlarge grid P2 (see Appendix B) and estimate the total volume of the lung from all sections.

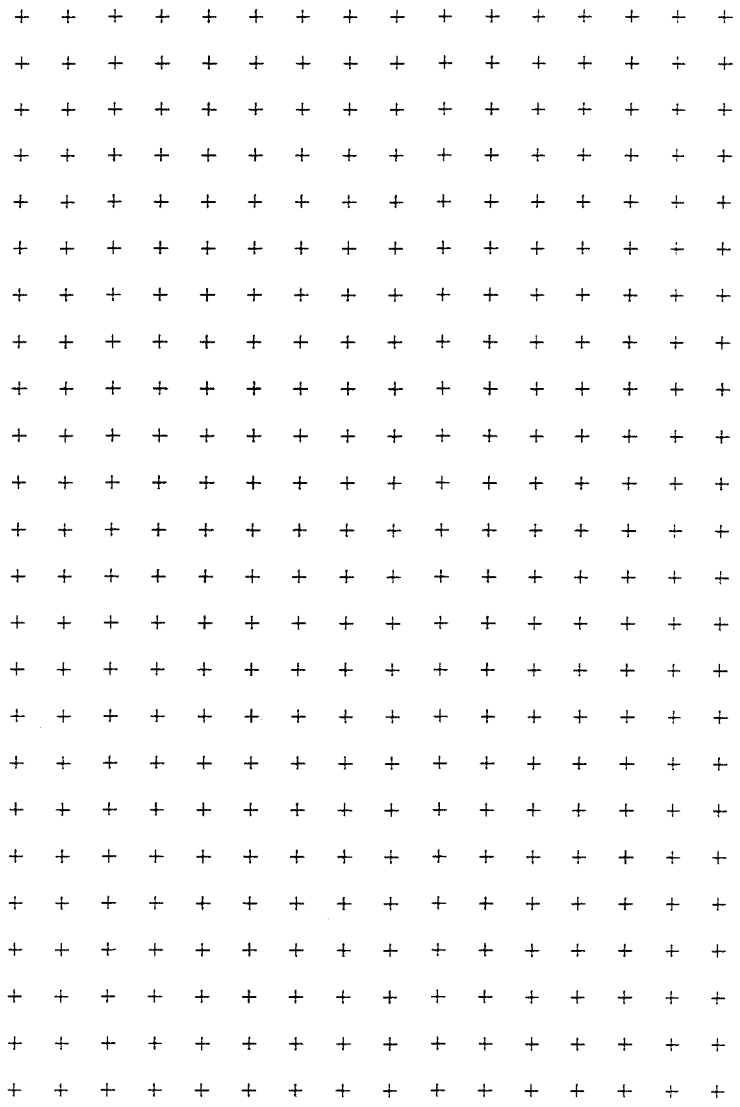

Grid P2 $= 10 \cdot \Delta x$

4. Conclusões e perspectivas

A execução deste trabalho permitiu: 1- A criação um protocolo rápido e preciso para execução de medidas de densidade óptica com o auxílio do *software* Image Pro Plus 4.1 (Artigo submetido- Brain Research Protocols "A simple and fast densitometric method to analyze tyrosine hydroxilase immunoreactivity in the substantia nigra pars compacta and in the ventral tegmental area") ; 2- A implementação da metodologia de estimativa de volume estrutural pelo procedimento de Cavalieri, como seu respectivo cálculo de coeficiente de erro, procedimentos estes realizados de forma semi-automática nos *softwares* Image Pro Plus 4.1 e Microsoft Excel (texto anexo).

A seguir apresentamos os principais resultados obtidos, divididos nos cinco artigos, "não metodológicos", publicados ou submetidos. Nesta seção do trabalho, serão apresentadas apenas as considerações metodológicas particulares de cada investigação, uma vez que, todas as considerações não metodológicas foram previamente discutidas nos artigos científicos publicados ou submetidos.

1-Relativas ao artigo "Glial fibrillary acidic protein immunodetection and immunoreactivity in the anterior and posterior medial amygdala of male and female rats"; Brain Research Bulletin, 58: 67-75 (2002).

- A reação imunohistoquímca para a proteína glial fibrilar ácida (GFAP) foi detectada nas diferentes subregiões da amígdala medial (AMe): amígdala medial ântero-

dorsal (AMeAD), amígdala medial póstero-dorsal (AMePD) e amígdala medial póstero-ventral (AMePV).

-Em ratas fêmeas em diestro, as subregiões posteriores da amígdala medial (AMePD e AMePV) apresentam uma maior imunoreatividade para GFAP quando comparadas a AMeAD.

-Na AMe de ratos machos não há nenhuma diferença significativa na imunoreatividade para GFAP entre as diferentes subregiões analisadas, AMeAD, AMePD e AMePV.

-As subregiões AMePD e AMePV da AMe de ratas fêmeas em diestro apresentam uma maior imunoreatividade para GFAP, quando comparadas as mesmas subregiões de ratos machos.

Considerações técnicas

A análise quantitativa dos resultados obtidos com a utilização da técnica imunohistoquímica para detecção da GFAP nos diferentes subnúcleos que compõem a AMe, não é uma tarefa simples, pois estas estruturas encefálicas não atendem uma das premissas básicas para o emprego das técnicas estereológicas, que é a presença de limites estruturais bem definidos (Paxinos e Watson, 1986; Paxinos e Watson, 1998). Portanto, procedimentos estereológicos como: a estimativa de volume estrutural dos distintos subnúcleos da AMe pelo método de Cavalieri (Gundersen, 1988; Cruz-Orive, 1997); a estimativa do número total de astrócitos imunorreativos para GFAP nos distintos subnúcleos da AMe pelo método do disector óptico (Sterio, 1984; Pakkenberg e Gundersen, 1988) ou a medida de densidade de superfície dos astrócitos GFAP imunoreativos (Baddeley *et al.*, 1986), não podem ser realizados na AMe. Deste modo,

nestas regiões, a análise semi-quantitiva por medida de densitometria óptica se caracteriza como a ferramenta mais adequada para a mensuração da imunoreatividade para GFAP.

2-Relativas ao artigo "Sciatic nerve transection decrease substance P immunoreactivity in the lumbosacral spinal cord of frog *Rana catesbeiana*"; Comparative Biochemistry and Physiology"; 131:807-814 (2002).

-Após a secção do nervo ciático de rãs (*Rana catesbeiana*) houve uma redução significativa da imunoreatividade para susbtância P no corno dorsal da medula espinhal ipsilateral ao local da lesão , quando comparado a mesma região contralateral.

-Esta diminuição da imunoreatividade para substância P permaneceu nos animais que tiveram uma sobrevida, pós transecção ciática, de 3, 5, 8 e 15 dias, os animais que tiveram uma sobrevida de 20 dias não apresentaram qualquer diferença na imunoreatividade detectada entre os lados ipsilateral e contraleteral a lesão, indicando uma restauração da imunoreatividade neste período.

Considerações técnicas

Neste experimento, os procedimentos imunohistoquímicos, para detecção da substância P, foram realizados em dias distintos, portanto com soluções distintas. Embora parâmetros como a concentração dos reagentes empregados e o tempo de incubação, tenham sido rigorosamente controlados, inevitavelmente existem diferenças na coloração basal entre estes procedimentos imunohistoquímicos. Portanto, neste caso, não é correta a comparação entre os diferentes grupos experimentais (controle, 3, 5,8,15 e 20 dias após deaferentação), deste modo, foram estatisticamente comparados, através da realização de

um teste *t* pareado, os lados ipsilateral e contralateral à deaferentação, em cada uma das secções analisadas por densitometria óptica.

3-Relativas ao artigo "Substance P immunoreactivity in the lumbar spinal cord of the turtle Trachemys dorbigni following peripheral nerve injury"; Brazilian Journal of Medical and Biological Research, 36: 515-520 (2003).

-Não há nenhuma alteração na imunoreatividade para substância P em tartarugas *Trachemys dorbigni* submetidas a desnervação, quando comparados os lados ipsilateral e contralateral à lesão, nos diferentes tempos de sobrevida após a secção do nervo ciático (7 dias, 15 dias, 30 dias, 60 dias e 90 dias).

Considerações técnicas

As mesmas considerações técnicas, descritas no artigo anterior, são válidas para esta investigação.

4- Relativas ao artigo "Failure of estrogen to protect the substantia nigra pars compacta of female rats from lesion induced by 6-hydroxydopamine"; Brain Research, 986-200-205 (2003).

-A infusão intraencefálica de 6OHDA é responsável pela diminuição do número de células imunoreativas para tirosina hidroxilase na porção compacta da substância nigra e o tratamento com estrógeno não tem qualquer efeito neuroprotetor sobre a lesão induzida por 6OHDA.

Estes resultados, sugerem uma cuidadosa análise sobre a utilização terapêutica da reposição de estrógeno para prevenção e/ou tratamento do mal de Parkinson, devido aos riscos potenciais deste tipo de tratamento.

Considerações técnicas

A estimativa precisa do número total de neurônios dopaminérgicos perdidos na porção compacta dá substancia nigra após a infusão de 6OHDA, somente pode ser realizada, com a utilização de metodologias estereológicas como o disector óptico ou fracionador óptico (Sterio, 1984; Cruz-Orive, 1997), contudo, para a emprego correto destas metodologias, se faz necessária a utilização de um microscópio óptico equipado com um platina motorizada (microcator), que se mova nos eixos (x, y e z), informando as variações de distância nestes três eixos. Atualmente o Laboratótio de Análise de Imagens do DCM-ICBS-UFGRS não conta com este tipo de equipamento, o que nos conduziu, a realização de uma avaliação bidimensional da morte neuronal gerada pelo tratamento com 6OHDA e do possível efeito neuroprotetor do estrógeno. Embora este tipo de metodologia não apresente a mesma precisão da estimativa estereológica, o resultado obtido através desta abordagem certamente será confirmado com o uso das técnicas estereológicas, devido a magnitude da lesão causada pela infusão de 6OHDA na porção compacta da substância nigra.

5-Relativa ao artigo "Preconditioning changes cytochrome oxidase activity and hippocampal volume after global cerebral ischemia". Submetido- Neuroscience Research.

- Imediatamente após o evento isquêmico há um aumento da atividade da enzima citocromo oxidase nos estratos oriens, piramidal e radial do hipocampo de ratos submetidos a isquemia letal e subletal, entretanto este aumento não é encontrado nos animais submetidos ao pré condicionamento isquêmico.

- Vinte e quatro horas após o evento isquemico ocorre um aumento da atividade da enzima citocromo oxidase em todos os grupos analisados (isquemia subletal, letal e precondicionamento isquemico)

- Sete dias após o evento isquemico não há nenhuma diferença significativa entre a atividade da enzima citocromo oxidase encontrada no hipocampo de animais controle e submetidos a qualquer tipo de isquemia prosencefálica (subletal, letal e precondicionamento isquemico)

- O evento isquemico subletal não altera significativamente o volume estrutural da região CA1 do hipocampo e do giro denteado.

- O evento isquemico letal diminui o volume estrutural da região CA1 do hipocampo, sem entretanto alterar o volume estrutural do giro denteado.

- O pré condicionamento isquemico causa uma atenuação significativa da diminuição do volume estrutural da região CA1 induzida pelo evento isquemico letal.

Os resultados obtidos neste trabalho, confirmam, através da estereologia, os resultados descritos previamente com a utilização de outras metodologias, mostrando que o pré condicionamento isquêmico, diminui os efeitos de um evento isquêmico letal, na região CA1 da formação hipocampal.

Considerações técnicas

Devido ao grande número de animais utilizados neste trabalho, a técnica histoquímica para a detecção da enzima citocromo oxidase foi realizada em quatro experimentos distintos, os animais foram divididos de acordo com o tempo de reperfusão empregado (0, 24h, 48h e 7 dias) com 20 animais em cada experimento, divididos em cinco animais por cada subgrupo (controle, isquemia subletal, isquemia letal e pré condicionamento isquêmico). Deste modo, não foi possível a comparação direta da medida de DO entre os animais com diferentes tempos de reperfusão, devido a utilização de meios de incubação distintos para realização dos quatro procedimentos histoquímicos.

A preparação adequada do tecido nervoso, é uma característica essencial para a aplicação das técnicas estereológicas, neste sentido, o modo como o encéfalo é fixado, pós-fixado,seccionado, desidratado,colocado em lâminas histológicas e coberto com resina é fundamental para a correta estimativa do volume estrutural pelo método de Cavalieri (Schimitz *et al.*, 2001). No intuito de corrigir possíveis erros na estimativa de volume estrutural, induzidos pelo enrrugamento tecidual, foi constituído o fator de enrrugamento da espessura da secção, obtido através da divisão da espessura final da secção pela espessura "original" da secção. Portanto, um fator de enrrugamento da espessura da secção de 1.0 significa que não houve nenhuma alteração na espessura original da secção, gerada pelo processamento histológico, enquanto um fator de enrrugamento da espessura da secção de 0.33, indica que a espessura original da secção é três vezes maior que a espessura da secção após o processamento histológico (West, 1996; Schimitz *et al*, 2001). Os fatores de enrrugamento da espessura da secção variam de acordo com processamento histológico empregado e a região encefálica analisada, por exemplo: são descritos valores para os fatores de enrrugamento da secção variando entre 1.0 e 0.78 para as secções incluídas em

metacrilato (Sousa *et al.*, 1999; Lukoyanov *et al.*,2000); valores de 0.8 a 0.32 para tecido nervoso fixado com formol e seccionado em criostato (Heinsen *et al.*, 1999; Schimitz *et al*, 2000); e o valor de 0.7 para secções do hipocampo de camundongo, com uma espessura original de 50 μm, seccionadas com a utilização de vibrátomo (Jinno *et al*, 1998). Além disso, o enrrugamento tecidual gerado pelo processamento histológico pode variar de acordo com a região da secção analisada, Andersen e Gundersen (1999) demonstraram que secções de cerebelo humano com uma espessura original de 100 μm, obtidas com o uso de vibrátomo, apresentavam uma redução média de 57,8% na região médial da secção e uma redução de 48,7% nas região das bordas laterais da mesma secção (Andersen e Gundersen, 1999; Gardella *et al.*, 2003).

Portanto, o cálculo o do fator de enrrugamento da secção é fundamental para a correta estimativa do volume estrutural a partir da utilização do método de Cavalieri, para a realização deste cálculo é necessário a utilização de um microscópio óptico equipado com uma platina móvel, que se mova nos eixos (x, y e z) e informe com precisão a espessura do eixo z (West, 1996).

Como citado anteriormente, o Laboratório de Análise de Imagens DCM-ICBS-UFRGS não conta, até o momento, com este tipo de equipamento, deste modo, a estimativa de volume estrutural foi expressa neste trabalho sob a forma de percentagem do controle, devido a impossibilidade do cálculo do fator de enrugamento da espessura da secção, gerado pelos processamento histológico.

O cálculo do coeficiente de erro obtido à partir da utilização do método de Cavalieri, associado a técnica de contagem de pontos, utilizado para a estimativa volumétrica da região CA1 do hipocampo e do giro denteado, foi realizado como a utilização do protocolo para cálculo do CE desenvolvido no *software* Microsoft Excel,

descrito anteriormente. Os resultados obtidos com a utilização deste protocolo foram confirmados pela Dra Marta García Fiñana, pesquisadora dno Magnetic Resonance and Image Analysis Research Centre (MARIARC) da Universidade de Liverpool, utilizando-se do *software* S-Plus.

A realização deste trabalho permitiu a criação do Laboratório de Análise de Imagens no DCM-ICBS-UFRGS, e a partir da utilização das técnicas de análise de imagens desenvolvidas neste trabalho foram publicados outros dois artigos científicos, Comparative Biochemistry and Physiology- A, 124: 113-122 (1999) e Brain Research 973: 171-178 (2003), e submetidos a análise para publicação outros quatro artigos.

Além disso, em um futuro próximo, pretendemos executar de forma rotineira, metodologias estereológicas como o disector óptico, o fracionador e o nucleador no intuito de criar um centro de referência na região sul do Brasil para este tipo de investigação científica.

Bibliografia adicional (Introdução e conclusões)

1. Adams, J.C. Technical considerations on the use of horseradish peroxidase as a neuronal marker. Neuroscience.; 2: 141-145; 1977.

2. Alberts, B.; Johnson, A.; Lewis, J.; Raff, M.; Roberts, K.; Walter, P. Molecular biology of the cell. 4rd ed. New York. Garland Sciences. 2002. 1511pp

3. Alonso-Magdalena, P.; Arguelles, K.; Jimenez, N.C.; Gonzalez-Pardo, H.; Perillan, C.; Costales, M., Vijande, M. Quantitative histochemical assessment of oxidative metabolism in the subfornical organ after partial aortic ligature in rats. Neurosc Lett., 344: 49-52; 2003.

4. Andersen, B.B.; Gundersen, H.J.G. Pronounced loss of cell nuclei and anisotropic deformation of thick sections. J. Microsc.,196: 69-73; 1999.

5. Arteni, N.; Salgueiro, J.; Torres, I.; Achaval. M.; Netto, C.A. Neonatal cerebral hypoxia-ischemia causes lateralized memory impairments in the adult rat. Brain Research., 973: 171-178; 2003.

6. Baddeley, A .J.; Gundersen, H.J.G.; Cruz-Orive, L.M. Estimation of surface area from vertical sections. J. Microsc., 142: 259-276; 1986.

7. Bjungn, J. Estimation of total number of cells in the rat spinal cord using the optical disector. Micron. Microsc. Acta., 22:25-26; 1991.

8. Butcher, R.G. The measurements in tissue sections of the two formazans derived from nitroblue tetrazolium in dehydrogenase reactions. Histochem. J., 739-744; 1978.

9. Cavalieri, B. (1635) *Geometria indivisibilidus continuorum*. Typis Clementis Feronif, Bononi.. Reprinted as Geometria degli indivisibil. Uniane Tipografica Editrice. Torinese. Torino. 1966.

10. Celis, J.E. Cell biology- A laboratory handbook- London: Academic Press. Vol 2-3; 1998.

11. Chieco, P.; Jonker, A.; Melchiorri, C.; Vanni, G.; Van Noorden, C.J.F. A user's guide for avoiding errors in absorbance image cytometry: a review with original experimental observations. Histochem., J. 26: 1-19; 1994.

12. Chieco, P.; Jonker, A.; Van Noorden, C.J.F. Image Cytometry. New York: Springer. 118 p. 2001.

13. Conn, H.J. Biological stains. Baltimore: The Williams and Wilkins Company. 694 pp. 1977.

14. Contu, G.R.; Nelson, J.W. Densitometry: modern approaches advance an established technique. Biotechniques., 16: 322-327; 1994.

15. Cruz-Orive, L.M. Precision of Cavalieri sections and slices with local errors. J. Microsc., 193:182-198; 1999.

16. Cruz-Orive, L. M. Stereology of single objects. J. Microsc., 163:102-113; 1997.

17. Cruz-Orive, L.M. Toward a more objective biology. Neurobiol. Aging., 15:377-378; 1994.

18. Cruz-Orive, L.M. Systematic sampling in stereology. Bull. Inter. Statist., 55: 451-468; 1993/

19. Cruz-Orive, L.M. On the precision of systematic sampling: a review of Matheron's transitive methods. J. Microsc., 153: 315-333; 1989.

20. Cruz-Orive, L.M.; Weibel, E. Recent stereological methods for cell biology: a brief survey. Am. J. Physiol., 258: L148-L146; 1990.

21. De Felipe, J.; Jones, E. Santiago Ramón y Cajal and methods in neurohistology. TINS., 15: 237-246; 1992.

22. De Olmos, J.; Heimer, L. Mapping of colateral projections with the HRP method. Neurosci. Lett., 6: 107-114; 1977.

23. De Robertis, E.D.P.; Nowinski, W.W.; Sáez, F.A. Citología general. Quinta edición. Buenos Aires. El Ateneo. 1963. 604 pp.

24. Everbroeck, B.V.; Pals, P.; Martin, J.J.; Gras, P. Antigen retrieval in prion protein immunohistochemistry., J. Histochem. Cytochem. 41: 1465-1470; 1999.

25. Fukuda, M.; Bohm, N.; Fujita, S. Cytophotometry and its biological application. Prog. Histochem. Cytochem., 11: 1-19; 1978.

26. Garcia-Fiñana, M.; Cruz-Orive, L.M.; Mackay, C.E.; Pakkenberg, B.; Roberts, N. Comparison of MR imaging against physical sectioning to estimate the volume of human cerebral compartments, NeuroImage., 18: 505-516; 2003.

27. Gardella, D.; Hatton, W.J.; Rind, H.B.; Rosen, G.D.; von Bartheld, C.S. Differential tissue shrinkage and compression in the z-axis: implication for optical disector counting in vibratome, plastic and cryosections. J. Neurosc. Method., (2003) (no prelo).

28. Gonzalez-Lima, F.; Garrosa, M. Quantitative histochemistry of cytochrome oxidase in rat brain. Neurosci. Lett., 123:251-253; 1991.

29. Gonzales-Lima, F.; Jones, D. Quantitative mapping of cytochrome oxidase activity in the central auditory system of the gerbil: a study with calibrated activity standards and metal intensified histochemistry. Brain. Res., 660: 34-49; 1994.

30. Gundersen, H.J.G.; Bagger, P.; Bendtsen, T.F. A new stereological tools: disector, fractionator, and point sampled intercepts and their use in pathological research. Acta Pathol. Microbiol. Immunol. Scand., 96: 857-881; 1988.

31. Gundersen, H.J.G.; Jensen, E.B. The efficiency of systematic sampling in stereology and its prediction. J. Microsc., 147: 229-263; 1987.

32. Gundersen, H.J.G.; Jensen, E.B.V.; Kiêu, K.; Nielsen, J. The efficiency of systematic sampling in stereology- reconsidered. J. Microsc., 193:199-211; 1999.

33. Hammond, P.I.; Jelacic, T.; Padilla, S.; Brimijoin, S. Quantitative, video based histochemistry to measure regional effects of anticholinesterase pesticides in rat brain. Anal. Biochem., 241: 82-92; 1996.

34. Hardie, D.C.; Gregory, T.R.; Hebert, P.D.N. From pixels to picograms: a beginners's guide to genome quantification by Feulgen image analysis densitometry. J. Histochem. Cytochem., 50: 735-749; 2002.

35. Harley e Bielajew, C. A.; Bielajew, C. H. A comparison of glycogen phosphorylase a and cytochrome oxidase histochemical staining in rat brain. J. Comp. Neurol., 322: 377-89; 1992.

36. Haug, H. History of neuromorphometry. J. Neurosc. Method., 18: 1-17; 1986.

37. Heinsen, H.; Rüb, U.; Ulmar, G.; Bethke, B.; Schüler, M.; Böcker, F.; Eisenmenger, W.; Götz, M.; Korr, H.; Schmitz, C. Nerve cell loss in the thalamic mediodorsal nucleus in Huntington's disease. Acta Neuropathol., 97: 613-622; 1999.

38. Hovda, D.A; Villablanca, J.R. Cerebral metabolism following neonatal or adult hemineodecortication in cats: effect on oxidative capacity using cytochrome oxidase histochemistry. Dev. Brain. Res., 110: 39-50; 1998.

39. Howard, C.V.; Reed, M.G. Unbiased stereology. New York: Springer. 1998. 246p.

40. Idrizbegovic. E.; Bogdanovic. N.; Viberg, A.; Canlon, B. Auditory peripheral influences on calcium binding protein immunoreactivity in the cochlear nucleus during aging in the C57BL/6J mouse. Hearing Res., 179: 33-42; 2003

41. Jinno, S.; Aika, Y.; Fukuda, T.; Kosaka, T. Quantitative analysis of GABAergic neurons in the mouse hippocampus, with optical disector using confocal laser scanning microscopy. Brain Res., 814: 55-70; 1998.

42. Kiêu, K. Three lectures on systematic geometric sampling. Memoirs 13/1997. Department of Theoretical Statistics. University of Aarhus.1997.

43. Kiêu, K.; Souchet, S.; Istas, J. Precision of sytematic sampling and transitive methods. J. Statist. Plan. Inf., 77: 263-279; 1999.

44. Knyihar-Csilik, E.; Tajti, J.; Samsam, M.; Sáry, G.; Buzás, S.; Vécsei, L. Depletion of calcitonin gene-related peptide from the caudal trigeminal nucleus of the rat after electrical stimulation of the gasserian ganglion. Exp. Brain. Res., 118:111-114; 1998.

45. Larsson, E.; Lindvall, O.; Kokaia, Z. Stereological assessment of vulnerability of immunocytochemically identified striatal and hippocampal neurons after global cerebral ischemia in rats. Brain. Res., 913: 117-132; 2001.

46. Lin, A.M.Y.; Yang, C.H.; Ueng, Y.F.; Luh, T. Y.; Liu, T.Y.; Lay, Y.P.; L. T. Ho, L.T. Differential effects of carboxyfullerene on MPP^+/MPTP-induced neurotoxicity, Neurochem. Intern. 44: 99-105; 2004.

47. Lukoyanov, N.V.; Brandao, F.; Cadete-Leite, A.; Madeira, M.D.; Paula-Barbosa, M.M. Synaptic reorganization in the hippocampal formation of alcohol-fed rats may compensate for functional deficits related to neuronal loss. Alcohol., 20: 139-148; 2000.

48. Martin, R. Neuroscience Methods: A guide for advanced students. New York. Harwood Academic Publishers. 1997. 256 pp.

49. Matheron, G. Les variables régionalisées et leur estimation. Masson et Cie. Paris.1965.

50. Matheron, G. The theory of regionalized variables and its applications. Les cahiers du Centre de Morphologie Mathématique de Fontainebleau. no 5. Ecole Nationale Supérieure des Mines de Paris. Fontainebleau.1971.

51. Mathieu, O.; Cruz-Orive, L.M.; Hoppeler, H.; Weibel, E.R. Measuring error and sampling variation in stereology: comparison of the efficiency of various methods for planar image analysis. J. Microsc., 121: 75-88; 1980.

52. Osborn, N.G.; Weber, K. Tumor diagnosis by intermediate filament typing: A novel tool for surgical pathology. Lab Invest., 48: 372-394; 1983.

53. Pakkenberg, B.; Gundersen, H.J.G. Total number of neurons and glial cells in human brain estimated by the disector and fractionator. J. Microsc., 150: 1-20; 1988.

54. Pannese, E. The black reaction. Brain. Res. Bull., 41: 343-349; 1996.

55. Paxinos, G., Watson, C. The rat brain in stereotaxic coordinates, 2nd ed. San Diego: Academic Press; 1986.

56. Paxinos, G., Watson, C. The rat brain in stereotaxic coordinates, 4nd ed. San Diego: Academic Press; 1998.

57. Pillegard, K.; Ladefoged, O. Total number of astrocytes in the molecular layer of the dentate gyrus of rats at different ages. Anal. Quant. Cytol. Histol., 18: 279-285; 1996.

58. Polak, J.M.; Van Noorden, S. An introduction to imunocytochemistry: Current techniques and problems. New York. Oxford University Press. 1992. 76 pp.

59. Ramón Y Cajal S. Histologie du sytème nerveux de l'homme et des vertébrés. Paris. A. Maloine. 1909. 986 pp.

60. Regeur, L.; Pakkenberg, B. Optimizing sampling designs for volume measurements of components of human brain using a stereological method. J. Microsc., 155: 113-121; 1989.

61. Roberts, N.; Cruz-Orive, L.M. Reid, N.; Brodie, D.; Bourne, M.; Edwards, R.H.T. Unbiased estimation of human body composition by the Cavalieri method using magnetic resonance imaging. J. Microsc., 171: 239-253; 1993.

62. Roberts, N.; Garden, A.A.; Cruz-Orive, L.M.; Whitehouse, G.H.; Edwards, R.H.T. Estimation of fetal volume by MRI and stereology. Br. J. Radiol., 67: 1067-1077; 1994.

63. Rodríguez, C.; Guillamón, A.; Pinos, H.; Collado, P. Postpartum changes in the GABAergic system in the bed nucleus of the accessory olfactory tract. Neurochem Int., 44: 179-183; 2004.

64. Ruiz-Torner, A.; Bordonau, F.O.; Valverde-Navarro, A.A.; Martínez-Soriano, F. The chemical architecture of the rat's periaqueductal gray based on acetylcholinesterase histochemistry: a quantitative and qualitative study. J. Chem. Neuroanat., 21:295-312; 2001.

65. Schmitz, C.; Holf, P.R. Recommendations for straightforward and rigorous methods of counting neurons based on a computer simulation approach. J. Chem. Neuroanat., 20: 93-114; 2000.

66. Schmitz, C.; Dafotakis, M.; Heinsen, H.; Mugrauer, K.; Niesel, A.; Popken, G.J.; Stephan, M.; Van de Berg, W.D.J.; von Hörsten, S.; Korr, H. Use of cryostat sections from snap-frozen nervous tissue for combining stereological estimates with histological, cellular, or molecular analyses on adjacent sections. J. Chem. Neuroanat., 20: 21-29. 2000.

67. Singer, C. A short story of biology. London. Oxford University Press. 1931.

68. Souchet, S. Précision de l'estimateur de Cavalieri. Rapport de stage, D.E.A. de statistiques et modèles aleatoires appliqués à la Finance. Université Paris-VII. Laboratoire de Biométrie. INRA-Versailles; 1995.

69. Sousa, N.; Paula-Barbosa, M.M; Almeida, O.F. Ligand and subfield specificity of corticoid-induced neuronal loss in the rat hippocampal formation. Neuroscience., 89: 1079-1087; 1999.

70. Sterio, D.C. The unbiased estimation of number and sizes of arbitrary particles using the disector. J. Microsc., 134: 127-136; 1984.

71. Sternberger, L.A.; Sternberger, N.H. The unlabeled antibody method: comparision of peroxidase-antiperoxidase with avidin-biotin complex by a new method of quantification. J. Histochem. Cytochem., 34: 599-605; 1996.

72. Sternberger, L.A. Immunocytochemistry 3rd ed. New York. Johns Wiley & Sons; 1986.

73. Strazielle, C.; Sturchler-Pierrat, C.; Staufenbiel, M.; Lalonde, R. Regional brain cytochrome oxidase activity in amyloid precursor protein transgenic mice with the swedish mutation. Neurosci., 118: 1151-1163; 2003.

74. Tangeng, M.; Zhengwei, C.; Wellman, S.E.; Ho, I.K. A quantitative histochemistry technique for measuring regional distribution of acetilcholinesterase in the brain using digital scanning densitometry. Anal. Biochem., 296: 18-28; 2001.

75. Tashima, S.; Shimada, S.; Yamaguchi, K.; Tsuruta, J.; Ogawa, M. Expression of brain-type glycogen phosphorylase is a potentially novel early biomarker in the carcinogenesis of human colorectal carcinomas. Am. J. Gastroenterol., 255:263; 2000.

76. Thune, J.J.; Pakkenberg, B. Stereological studies of the schizophrenic brain. Brain. Res. Rev., 31: 200-204; 2000.

77. Vaid, R.R.; Yee, B.K.; Rawlins, J.N.P.; Totterdell, S. NADPH-diaphorase reactive pyramidal neurons in Ammon's horn and the subiculum of the rat hippocampal formation. Brain. Res., 733: 31-40; 1996.

78. Van Noorden, C.J.F.; Butcher, R.G. Quantitative enzyme cytochemistry. In: P.J. Stoward.; Pearse, A. G. E. Histochemistry, theoretical and applied, Vol 3: Enzime histochemistry 4th Edn. Churchill Livingstone. Edinburgh.1991. pp 355-432.

79. West, M.J. Stereological methods for estimating the total number of neurons and synapses: issues of precision and bias. TINS., 22(2): 51-61; 1999.

80. Wong-Riley, M.; Antuono, P., Ho, K.; Egan, R.; Hevner, R.; Liebl, W.; Huang, Z.; Rachel, R.; Jones, J. Cytochrome oxidase in Alzheimer's Disease: biochemical, histochemical and immunohistochemical analyses of the visual and other systems. Vision Res., 37: 3593-3608; 1997.